CP27: Expression, Regulation, and Function of a Chromatin Complex Member

BY

Yoshihiro Ito
D.D.S. Nihon University, School of Dentistry, 1996

THESIS

Submitted as partial fulfillment of the requirements
for the degree of Doctor of Philosophy in Oral Science
in the Graduate College of the
University of Illinois at Chicago, 2012

Chicago, Illinois

Defense Committee:

Dr. Thomas Diekwisch, Chair and Advisor
Dr. Xianghong Luan, Department of Oral Biology
Dr. David Crowe, Center for Molecular Biology of Oral Diseases
Dr. Alison Doubleday, Department of Oral Biology
Dr. Michel Allen, University of Chicago

Acknowledgments

I would like to thank my thesis committee (Dr. Diekwisch, Dr. Luan, Dr Crowe, Dr. Doubleday, and Dr. Allen) for their unwavering support and assistance. They provided guidance in all areas that helped me accomplish my research goals. I would also like to acknowledge MOST programs in Oral Science. Also I would like to thank all my lab members for their support and advice.

This research was supported by NIDCR grant DE13095 to TGHD and 1T32DE018381 MOST grant.

YI

TABLE OF CONTENTS

TABLE OF CONTENTS (continued)

TABLE OF CONTENTS (continued)

LIST OF TABLES

LIST OF FUGURES

LIST OF ABBREVIATIONS

AMV	Avian myeloblastosis virus;
AP-1	Activator protein transcription factor;
BSA	Bovine serum albumin
BrdU	Bromodeoxyuridine
BAF	BRG1/brm-associated factor
BCNT	Bucentaur
C/EBP	CCAAT/enhancer binding protein;
CBF	Core binding factor;
CBF-B	Core binding transcription factor-subunit B
CDC25c	CDC25 phosphatase;
ChIP	Chromatin immunoprecipitation
CP27	Craniofacial protein
Csx/Nkx 2.5	cardiac homeobox transcription factor;
DMEM	Dulbecco's modified eagle medium
DMAP1	DNA methyltransferase 1-associated protein 1
EMSA	Electrophoretic mobility shift assay
ES	Embryonic stem cell
ETS	E-twenty-six transcription factor;
EED	Embryonic ectoderm development
een	extraembryonic endoderm
ee	extraembryonic ectoderm layer
FCS	Fetal calf serum
FGF	Fibroblast growth factor;
GATA	Transcription factor that binds to the GATA DNA sequence;
H2A.Z	H2A histone family, member Z
HOX	Homeobox protein
HSP 70	Heat shock protein 70;
HDAC	histone deacyltransferases
ICM	inner cell mass
KLF	Krueppel-like factor
LIF	Leukemia inhibitory factor
NF-1	Nuclear factor 1;
NF1	Nuclear transcription factor 1
NF-Y	Nuclear transcription factor Y
NF-Y	Nuclear factor Y;
NF-YA	Nuclear transcription factor Y subunit alpha
Oct	Octamer binding factor;
PCR	Polymerase chain reaction
POU	Pit-1, Oct-1, Unc-86 transcription factor family;
pI	Isoelectric point
RLM-RACE,	RNA ligase mediated rapid amplification of cDNA ends;
SOX	Sry-related high mobility group box transcription factor
SRCAP	Snf2-related CREBBP activator protein Snf2-related CREBBP activator protein

TIP	TATA box-binding protein-interacting protein
USF1	Upstream stimulatory factor 1
USF2	Upstream stimulatory factor 2

Summary

CP27 is a novel gene involved in early vertebrate development that features a distinct expression pattern during development. The cp27 gene contains an open reading frame of 295 amino acids corresponding to a predicted molecular mass of 33kDa. Here we have characterized the CP27 promoter and performed a first analysis of CP27 function in development.

To study *cp27* gene regulation, we have cloned the promoter of the mouse *cp27* gene, examined its transcriptional activity, and identified transcription factor binding sites in the proximal promoter region. Two major transcription start sites were mapped adjacent to exon 1. Promoter function analysis of the 5′ flanking region by progressive 5′ deletion mutations localized transcription repression elements between −1993 bp and −969 bp and several positive elements between −968 bp and the preferred transcription start site. EMSA and functional studies indicated two function-cooperative CCAAT boxes and identified the NF-Y transcription factor as the CCAAT activator controlling transactivation of the CP27 promoter. In addition, this study demonstrated that for its effective binding and function, NF-Y required not only the minimal DNA segment length identified by deletion studies, but also a defined nucleotide sequence in the distal 3′ flanking region of the CP27 proximal promoter CCAAT box. These results provide a basis for our understanding of the specific regulation of the cp27 gene in the NF-Y-mediated gene transcription network.

The maintenance and differentiation of embryonic stem cells (ES cells) depends on the regulation of gene expression through the coordinated binding of transcription factors to regulatory promoter elements. One of the genes involved in embryonic development is the chromatin factor CP27. Previously, we have shown that NF-Y interacted with the CP27 proximal promoter CCAAT-box. Here we report that CP27 gene expression in mouse ES cells is

controlled by CCAAT and E-box cis-acting regulatory elements and their corresponding transcription factors NF-Y and USF1. Specifically, USF1 interacts with the E-box of the *cp27* proximal promoter and NF-Y interacts with the CCAAT-box. NF-Y and USF1 also interacted with each other and activated the *cp27* promoter in a synergistic fashion. Together, these studies demonstrate that gene expression of the chromatin factor CP27 is regulated through the interaction of the transcription factors NF-Y and USF1 with the *cp27* proximal promoter.

Chromatin dynamics assume key functions in the lineage differentiation and gastrulation of bilaterian embryos. Here we demonstrate that a novel chromatin factor CP27 is required for mouse development, germ layer differentiation, and the formation of an archenteron. Loss of CP27 caused severely disturbed epiblast development and prolonged endoderm survival. *cp27* Null mice expressed residual levels of the pluripotency factor Nanog and the variant histone H2A.Z, and resembled slightly advanced stages of either phenotype. In embryoid bodies and cells, CP27 regulated both Nanog and H2A.Z expression. CP27 interacted with the variant histone H2A.Z on a chromatin level, and a chromatin complex containing both CP27 and H2A.Z differentially bound to the Nanog promoter. Together, these findings suggest a direct link between CP27 and H2A.Z chromatin complex interactions and ES cell lineage specification via Nanog. Studies presented here shed light on the chromatin-level regulation of pluripotency factors and the resulting effect on ES cell lineage specification and gastrulation.

Together, our data indicate that CP27 is chromatin factor involved in early embryonic development that is regulated by the universal transcription factor NF-Y in combination with the USF-1 enhancer.

I. INTRODUCTION

A. Background

Therapeutic promise of stem cells. Stem cells are unique cells that have the capacity for self-renewal and are capable of forming at least one, and sometimes many specialized cell types (Donovan and Gearhart 2001). It is conceivable that such pluripotent cells could be used to treat a wide variety of human diseases, particularly those in which specific cells types (such as cardiomyocytes, dopaminergic neurons, and l3-islet cells) have been lost or disabled (Donovan and Gearhart 2001). Recent studies have demonstrated that transplanted bone marrow cells can turn into unexpected lineages including myocytes, hepatocytes, neurons, and many others (Weissman 2000). However, it has been suggested that some of these effects that have been originally interpreted as transdifferentiation may be due to spontaneous cell fusion (Terada et al. 2002, Ying et al. 2002). Together, these findings have shed light on the puzzling behavior of stem cells and once more renewed interest in embryonic stem cells. Embryonic stem (ES) cell lines are derived from explanted cultures of the inner cell mass (ICM) of blastocysts (Thomson et al. 1998) and can be kept in an undifferentiated and pluripotent state in culture.

Unfortunately, many promising derivatives of ES cells have proven to function poorly in animal engraftment models (Rasmussen 2003). These difficulties point to the need for a more sophisticated understanding of the processes and mechanisms that govern differentiation and of the developmental pathways that they attempt to recapitulate (Rasmussen 2003).

Chromatin remodeling as a key mechanism for epigenetic regulation of gene expression during cell differentiation. A number of studies have indicated that the transcriptional state of a gene in ES cells can be viewed as a reflection of its underlying chromatin state (reviewed in Cavalli 2006). It has been suggested that studies of chromatin in differentiating ES cells will greatly aid the subsequent clinical development of stem cell therapies because stem cell differentiation is essentially an attempt to achieve tissue-specific patterns of gene expression *in vitro* (Rasmussen 2003, Meshorer and Misteli 2006). In order to modify and achieve fine-tuned patterns of gene expression, ES cells contain robust chromatin-remodeling and reprogramming activities, including the mammalian SWI/SNF chromatin remodeling complex, a network of polycomb proteins, and the SWRAP complex (Puente et al. 2005, Meshorer and Misteli 2006). In addition, transcription factors interact with transcription promoting histone acetyltransferase (HAT) proteins resulting in histone modifications, which in turn cause changes in the activation or repression of gene expression (Cheung and Briggs 2000). One of the examples of histones that affect gene expression is the histone variant H2A.Z, which protects euchromatin from becoming transcriptionally inactive by preventing ectopic spreading of heterochromatin (Meneghini et al. 2003). This histone variant H2A.Z has been tightly linked to the function of CP27, a unique gene that has been discovered in our laboratory.

The cp27 gene an essential gene in embryonal development and cell specification. CP27 is a unique gene product expressed during early embryogenesis and during the formation of embryonal organs (Diekwisch et al. 1999). Originally, *cp27* was cloned from a mouse E11 age library and mapped to the human chromosome region

16q22.2-22.3 close to a region associated with several myeloid anemias (Diekwisch, 1996; Diekwisch et aI., 1999). In more recent studies, we have shown that CP27 affects viability, proliferation, attachment and gene expression in embryonic fibroblasts (Luan and Diekwisch 2002). We have localized CP27 to the stellate reticulum of developing tooth organs, a transitory celilayer of developing enamel organs (Diekwisch et al. 2002) and we have demonstrated that CP27 is necessary for cell survival and differentiation during tooth morphogenesis in organ culture (Diekwisch and Luan 2002).

Evolutionary conservation of the cp27 gene as part of a yeast chromatin remodeling complex. From an evolutionary point of view, the *cp27* gene is highly conserved. A number of vertebrate homologues have been cloned (Nobokuni et aI., 1997) and database searches have identified cp27 homologues in species as distant as pufferfish *(Fugu rubripes)* or yeast *(Saccharomyces* cerevisiae)(Diekwisch et al. 1999). The yeast protein swc5 shares 45% homology with cp27 (Diekwisch et al. 1999) and has been characterized as a component of the Swr1 complex that incorporates the histone H2A.Z into euchromatin (Kobor et al. 2004). H2A.Z is an essential histone variant that affects the equilibrium between different chromatin conformational states (Fan et al. 2002) while Swr1 chromatin remodeling enzymes regulate cell cycle checkpoint responses to DNA damage (Papamichos-Chronakis et al. 2006, Downs et al. 2004) and have been associated with the regulation of chromosome stability (Krogan et al. 2004) and chromatin remodeling (Li et al. 2005).

Chromatin mediated regulation of gene expression via histone acetylation/deacetylation mechanisms. The profound impact of dynamic chromatin architecture on eukaryotic gene expression has only been fully recognized in recent years

(Kraus and Wang 2002, Dillon 2006, Zhang and Reinberg 2006). Chromatin-mediated gene expression activation is often accomplished by de-repression of silencing mechanisms that involve histone acetyltransferase (HAT)-mediated chromatin decondensation, while histone deacyltransferases (HDAC) contribute to chromatin condensation and repression of gene expression (Kraus and Wang 2002, Bulger 2005, Yang and Gregoire 2005). These histone acetylation dynamics not only play key roles in the regulation of gene expression but also contribute significantly to changes in pluripotency/lineage commitment states in embryonic stem cells (Forsberg et al. 2000, Tada and Tada 2001, Lee et al. 2004).

The role of the chromatin in embryonic stem cell puripotency and differentiation. Inside of their chromatin, embryonic stem cells harbor an extraordinary molecular machinery responsible for complex tasks such as maintenance of pluripotency, self-renewal and lineage specification (Meshorer and Misteli 2006). There has been emerging evidence that lineage specific genes are poised for activity but are held in check by the repressive machinery (Meshorer and Misteli 2006) and that polycomb-group proteins and DNA methylation play a major role in the maintanence of the pluripotent state (Auzara et al. 2006, Hattori et al. 2006, Jorgensen et al. 2006). Moreover, core transcriptional regulatory circuitry factors in human embryonic stem cells, OCT4, SOX2, and NANOG, co-occupy a substantial portion of the transcriptional landscape of ES-cell target genes (Boyer et al. 2005). In turn, the embryonic transcriptional machinery is controlled by loose binding of architectural chromatin proteins which control the pluripotency differentiation equilibrium through hyper-dynamic binding mechanisms (Meshorer et al. 2006). Together, this tight relationship between chromatin structure

histone acetylation dynamics and ES cell transcriptional core circuitry exerts profound control on ES cell pluripotency and lineage derivation.

CP27 and ES cell pluripotency. Here we are proposing that CP27 is a major factor in the embryonic epigenetic chromatin network that contributes to ES cell pluripotency and differentiation. As a homologue to the yeast protein swc5, in light of its functional significance, and because of its chromatin localization as visualized by immunohistochemistry and GFP-fusion protein, we were poised to explore putative mechanisms by which CP27 might exert a control on the eukaryotic ES cell transcriptional machinery. Using ChIP-IP studies, we identified the histone variant H2A.Z as a potential regulating factor that might be involved in CP27 mediated transcriptional regulation. H2A.Z might be an in chromatin-associated for CP27 in its role to regulates ES gene.

Evidence for a functional synergism between CP27 and H2A.Z has been corroborated by *co*localization using confocal microscopy and functional assays using the CP27 knock-down and H2A.Z immunolocalization (Fig. 4). In addition, we found a 4-fold decrease in Nanog, a significant 4-fold increase in Sox2, anda co-localization between Nanog and CP27 as additional supportive evidence for our hypothesis that CP27 is a chromatin-associated co-factor that affects the ES cell transcriptional core circuitry that controls the maintenance ·of ES cell pluripotency.

B. Characterization of the mouse CP27 promoter and NF-Y mediated gene regulation

Craniofacial development occurs in a complex signaling environment in which growth factors, transcription factors and structural genes of the extracellular matrix maintain signal-response cascades that ultimately result in the formation of the vertebrate head (Davidson, 1993, Slavkin and Diekwisch, 1996 and Thesleff and Sharpe, 1997). These signaling cascades involve a continuous communication between epithelial and mesenchymal components of adjacent tissues (Thesleff, 1995 and Thesleff and Sharpe, 1997). One such gene that is expressed at several crucial sites in the epithelial–mesenchymal interface during craniofacial development is CP27 (Diekwisch et al., 1999 and Diekwisch et al., 2002).

CP27 is a unique gene that is highly conserved in many species such as human, mouse, bovine, deer, goat, sheep, giraffe, and pig (Nobukuni et al., 1997 and Diekwisch et al., 2002). Sequence analysis has also revealed significant homologues in zebrafish (Danio rerio) and yeast (Saccharomyces cerevisiae) (Diekwisch et al., 2002; unpublished observation). Originally, CP27 was cloned from an E11 early embryonic library (Nobukuni et al., 1997, Diekwisch and Marches, 1997 and Diekwisch et al., 2002). Northern blot analysis of RNA from multiple mouse tissues demonstrated high levels of expression in developing mouse teeth, heart, lungs, and liver. Both the expression in presumably important sites related to organogenesis and the distinct changes in localization during development (Nobukuni et al., 1997, Diekwisch and Marches, 1997 and Diekwisch et al., 2002) as well as gain- or loss-of-function studies (Diekwisch

and Luan, 2002 and Luan and Diekwisch, 2002) suggest that CP27 may play important roles during development.

To understand the expression of the cp27 gene and elucidate the mechanisms that govern it, we have cloned the promoter region of the mouse cp27 gene and characterized the cell-specific elements in the 5′ flanking region in embryonic fibroblasts. Using gel-shift and functional studies, we have identified NF-Y as a transactivator of the CP27 promoter that regulates cp27 gene expression via multiple CCAAT boxes. Our results document for the first time the importance of the 5′ 2-kb flanking region in the expression of the mouse cp27 gene and establish NF-Y as a transcriptional regulator of cp27 gene expression.

C. The H2A.Z Exchange Histone Chaperone CP27 regulates ES cell Pluripotency through Nanog

The eukaryotic transcriptional machinery controls gene expression through its interaction with the promoters of target genes, most commonly through specific promoter elements such as TATA boxes. Frequently, eukaryotic promoter elements act in concert with other regulatory elements such as enhancers or silencers (Griffiths et al., 2000). For example, the CCAAT-box acts in conjunction with the NF-Y transcription factor as a crucial promoter organizer, facilitating the recruitment of polymerase II and of neighboring transcription factors (Frontini and Imbriano, 2002, Kabe et al., 2005 and Donati et al., 2006). The combinatorial binding of transcription factors to promoter elements plays a key role during eukaryotic development, when unique combinations of

transcription factor binding sites establish specific regulatory codes (Narlikar and Ovcharenko, 2009). The quintessential role of a finely tuned transcriptional machinery is illustrated by the regulatory circuitry involved in the maintenance of embryonic stem cell (ES cell) pluripotency and progression into differentiated lineages, which is controlled by the promoters of chromatin factors (Boyer et al., 2005).

One of the chromatin factors required for ES cell pluripotency maintenance is the CP27 gene, a highly conserved transcriptional co-regulator characterized by a TATA-less proximal promoter (Luan et al., 2010). Previously we have reported that CP27 function elimination caused early embryonic lethality and failure of epiblast expansion in CP27-null mouse embryos (Ito et al., 2005). The CP27 promoter contains several CCAAT-boxes, common regulatory elements in eukaryotic promoters usually found in the vicinity of other promoter elements such as E-box and GC-rich elements (Luan et al., 2010, Bucher and Trifonov, 1988, Magan et al., 2003, Schuettengruber et al., 2003 , Zhu et al., 2003 and Zhu et al., 2005). Most prominent among CCAAT-box binding factors is the ubiquitous transcription factor NF-Y, a trimeric transcriptional activator with histone-like subunits (Mantovani, 1999 and Guerra et al., 2007). NF-Y binding to the CCAAT-box is required for ES cell proliferation (Grskovic et al., 2007).

To understand the mechanisms that govern CP27 regulation in ES cell maintenance and differentiation, we turned to the CP27 promoter to identify specific regulatory elements and to test their function in mouse ES cells. We found two major cis-acting elements in the CP27 proximal promoter, a CCAAT-box and an E-box. Here we report how these two key CP27 proximal promoter elements are regulated by the

transcription factors NF-Y and USF1 and provide an explanation for the role of CP27 in ES cell growth.

D. The H2A.Z Exchange Histone Chaperone CP27 regulates ES cell Pluripotency through Nanog

Chromatin remodeling complexes are large, multi-subunit protein complexes that fine-tune the action of the transcriptional machinery through combinations of individual building blocks, allowing for a sophisticated, nuanced control of gene expression (Berger 2007). Among these are the several large ATP-dependent chromatin complexes, including the SWI/SNF complex, the CHD complex, the INO80 complex, and the ISWI complex. Commonly, these complexes contain a large ATPase subunit, which mobilizes the nucleosome to allow access to DNA for transcriptional control, while other complex members are involved in fine-tuning the ATPase action and DNA recognition.

Recently, a number of studies have demonstrated that ATP remodeling enzymes such as Tip60/p400 and SWI/SNF as well as chromatin complex members such as Brg, BAF155 and BAF250A are essential for the regulation of core transcriptional circuitry involved in the maintenance and function of ES cells as well as embryonic survival (15-18 from Ho et al. Gaspar-Maia et al. 2011.). ES cell core circuitry involves factors such as Oct4, Sox2, Nanog, and Klf4, which collaborate to stably maintain the expression of pluripotency genes (after Ho et al.). This delicate balance of pluripotency factors is profoundly affected by epigenetic mechanisms involving not only chromatin complex members, but also Polycomb complexes, microRNAs, and histone modifying enzymes (Ho et al.). Together, these establish a stem cell chromatin state in ES cell progenitors by

activating or repressing multiple target genes (Spivakov and Fisher, 2007). One of these three regulators, Nanog, has recently been defined as a molecular gatekeeper that confers variable resistance to differentiation upon ES cells and acts primarily in the construction of inner cell mass and germ cell states.

The histone variant H2A.Z is one of the key chromatin components that affects gene expression during early development and gastrulation. H2A.Z replaces conventional H2A in many nucleosomes and protects euchromatin from becoming transcriptionally inactive by preventing ectopic spreading of heterochromatin (Fan et al., 2002, Meneghini et al. 2003). H2A.Z also plays a critical role during early mammalian development and gastrulation and is enriched in the chordamesoderm, where it may affect proliferation and migration (Faast et al. 2001, Ridgway et al. 2004). The incorporation of H2A.Z into nucleosomes is mediated by the SWR (SRCAP in mammal) multiprotein complex (Kobor et al., 2004; Ruhl et al., 2006). One of the members of the SWR complex is Swc5, the yeast orthologue of the mouse CP27 protein, in yeast loss of SWR complex subunits such as Swc2, Arp6, Swc5 and Swc6, function failed to incorporation of Hiz1 (H2A.Z) to nucleosomes (Wu et al. 2005).

The *cp27* gene is expressed during early embryogenesis and during the formation of embryonic organs (Diekwisch et al., 1999), affects viability, proliferation, attachment, and gene expression in embryonic fibroblasts, and is necessary for cell survival and differentiation during organogenesis (Diekwisch and Luan, 2002, Luan and Diekwisch 2002). In the present study we are exploiting the presence of residual or reduced levels of Nanog and H2A.Z expression in the *cp27* null phenotype to decipher the impact of chromatin dynamics on embryonic lineage specification. Evidence for a relationship

between CP27 and Nanog is provided through multiple CP27 loss of function studies and by demonstrating that CP27 specifically regulates Nanog expression in ES cells. Based on the role of the CP27 yeast homologue Swc5 in the incorporation of H2A.Z into nucleosomes we have performed studies to confirm that SRCAP complex interacts with CP27 on a chromatin-level and that CP27 function modulation affects H2A.Z expression and exchange. Moreover, we demonstrates Cp27 function not only histone exchange via SRCAP complex, also unique function of gene regulation. Our findings provide the first evidence of an intimate link between chromatin complex members, ES cell pluripotency factors, and germ layer specification.

II. MATERIAL AND METHODS

A. 1. Library screening and DNA sequencing

A mouse genomic lambda Fix II 129/SVJ library (Stratagene, La Jolla, CA) was screened with a full-length mouse CP27 cDNA, and five clones were identified. Using the EcoRI restriction enzyme, the DNA insert was cut and fragments were subcloned into the pBluescript vector (Stratagene). The resulting DNA sequence was determined with an ABI 373 automatic sequencer. One of the five genomic clones contained 2.1 kb of the 5′ flanking region of the cp27 gene and was used for further analysis. The transcription factor binding sites within the 5′ flanking region were determined using MatInspector (www.genomatrix.de) and Signal Scan (www.bimas.cit.nih.gov/molbio/signal/).

A. 2. Primer Extension Analysis

Primer extension was carried out using the Primer Extension System kit (Promega, Madison, WI). An antisense primer CP 82-61 (5′ GCTACCCACACGACTGCGCCAC 3′) was labeled with r-32P using T4 polynucleotide kinase and annealed in AMV primer extension buffer at 58 °C for 40 min to 10 μg of total RNA from NIH 3T3 cells, which have been previously shown to express CP27 (Luan and Diekwisch, 2002) or tRNA. The primer was extended with AMV reverse transcriptase at 42 °C for 30 min. Resulting products were electrophoresed in an 8% denaturing urea polyacrylamide gel and autoradiographed. The sizes of the products were determined by 32P-labeled ΦX 174 Hinf I DNA markers.

A. 3. Ribonuclease protection assay (RPA)

The 5′ flanking region and partial exon 1 of the cp27 gene were amplified via polymerase chain reaction using sense primer CP-261/-242 (5′ TATTAGCTTGTGAGCAAATT 3′) and antisense primer CP 82/61. The 343-bp fragment was then subcloned into the plasmid pCR II-TOPO (Invitrogen, Carlsbad, CA). Transcription was performed with T7 RNA polymerase and yielded α 32P-labeled antisense RNA that was then used as a probe. The probe was annealed to 10 μg of total RNA from NIH 3T3 cells or yeast RNA at 42 °C for 16 h. Following digestion with RNase A and RNase T1 (Ambion, Austin, TX) according to manufacturer's instructions, the RNase-resistant radioactivity was size-fractionated in an 8% denaturing urea polyacrylamide gel and autoradiographed. The sizes of the protected fragments were determined by 32P-labeled ΦX 174 Hinf I DNA markers.

A. 4. 5′-Rapid amplification of cDNA ends (5′ RACE)

Rapid amplification of cDNA 5′ ends was performed using a RLM-RACE kit (Ambion). 10 μg of total RNA was treated with Calf intestine alkaline phosphatase to remove free 5′-phosphate. Tobacco acid pyrophosphatase was added to the reaction to remove the cap structure from full-length mRNA. A 45-base RNA adaptor oligonucleotide was ligated to the RNAs using T4 ligase. The first-strand cDNA was synthesized in a random-primed reverse transcription reaction. Amplification of the 5′ ends of CP27 transcripts was accomplished with two pairs of nested primers: a 5′ RACE outer primer 5′ GCTGATGGCGATGAATGAACACTG 3′ and a CP27 antisense outer primer 5′ TCTCTTCAGTCTCCTCGGCT 3′; a 5′ RACE inner primer 5′

CGCGGATCCGAACACTGCGTTTGCTGGCTTTGATG 3′ and a CP27 antisense inner primer 5′ GCTCCTCTTCATCTTCTTCACTGC 3′. The RACE products were subcloned into pCR II-TOPO and then sequenced.

A. 5. Promoter–reporter gene constructs

For this promoter study, a total of 15 promoter–reporter gene constructs were generated. The inserts for 14 of the 15 constructs were amplified by PCR with the screened genomic clone as a template using a common 3′ primer and selected 5′ primers (Table 1 and Table 2). These primers also introduced a SacI site at the 5′ end and a HindIII site at the 3′ end of the amplified fragments. The PCR fragments were gel-purified using Qiaquick PCR preps (QIAGEN, Valencia, CA), digested with SacI and HindIII and subcloned into the pGL3-basic vector (Promega). Correct orientation of all inserts with respect to the pGL3 vector was verified by DNA sequencing. Only the pGL −1475/+48 plasmid was generated using a pGL3 vector into which a 1.5 kb BglII and HindIII fragment from pGL −1993/+48 was inserted. The constructs used for deletion mutation studies were pGL3-1993, pGL3-1475, pGL3-969, pGL3-720, pGL3-207, pGL3-93, and pGL3-17 (Fig. 3). The constructs pGL-93/-56M10-12, pGL3-1255, pGL3-1190, pGL−93/+48CATm, pGL-93-56M10-12, pGL−1255/+48CAT1m, pGL-1255/+48CAT5m, and pGL−1255/+48CAT1,5m were used for CCAAT box function studies. Plasmids carrying an “m” denominator were subjected to a mutation, and pGL−1255/+48CAT1,5m was subjected to a double mutation. All plasmid constructs contained part of the exon 1 noncoding region.

A. 6. Transient Transfection and Dual Luciferase Assay

The mouse embryonic fibroblast cell line NIH 3T3 was used as the recipient cell line for transient transfection assays. NIH 3T3 cells (3 × 105 cells/well) were placed in 6-well plates and cultured for 24 h. For each transfection, cells were incubated with 1 μg of each promoter–reporter plasmid, 0.01 μg of pRL-TK (Promega), which was used as internal control for transfection efficiency, 4 μl of LipofectAMINE PLUS REAGENT (Invitrogen), and 2 μl of LipofectAMINE reagent (Invitrogen) in serum-free medium for 3 h. For co-transfection, 1 μg of the pGL−1475/+48 construct was introduced with 0.4 or 0.8 μg of expression vector pIRES-NFYA or with 0.8 μg of pIRES-NFYAm29, a domain negative NF-YA (courtesy of Dr. S. Chen, UTHSCSA). After removal of the DNA–PLUS-LipofectAMINE complex, cells were incubated in 2 ml of complemented medium for 48 h and then subjected to a dual luciferase assay according to the manufacturer's instructions (Promega). In this dual luciferase system, CP27 promoter fragments were linked to the firefly luciferase gene while the co-transfected renilla luciferase gene (pRL-TK) was driven by the SV40 promoter. The firefly and renilla luciferase activities were measured using TD-20/20 (Promega). Promoter activity measurements were a reflection of the ratio of firefly/renilla luciferase for each construct. For luciferase activity measurements, the means of luciferase activity measurements from five independent sets of experiments using a triplicate set of wells in each experiment were determined for each construct.

A. 7. Nuclear extract preparation

NIH 3T3 cells (5 × 107) in 100 mm dishes were washed twice with cold phosphate-buffered saline (pH 7.4) and scraped off in 1 ml of lysis buffer (10 mM Hepes

(pH 7.9), 1.5 mM MgCl2, 10 mM KCl, 0.5 mM DDT, 0.5 mM phenyl-methylsulphonyl fluoride (PMSF), 0.05% Nonidet P-40 (NP-40). Cell lysates were homogenized with 20 strokes using a tight-fitting Dounce homogenizer and centrifuged at 250g for 10 min at 4 °C to pellet the nuclei. The pelleted nuclei were resuspended in 1 ml of nuclear extraction buffer (5 mM Hepes (pH 7.9), 26% glycerol, 1.5 mM MgCl2, 0.2 mM EDTA, 0.5 mM DTT, 0.5 mM PMSF) with a final concentration of 300 mM NaCl, and mixed on a rotator at 4 °C for 1 h. Nuclear debris was centrifuged at 24,000g for 20 min at 4 °C. Aliquots were frozen at −70 °C. Protein concentrations were determined using the Bio-Rad Laboratories protein assay reagent (Bio-Rad, Philadelphia, PA).

A. 8. Electrophoretic mobility shift assay (EMSA)

Double-stranded oligonucleotides (Table 2) for EMSAs were labeled with (r-32P) ATP using T4 kinase and purified with the Qiaquick nucleotide removal kit (QIAGEN). EMSAs were performed by incubating 5 μg of nuclear extract with labeled double-stranded oligonucleotide in 20 μl reaction buffer [(10 mM Hepes (pH 7.9), 50 mM KCl, 2.5 mM MgCl2, 1 mM DDT, 10% glycerol, 2 μg of poly (dI–dC)] at room temperature for 20 min. For competition analysis, 25- or 50-fold molar excess of unlabeled double-stranded oligonucleotide was added to the nuclear extracts prior to the addition of the labeled probe. For supershift assays, polyclonal antibodies CBFA, CBFB, CBFC and Est 1/2 (Santa Cruz Biotechnology), NF1 and SOX5 (Abcam, Cambridge, MA), were incubated with the nuclear extracts for 15 min followed by the addition of radio-labeled probe. DNA–protein complexes were resolved in a 5% non-denaturing polyacrylamide gel in 1x TBE.

A.9. Immunoblotting

Nuclear extracts separated by EMSA under native conditions were electrophoretically transferred to nitrocellulose in a blotting apparatus filled with transfer buffer (25 mM Tris, 190 mM glycine, 20% methanol) for 1 h at 75 mA. Nitrocellulose filters were blocked in 2% BSA overnight at room temperature. The blot was incubated with 1:200 diluted anti-mouse CBF-B antibody (Santa Cruz) for 2 h, and a 1:2000 diluted AP-conjugated rabbit anti-goat secondary antibody (Invitrogen) for 1 h, and then with NB/ BCIP substrate. For controls, the primary antibody was omitted.

A.10. Mutagenesis

Site-directed mutagenesis was performed using the GeneEditor in vitro Site-Directed Mutagenesis System (Promega). The sense oligonucleotides (Table 2) used in the mutation analysis of competition EMSA served as mutagenesis primers. The templates for the mutagenesis of the CCAAT box and the CGGA site within the proximal promoter region and the CCAAT box in a distant region were constructs pGL −93/+48 and pGL −1255/+48, respectively. The DNA templates, sense oligonucleotide and bottom selection oligonucleotide were annealed at 75 °C for 5 min and then cooled slowly to 37 °C. Mutant strands were synthesized and ligated in synthesis buffer using T4 DNA polymerase and T4 DNA ligase (Promega). To confirm the fidelity of mutations, plasmids pGL−93/+48CATm, pGL-93-56M10-12, pGL−1255/+48CAT1m, pGL−1255/+48CAT5m, and pGL−1255/+48CAT1,5m were analyzed by DNA sequencing.

A.11. Chromatin immunoprecipitation (ChIP)

ChIP was performed using a Chromatin Immunoprecipitation Assay kit (Invitrogen). For this study, NIH 3T3 cells were fixed in 1% formaldehyde. Nuclei were isolated, sonicated and pre-cleaned with protein A Agarose/Salmon Sperm DNA. For ChIP, the pre-cleaned chromatin solution was set as input or incubated with 5 μg of either anti-CBF-B (Santa Cruz) or anti-Flag antibody (SIGMA, St Luis, MO) on a rotation platform at 4 °C overnight. After reversal of the cross-links, the DNA was purified from the immune complex and amplified using PCR primer sets CP−93/−73 and CP + 48/+25 or CP−1255/−1234 (Table 1) and CP−1132/−1152 (5′ATCCGTAGGAACAACCAATA3′) specific for the CP27 promoter region.

B. 1. Mouse embryonic stem (ES) cell culture

Mouse ES cells were cultured in DMEM supplemented with 15% FCS, 2 mM L-glutamine, 0.1 mM non-essential amino acids, 0.1 mM 2-mercaptoethanol and 1000 U/ml leukemia inhibitory factor (LIF) (Chemicon, Temecula, CA). The culture medium was changed everyday and the cells were passed onto gelatin coated cell culture dish at subconfluence every 3 days.

B. 2. Nuclear extract preparation

ES cells (5×10^7) in 100 mm dishes were harvested and cell lysates were centrifuged. The pelleted nuclei were resuspended in nuclear extraction buffer with a final concentration of 300 mM NaCl, and centrifuged at 24,000*g* for 20 min at 4 °C. Aliquots of the supernatant were frozen at −70 °C. Protein concentrations were determined using a protein assay reagent (Bio-Rad, Philadelphia, PA).

B. 3. Electrophoretic mobility shift assay (EMSA)

Double-stranded oligonucleotides (Table 3) for EMSAs were labeled with (gamma-^{32}P) ATP using T4 kinase. EMSAs were performed by incubating 5 μg of nuclear extract with labeled double-stranded oligonucleotide at room temperature for 20 min. For competition analysis, 25- or 50-fold molar excess of unlabeled double-stranded oligonucleotide was added to the nuclear extracts prior to the addition of the labeled probe. For supershift assays, polyclonal antibodies against NF-YA, NF1, USF1 and USF2 (Santa Cruz Biotechnology, Santa Cruz, CA) were incubated with the nuclear extracts for 15 min followed by the addition of radio-labeled probe. NF1 antibody was used as antibody control. DNA–protein complexes were resolved on a 5% non-denaturing polyacrylamide gel in 1× TBE.

B. 4. DNase I footprinting analysis

This assay was performed using the Core Footprinting System (Promega, Madison, WI). An end-labeled probe CP − 207/+48 was generated from the plasmid pGL −207/+48 by first digesting the DNA with Sac I, end-labeling with T4 polynucleotide using (gamma-^{32}P) ATP, and then digesting the DNA with Hind III. DNA–protein complexes were formed by incubating the end-labeled DNA with 100 μg of nuclear extracts in binding buffer. BSA was used as negative control. RQ1 RNase-free DNase was added to the reaction containing Ca^{2+}/Mg^{2+}. DNA samples were then separated by denaturing polyacrylamide gel electrophoresis.

B. 5. DNA constructs

For reporter constructs, fragments of the mouse CP27 promoter were amplified by PCR with a screened genomic clone as a template using a common 3′ primer and selected 5′ primers (Table 3). These primers also introduced a Sac I site at the 5′ end and a Hind III site at 3′ end of the amplified fragments. The PCR fragments were subcloned into the pGL3-basic vector (Promega). Correct sequence and orientation of all inserts in respect to the pGL3 vector were verified by DNA sequencing. Four reporter constructs (pGL-207, pGL-93, pGL-55, and pGL-17) were generated and each construct contained part of the exon 1 noncoding region. For the generation of expression constructs, the full length of NF-YA (long isoform) cDNA was generously provided by Dr. Sanker N. Maity (M.D. Anderson Cancer Center, University of Texas, Huston, TX), and subcloned into the Sal I and Sac I sites of the pIRES-GFP vector (Clontech, San Francisco, CA). The USF1 expression vector pCMV-SPORT6.1-USF1 was obtained from Open Biosystems

(Huntsville, AL). The position of probes, constructs, the E-box, and the CCAAT-box on the proximal CP27 promoter are annotated in Table 4.

B. 6. Transient transfection and dual luciferase assay

Mouse ES cells were used as the recipient cells for transient transfection assays. Cells (10^6 cells/transfection) were transfected with 5 μg of each promoter–reporter plasmid only or with expression vectors pIRES-NF-YA and/or pCMV-SPORT6.1-USF1 using an electroporator (Nucleofector, Amaxa, Gaithersburg, MD). pRL-TK (0.01 μg) (Promega) was co-transfected with promoter–reporter plasmid as internal control for transfection efficiency. Cells were incubated in 3 ml complemented medium for 48 h and then subjected to a dual luciferase assay (Promega) or RNA extraction. Overexpression of NF-Ya and USF1 was monitored by RT-PCR and compared with β-actin.

B. 7. Mutagenesis

Site-directed mutagenesis was performed using the GeneEditor *in vitro* Site-Directed Mutagenesis System (Promega). The sense oligonucleotides (Table 3) used in the mutation analysis of competition EMSA served as mutagenesis primers. The template for the mutagenesis of the CCAAT-box and the E-box was construct pGL − 93/+48. Mutant strands were synthesized and ligated in synthesis buffer using T4 DNA polymerase and T4 DNA ligase (Promega). To confirm the fidelity of mutations, plasmids were analyzed by DNA sequencing.

B. 8. Immunofluorescence

Cells were cultured on glass slides and fixed in 0.1% paraformaldehyde. For detection of NF-Ya and USF1 expression in ES cells, fluorescent immunohistochemistry was performed using goat anti-NF-Ya antibody or rabbit anti-USF1 antibody (Santa

Cruz). Samples were incubated overnight at 4 °C with primary antibodies and then with secondary FITC-conjugated anti-goat IgG antibody or Texas Red-conjugated anti-rabbit antibody (Invitrogen, Carlsbad, CA) and then analyzed using fluorescence microscopy. The same fluorescence settings and intensities were used for all experiments.

B.9. Chromatin immunoprecipitation (ChIP)

ChIP was performed using Chromatin-Immunoprecipitation Assay Kit (Millipore, Billerica, MA). ES cells were fixed in 1% formaldehyde. Nuclei were isolated, sonicated and pre-cleaned with protein A Agarose/Salmon Sperm DNA. For ChIP, the pre-cleaned chromatin solution was set as input or incubated with 5 μg of anti-NF-Ya, anti-USF1 (Santa Cruz) or anti-Flag antibody (Sigma, St. Louis, MO) on a rotation platform at 4 °C overnight. After reversal of the cross-links, the DNA was purified from the immune complex and amplified using PCR primers (Table 3) specific for the CP27 promoter region.

B.10. Coimmunoprecipitation and Western blotting

Whole cell lysates were centrifuged at 10,000*g* to pellet cellular debris. The supernatants were precleared with protein A-agarose beads and then incubated with NF-YA or USF1 antibodies (Santa Cruz) at 4 °C overnight and with protein A-agarose beads for 1 h. The bead–antibody pellets were washed and fragmented by SDS-PAGE on 15% gels. The separated proteins were transferred to a nitrocellular membrane. The membranes were blocked with 5% non-fat dried milk in PBS overnight at 4 °C and incubated with 1:2000 diluted USF1 or NF-YA (Santa Cruz), and then with a 1:2000 diluted HRP-conjugated secondary antibody (Invitrogen, Carlsbad, CA). The immune

complexes were detected with SuperSignal West Pico Chemilumnescent Substrate (Thermo Scientific, Rockford, IL).

B.11. Quantitative real time RT-PCR

Total RNA was extracted from mES cells using Trizol (Invitrogen). Total RNA quality and quantity were tested by spectrophotometry and agarose gel electrophoresis. 2 μg RNA was reverse transcribed and cDNA amplified using selected primers. Real time quantitative PCR was conducted using SuperScript III Platinum two step qPCR kit with LUX fluorogenic primer (Invitrogen). Primers were designed using the LUX™ Designer software (FAM labeled LUX primer, Invitrogen) and listed in Table 3. Reaction conditions were as follows: 2 min at 50 °C (1 cycle), 10 min at 95 °C (1 cycle), and 15 s at 95 °C and 1 min at 60 °C (40 cycles). PCR products were continuously monitored with an ABI PRISM 7900 detection system (RRC-Core at UIC). Samples were normalized using ribosome 18 RNA (JOE labeled LUX primer set, Invitrogen). CP27 expression levels were calculated in relationship to the β-actin internal control using the $2^{-\Delta\Delta Ct}$ method (Livak and Schmittgen, 2001).

B.12. Statistical analysis

All experiments were performed in triplicate unless stated otherwise. Final values were reported as means +/- standard deviation or 1-way analysis of variance (ANOVA). Data were analyzed using Student's t-test and p-values less than 0.05 were considered statistically significant.

C. 1. Protein alignment, phylogenetic tree, and isoelectric point analysis

CP27 homologous sequences from ten different species ranging from mycoplasms and plants to animals and humans were identified (supplement 1) and multiple sequence alignment and phylogenetic tree analysis were performed using the ClustalW2software (EMBL- EBI, European Bioinformatics Institute, http://www.ebi.ac.uk/). CP27 protein isoelectric point calculations were carried out on the basis of the Henderson–Hasselbalch equation using publicly available software (http://isoelectric.ovh.org/) (Lukasz Kozlowski, Kielce, Poland 2011) to obtain pI average values.

C. 2. CP27 targeting and CP27 overexpression

A ~9.6kb genomic DNA region employed to construct the targeting vector was first subcloned from a positively identified BAC clone using a homologous recombination-based technique. The region was designed that the short homology arm (SA, Fig. 1) extends 1.2kb 3' into exon 1. The long homology arm (LA, Fig. 1) started at the 5'end of exon 1 before the ATG start codon and was ~8kb long. A LacZ/Neo cassette was inserted before the ATG of Exon 1 and replaced ~376 bps of the gene sequence. The total size of the targeting construct (including vector backbone and LacZ/Neo cassette) was ~16.8kb. The CP27 overexpression vector was constructed using the pIRES-EGFP vector (Clontech). The CP27/Flag gene was amplified by PCR. A Flag tag was added at the 3' prime site before the stop site using a reverse primer.

C. 3. Genotype analysis by Southern blot

CP27 knockout mice were identified by Southern blot analysis of DNA from founder mouse tails. Tails were lysed with 100mM Tris–HCl, pH 8.5, 5 mM EDTA, pH

8.0, 0.2% SDS, 200 mM NaCl/proteinase K, and then treated with phenol/chloroform, 1:1 (by volume), precipitated with ethanol, and dissolved in TE buffer (10 mM Tris–HCl, pH 7.5/1 mM EDTA). Genomic DNA was digested with the restriction enzyme PstI. After transfer to nylon membranes (Immunobilon-NY+, Millipore), Southern hybridization was performed using a probe based on 329bp of intron 1 labeled with ^{32}P by random priming. Following PCR-amplification, a wild type band of ~5.1kb and a mutant band of ~3.8kb were detected.

C. 4. Genotype analysis by PCR

Blastocysts and preimplantation embryos were lysed for 10 min at 98°C (10 µl of PBS diluted 1:1 with water) and then cooled to 4°C. To analyze genomic DNA from tails and embryos, DNA was lysed using proteinase K and extracted using the phenol/chloroform strategy. DNA extracts were subjected to 35 cycles of amplification (with each cycle consisting of 94°C, 60°C, 72°C, 1 min for each) in a thermal cycler. The PCR product size was 479bp for wild-type and 345 for mutant mice.

C. 5. Blastocyst culture

Blastocysts were obtained from the uteri of 3.5 day pregnant CP27 heterozygous female mice. In order to generate blastocysts, pregnant mice were mated with CP27 heterozygous male mice, and pregnancy was checked by plug. Blastocysts were flushed out from uteri and then recovered in PBS. Subsequently, blastocysts were placed on gelatin coated culture plates with ES cell culture medium without LEF for 5 days.

C. 6. BrdU injections and tissue preparation

Bromodeoxyuridine (BrdU, Sigma, St. Louis, MO) was dissolved in sterile 0.9% NaCl and filtered. BrdU was injected intraperitoneally at a concentration of 40 mg/kg body weight. Samples were harvested after 4 hours of BrdU incubation and fixed with ice-cold 4% paraformaldehyde overnight, then embedded in paraffin and sectioned at 6μm. Sections were deparaffinized and rehydrated, then incubated in 1.5M HCL for 15 min at 37 °C, followed by a further incubation in 0.1M boric buffer (pH 8.5) for 10 min at room temperature, enabling visualization of proliferating cells by immunohistochemistry.

C. 7. Histology and Immunohistochemistry

For histological and immunohistochemical analysis, embryos were fixed in 10% buffered formalin overnight at 4°C, dehydrated and embedded in paraffin. All samples were sectioned at 6μm. Embryo sections were either stained with hematoxylin–eosin or subjected to immunohistochemistry for protein localization. Primary antibodies against marker proteins were applied (sources and antibody concentrations provided online) and CP27 mutant and wild-type sections were compared in a single reaction. Standard immunohistochemistry procedures for polyclonal primary antibodies were applied using the instructions of the Zymed Histostain kit (Zymed, South San Francisco, CA). For cell proliferation analysis, 6-day pregnant CP27 heterozygous female mice were intraperitoneally injected with BrdU (5-bromo-29-deoxy-uridine, Sigma) at a concentration of 40 mg/kg body weight and sacrificed 4 hours after injection. BrdU-labeled embryos were harvested and fixed in paraformaldehyde overnight, and then

processed for paraffin sectioning. Tissue samples were stained using the Zymed BrdU staining kit (Zymed, South San Francisco, CA). For whole mount immunohistochemistry of blastocysts, E3.5 preimplantation embryos were flushed from the uterus and fixed with 10% buffered formalin. Antibodies against CP27 and H2A.Z were used for the primary antibody reaction. For H2A.Z staining, CP27 knockout blastocysts were then immersed in horseradish peroxidase conjugated anti-rabbit IgG secondary antibody, washed, and then stained with the AEC substrate (Zymed kit). CP27 and H2A.Z double staining was performed using FITC-conjugated rabbit anti-mouse immunoglobulins (Sigma) and Texas-red-conjugated sheep anti-rabbit immunoglobulins as secondary antibodies. After fluorescent micrographs were exposed, DNA was extracted from stained embryos, and embryos were genotyped by PCR.

C. 8. Real time qPCR and laser dissection

In order to compare levels of Nanog and H2A.Z expression between wildtype and cp27 E6.5 knockout mouse embryos, frozen samples were prepared by laser dissection (LMD, Leica), and levels of Nanog and H2A.Z expression were determined using real time qPCR analysis. Samples were fixed in 0.2% paraformaldehyde, embedded in frozen tissue embedding media (Fisher), and then cryosectioned. Total RNA was isolated from frozen sections using the RNeasy mini kit (Qiagen) and reverse transcribed (Invitrogen) following total RNA quantification. RT was performed with the oligo-dt primer. Real-time quantitative PCR was performed to quantify mRNA levels using the 2X Fast SYBR Green Master Mix (ABI) combined with 500 nM of each forward and reverse primer designed for the region of interest (primers provided online). The real-time PCR protocol was: 20 sec at 95 °C for activation of AmpliTaq Fast DNA polymerase followed by a

two-step reaction (denaturation: 95 °C for 3 sec, annealing and extension: 60 °C for 20 sec), and 40 cycles of amplification. Primer information (Table 5).

C. 9. Co- immuneprecipitation (Co-IP) ES cells

Protein samples were obtained from ES cells and homogenized with non-denature lysis buffer (20 mM Tris HCl pH 8, 137 mM NaCl, 10% glycerol, 1% Nonidet P-40, 2 mM EDTA, protease inhibitors). Samples were then centrifuged to remove cell debris and the supernatant was transferred to a centrifuge tube. To remove endogenous IgG to reduce background, the samples were incubated with protein A agarose/salmon sperm DNA agarose beads (Millipore, Bedford, MA) for 1 hour. Agarose beads were pelleted by brief centrifugation and the supernatant fraction was collected. This fraction was then incubated with immunoprecipitating antibody (CP27 Polyclonal rabbit IgG, and TIP49a and TIP49b) overnight at 4^0C. Non-immune rabbit IgG was used as a negative control. To recover protein for immuneprecipitation, the sample was incubated with protein A magnetic beads (Millipore) and incubated for 1 hour. After washing with lysis buffer for three times, protein was eluted with Laemmli buffer for western blot. Western blot was performed with anti-DMAP1, BAF53A, and CP27 antibody. Antibody information (Table 6).

C. 10. Western Blotting

Protein samples were extracted in SDS sample buffer and resolved by SDS-PAGE. 30 mg total protein was transferred to PVDF (Bio-Rad, Hercules, CA) using transfer buffer (48 mM Tris-HCl 40 mM glycine 0.05% SDS) and semi-dry transfer apparatus (Trans Blot SD, Bio-Rad). Membranes were blotted with affinity purified

primary antibodies against CP27, Nanog, Oct4, Sox2, H2A.Z, DMAP1, Baf53a, Cyclin C, GAPDH, and actin. Anti-rabbit or anti-mouse HRP-conjugated secondary antibody (Abcam) for Western blot or Clean-Blot IP Detection (Thermo Scientific, Waltham, MA) for Co-Immunoprecipitation were used at a 1:1000 to 5000 dilution for 2 hrs at room temperature in TBS with 0.1% Tween 20. Detection was performed using Super Signal West Pico Chemiluminescent Substrate according to the manufacturer's specifications (Thermo Scientific). Antibody information; (Table 6).

C. 11. ChIP Assay

Chromatin cross-linking was performed with 1% formaldehyde and was stopped by the addition of glycine to a final concentration of 125 mM. ES cells were washed twice using ice cold PBS containing protease inhibitors (PMSF, Sigma), harvested with ice cold PBS, pelleted by centrifugation for 4 minutes at 2000 rpm and at 4°C. Cell pellets were resuspended in 200 µl of SDS lysis buffer (1% SDS, 10 mM EDTA, 50 mM Tris-HCl, pH 8.1.) and incubated for 10 minutes on ice. Cell lysates were sonicated to shear chromatin to 200 and 1000 basepairs fragments (amplitude 4, 10 sec for 5 times at 20 sec interval, Qsonica S3000, Qsonica, Newtown, CT). Samples were diluted 10 fold in ChIP dilution buffer and precleared to reduce nonspecific background with protein A Agarose/Salmon Sperm DNA (50% slurry) in ChIP dilution buffer. The precleared extract was incubated overnight with 5µg of the antibody at 4 °C. The immune complex was recovered with protein A magnetic beads after incubating at 4 °C for 2 hours. The bead complexes were washed twice for 5 min each with low salt wash buffer (20mM Tris (pH8), 150mM NaCl, 2mM EDTA, 1% Triton X-100, and 0.1% SDS), high salt wash buffer (20mM Tris (pH8), 500mM NaCl, 2mM EDTA, 1% Triton X-100, and 0.1%

SDS), LiCl wash buffer (20 mM Tris-HCl (pH 8.0), 1 mM EDTA, 250 mM LiCl, 0.5% sodium deoxycholate, and 0.5% Nonidet P-40), and TEbuffer (10mM Tris-HCl and 1mM EDTA (pH 8.0)). The precipitated chromatin complex was eluted from beads by two times 30 min incubation with elution buffer (1% SDS and 0.1 M NaHCO3) at room temperature and brief vortexing. Eluates were combined and crosslinking was reversed by overnight incubation with 250mM NaCl at 65 °C. The combined eluates were then incubated with Proteinase K (Roche, Pleasanton, CA) with 10 mM EDTA and 40 mM Tris-HCl (pH6.5) for 1h at 45°C. DNA was recovered by phenol/chloroform extraction and ethanol precipitation with 0 μg glycogen to visualize the DNA pellet. Pellets were washed with 70% ethanol and air dried. Immunoprecipitated samples were resuspended in deionized H_2O. The DNA from ChIP assays was analyzed by real-time PCR (ABI 7500FAST, ABI) with 2X Fast SYBR Green Master Mix (ABI), 500 nM of each forward and reverse primer that represented the region of interest. Primer information (Table 5).

III. RESULTS

A.1. Sequence analysis of the mouse CP27 promoter region

Our sequence analysis of the mouse CP27 promoter region was based on a clone that contained 2.1 kb of the 5′ CP27 flanking sequence. The clone was isolated from a murine 129/SVJ genomic library using the CP27 cDNA as a probe. The sequence of the 5′ flanking region and partial exon 1 is shown in Fig. 1. Computer searches using MatInspector from www.genomatrix.de and Signal Scan from www.bimas.cit.nih.gov/molbio/signal/ revealed a CCAAT box at position −79 and an unknown motif (CGGA) in the CCAAT 3′ flanking region. In addition, multiple CCAAT elements were also identified between −1227 and −785. The CCAAT box is a DNA element present in the promoter region of many constitutive, inducible and cell-cycle regulating eukaryotic genes (Caretti et al., 2003 and Hu et al., 2000). CCAAT box binding by the transcription factor NF-Y is thought to be a major mechanism required for transcriptional activation (Ceribelli et al., 2008, Donati et al., 2008 and Gatta and Mantonani, 2008). Our sequence analysis identified several potential transcription factor binding sites in the proximal promoter region, including an E box core consensus (ccaCGTGg) site at position −44, and a c-myb core consensus (ttCAACggt) site at position −160. Interestingly, there were seven Octamer-binding factor 1 (Oct 1) binding sites in the 5′ CP27 flanking sequence, suggesting a potential regulation of the cp27 gene by the POU homeodomain transcription factor. Two binding sites for the homeobox factor Csx/Nkx 2.5 were located in the promoter sequence as well. In addition, our CP27

promoter sequence analysis revealed the presence of consensus binding sequences for common transcription factors such as AP1 and GATA (Fig. 1).

A.2. Mapping of CP27 transcription start sites

A primer extension study was performed to map the mouse cp27 gene transcription start sites. For this study, CP27 antisense oligonucleotides CP 82-61 corresponding to nucleotides in exon 1 were synthesized and annealed to total RNA extracted from NIH 3T3 cells. The primer extension reaction yielded three bands of about 80, 100 and 120 nucleotides, respectively (Fig. 2A, lane 3). tRNA was used as a source of control RNA. No primer extension product was detected in the control RNA from these cells (Fig. 2A, lane 2).

To confirm the identity of the transcription start sites determined by primer extension, ribonuclease protection assays were performed. An RNA probe was generated from a TOPO-5′ CP27 plasmid containing a 289 bp PCR product from −207 to + 82 bp of the cp27 gene, hybridized to total RNA extracted from NIH 3T3 cells or yeast RNA, and digested with RNase A and T1. The RNA protection assay yielded protected fragments of about 80, 110 and 120 bp in length (Fig. 2B, lane 3). No protected bands were observed in the control RNA (Fig. 2B, lane 2). The size of two protected fragments was similar to the length of two primer extension products, since the 5′-end of the antisense probe used in the RPA was defined by the same antisense oligonucleotide CP 82-61 used in the primer extension assay. However, the size of the second-largest protected fragment ran at a higher molecular weight in the RNA protection assay compared to the primer extension study (Fig. 2A, B, lane 3).

For precise determination of transcription start sites, 5′-RACE assays were performed on NIH 3T3 RNA using two nested CP27 antisense primers. Sequencing 10 RACE subclones yielded two different transcription start sites, as indicated in Fig. 2C. The 5′ end of the longer product (five of ten) corresponded to an adenine purine residue 140 nucleotides upstream from the ATG initiation codon, and the shorter product (four of ten) mapped a second start site to an adenine purine residue located 102 nucleotides upstream of the ATG codon. The two products resulting from the 5′ RACE were identical to the sizes of the first and third bands of the primer extension and ribonuclease protection assays.

A.3. Promoter activity of the 5′ flanking region of the mouse cp27 gene

The function of the 5′ flanking region in the regulation of the mouse CP27 gene was determined by luciferase reporter gene expression. We inserted a 2.0 kb fragment including the 5′ CP27 flanking region and + 48 bp of the CP27 exon 1 into the promoterless expression vector pGL3-basic upstream of the luciferase reporter gene (Fig. 3A). Using this assay, the expression of luciferase via the pGL −1993/+48 vector was 500-fold greater than the background measured with pGL-basic.

To localize putative cis-acting elements regulating transcription of the cp27 gene, progressive 5′ deletion mutations of the 2.0 kb promoter (−1993 to + 48) were performed using reporter gene constructs. Expression of the reporter gene driven by the mutants was examined by transient transfection assays. The initial deletion removed approximately 500 bp from the upstream end of the pGL −1993/+48 construct. The resulting construct (pGL −1475/+48) produced a slight increase in luciferase activity in NIH 3T3 cells. Deletion of another 506 bp from the 5′ end generated the construct pGL−969/+48 and

resulted in a 2.5-fold increase compared with the construct pGL −1475/+48. Further deletions from −969 to −93 led to a progressive decrease in promoter activity. Removal of approximate 250 bp from the upstream end of the pGL −969/+48 plasmid generated the construct pGL −720/+48 which resulted in a 1.4-fold decrease in luciferase expression acitivity compared to the construct pGL −969/+48. Deletion of the next 520 nucleotides also resulted in a 1.4 fold decrease in expression activity. A further deletion of 104 bp generated the construct pGL −93/+48 and led to a further 1.6-fold decrease in luciferase activity. The activity of the pGL −17/+48 construct was on the same level with the pGL3-basic vector (Fig. 3B).

Together, the results of the deletion analysis revealed the following three regulatory elements: (i) a positive element in the small interval between −17 and −93 bp, (ii) several enhancer elements located within the first −969 bp, and (iii) a general repression region between nucleotides −969 and −1993.

A.4. Identification of NFY as the nuclear factor binding to the CP27 proximal promoter CCAAT box

The transient transfection experiments described above indicated the presence of positive regulatory elements within 93 bp of the mouse CP27 proximal promoter region. To answer whether the CCAAT box is a basal regulatory element in the mouse CP27 proximal promoter, an oligonucleotide containing the CCAAT box (CP−93/−56) was subjected to an EMSA. The EMSA revealed formation of a protein–DNA complex using the radioactively labeled oligonucleotide CP−93/−56 and nuclear extracts from NIH 3T3 cells (Fig. 4A, lane2). Competition experiments were performed to determine the sequence specificity of the protein–DNA complex. Molar excesses (25- or 50-fold) of

unlabeled CP−93/−56 eliminated the formation of the complex (Fig. 4A, lanes 3 and 4). However, when a mutation in the CCAAT box was introduced by mutating CCAAT to CACAT (Table 2), the mutated CP−93/−56 did not affect protein/DNA binding (Fig 4A, lanes 5 and 6).

CCAAT box binding proteins may bind to elements containing a CCAAT box. These proteins include the C/EBP family, NF-Y, Y box factor, and CBT/NF1 (Dorn et al., 1987, Didier et al., 1988, Zorbas et al., 1992 and Sylvester et al., 1994). To identify the specific factor(s) that binds to the CCAAT box of the CP27 proximal promoter, nuclear proteins from NIH 3T3 cells were characterized using EMSA. Taking advantage of the heat-stability of the C/EBP family DNA binding proteins (MacDougald and Jump, 1991), nuclear extracts were heated to 85 °C prior to incubation with the radioactively-labeled oligonucleotide CP−93/−56. The heat treatment led to an abolishment of the shift and to a loss of the DNA–protein complex band (Fig. 4B, lane 3), indicating that the factor binding to the proximal CP27 promoter is heat-sensitive and thus excluding the heat-stable C/EBP as a candidate factor for CP27 proximal CCAAT box binding. Following exclusion of C/EBP as a candidate CCAAT binding protein, focus was directed toward the heterotrimeric transcription factor NF-Y, which had been characterized as the most ubiquitous and specific factor involved in the regulation of CCAAT box (Mantovani, 1998). To examine whether NF-Y functioned as a binding protein in the DNA–protein complex formed by NIH 3T3 nuclear extracts and oligonucleotide CP−93/−56 in EMSA, anti-NF-YA antibody was applied to EMSA gel blots after Western blotting (Novak and Paradiso, 1995). Immunoblot analysis demonstrated that NF-Y was present in the DNA–protein complex (Fig. 4C, lane 4).

Incubation of anti-NF-YA antibody together with the DNA–protein complex led to the formation of a slower migrating supershifted band (Fig. 4D, lane 3), while anti-NF-YC antibody abolished the DNA–protein complex (Fig. 4D, lane 4). However, anti-NF1, anti-EST1/2, and anti-SOX5 antibodies did not affect the formation of the DNA–protein complex (Fig. 4D, lanes 5–7), further confirming that the DNA–protein complex contained the NF-Y transcription factor. These results suggest that NF-Y binds to the CCAAT sequence in the mouse CP27 proximal promoter.

To further confirm that the CCAAT box is involved in the regulation of the CP27 promoter, the CCAAT box of the intact CP27 promoter was mutated by means of a mutated construct (Table 2). Specifically, the activity of the mutated plasmid pGL−93/+48 CAT-mut was compared with that of the wild-type pGL−93/+48. The mutations had significant effects on the activity of the CP27 promoter. Mutation in the CCAAT box reduced the activity by 90% (Fig. 4E). These results demonstrated that the CCAAT box is a significant regulatory element located in the mouse CP27 proximal promoter.

To verify the binding of NFY to the CP27 promoter in vivo in NIH 3T3 cells, Chromatin immuno-precipitation was performed. The cross-linked chromatin was immuno-precipitated with anti-NFYA antibody and subjected to PCR amplification using primers spanning the CCAAT box of the CP27 proximal promoter region. A 140 bp DNA fragment of expected length was amplified (Fig. 4F, lane 3). In contrast, a control anti-flag antibody failed to precipitate chromatin fragments containing the endogenous CP27 promoter (Fig. 4F, lane 4).

A.5. Specific sequence determination of the CCAAT box 3′ flanking region required for NF-Y binding

Specific neighboring nucleotides on both 5′ and 3′ sides of the CCAAT box are involved in the efficient binding of NF-Y (Mantovani, 1998). In addition, minimal DNA fragments in both the upstream and downstream distal regions are required for the formation of a stable NF-Y–DNA complex (Sugira and Takishima, 2003). We therefore investigated what role the CCAAT 3′ flanking region (i.e. the CGGA motif) of the CP27 proximal promoter might play in regulating promoter function and DNA binding by NF-Y.

To determine the effect of the CGGA motif on the binding of NF-Y to the CCAAT box of the CP27 proximal promoter, EMSA was performed using oligonucleotides CP−93/−56 (D16) along with its deletion mutants CP−93/−65D9 (D9) and CP−93/−65D13 (D13), and the site-specific mutant CP-93/-65M10-12 (M10-12) (Table 2). In this EMSA, NF-Y efficiently bound to probes D16 and D13 (Fig. 5A, lanes 1 and 3), while binding affinity was substantially reduced when NF-Y bound to probe M10-12 (Fig. 5A, lane 4); and a diminishingly small NF-Y–DNA complex formed between NF-Y and probe D9 (Fig. 5A, lane 2).

To determine whether the CGGA motif altered NF-Y binding through interacting with NF-Y heterotrimeric complex, super EMSA was performed using anti-NF-YA and NF-YB antibodies. The reactivity of the NF-Y/M10-12 complex to each antibody was compared with the reactivity of the NF-Y/D16 and NF-Y/D13 complexes. While there were no differences in the supershift pattern between M10-12, D16, and D13, NF-Y binding was greatly reduced in the mutated motif M10-12 compared to D16 and D13

(Fig. 5B). Taken together, these observations suggest that the CGGA motif affects the binding of the NF-Y complexes to the CCAAT box.

To confirm that the CGGA motif indeed had an effect on NF-Y binding to the CCAAT box, a luciferase reporter construct pGL-93/-56M10-12 was generated (Table 2). This construct contained the mutated binding site (tacA vs. CGGA) and the intact CCAAT box. Compared with the wild-type construct (pGL−93/−65), this mutation reduced the activity of the intact promoter by 77%, indicating that the binding site is critical for NF-Y binding to the mouse CP27 proximal promoter (Fig. 5C).

A.6. Involvement of multiple NF-Y/CCAAT complexes in cp27 gene expression

To fully understand CP27 gene expression regulation via CCAAT boxes we explored the function of multiple CCAAT sites harboring in the CP27 promoter subsequent to our characterization of the proximal NF-Y binding CCAAT box. Altogether, a transcriptional cis-regulatory element analysis using MatInspector (www.genomatrix.de) and Signal Scan (www.bimas.dcrt.nih.gov) revealed five CCAAT boxes (CAT 1–5) in the CP27 promoter. The proximal CAT1 (−79 to −83) and CAT2 (−785 to −789) were in forward orientation and located in the enhancing regions (Fig. 1). The CAT boxes 3–5 (−1227 to −1150) were found in a general repression region in reverse orientation and located in close proximity to each other, separated only by 33 to 34 bp intervals (Fig. 1). Incubation of nuclear extract from NIH3T3 cells with the 32P-labeled probe CAT5 (CP-1255-1210) produced specific DNA/protein complexes (Fig. 6A, lane2) using EMSA. Twenty-five- and fifty-fold molar excess of wild type oligonucleotides CP-1255/-1213 completed the formation of the DNA/protein complex (Fig. 6A lanes 3–4), and the mutated oligonucleotide CP−1255/−1234 did not affect the

DNA/protein complexes (Fig. 6A, lane5). However, oligonucleotide CP−1233/−1213 containing a CCAAT box had the competition capability (Fig. 6A, lane 6). Addition of antibodies to NF1 and SOX5 did not recognize these bands (Fig. 6A, lanes 7–8), whereas the anti-NF-YA antibody (Fig. 6A, lane 9) formed a super-shifted band with the DNA/protein complex, indicating that NF-Y binds to the CCAAT-boxes within the CP27 promoter.

To determine whether the CAT5 CCAAT box serves as a stimulatory or a repressive site, we performed a 5′ deletion mutation analysis and also introduced mutations into the box (ATTGG to ATGTG). Three promoter–reporter constructors were generated either as a wild type (pGL−1255/+48) or a 5′ deletion (pGL-1190) or a mutation (pGL-1255CAT5m2) construct, and then transiently transfected into NIH3T3 cells. Our findings indicated that removal of the CAT5 CCAAT box and adjacent regions had a significant effect on the mouse CP27 promoter function, decreasing expression of the reporter gene by 74%. Moreover, mutation of CAT5 CCAAT box resulted in a 62% reduction when compared to the wild type construct (Fig. 6B). The decrease in CP27 promoter activity observed by CAT5 mutation suggests that this site is involved in the control of cp27 gene expression enhancement despite its placement in an overall repressive promoter region.

Chromatin immunoprecipitation was performed to verify the binding of NF-Y to the CAT5 CCAAT box in the CP27 promoter in NIH3T3 cells in vivo. The cross-linked chromatin was immuno-precipitated with anti-NF-YA antibody and subjected to PCR amplification using a pair of primers CP−1255/−1234 and CP−1132/−1152 spanning the CAT5 containing region. A DNA fragment (123 bp) corresponding in size to the CP27

promoter region was amplified (Fig. 6C, lanes 2). In contrast, a control anti-flag antibody failed to precipitate a chromatin fragment containing the endogenous CP27 promoter (Fig. 6C, lanes 3). These results confirmed the presence of the active NF-Y-binding CAT5 CCAAT box in the CP27 promoter.

Oligonucleotides containing the sequence for the CAT2 CCAAT box were used as a probe in EMSA experiments and for the generation of DNA–protein complexes. However, these complexes were not recognized by either anti-NF-YA, NF-YB, or NF-YC antibodies. Oligonucleotides containing the CAT3 or CAT4 CCAAT box sequence did not form substantially shifted bands when incubated with nuclear extracts from NIH3T3 cells (data not shown).

A.7. Requirement for functional cooperation among multiple NF-Y/CCAAT binding sites for cp27 gene expression

To investigate whether multiple NF-Y/CCAAT binding sites function independently from each other or are required to cooperate in the regulation of the CP27 promoter, four constructs were generated, including one containing the intact CP27 promoter and three constructs in which the CCAAT box was mutated. Specifically, the activity of the three mutated plasmids pGL−1255/+48 CAT1-mut, pGL−1255/+48 CAT5-mut or pGL−1255/+48 CAT 1,5-mut was compared with that of the wild-type pGL−1255/+48. The mutation in the CCAAT-box1 reduced luciferase activity by 61% (Fig. 7A). Mutation of the CAT5 box decreased CP27 promoter activity by 62% (Fig. 7A). Interestingly, simultaneous mutations in the CAT1 and CAT5 boxes reduced CP27 promoter activity by 90% (Fig. 7A). These results suggest that the two CAT boxes cooperate to activate the CP27 promoter.

To determine whether NF-Y can functionally activate the CP27 promoter, an expression vector for NF-YA (pIRES-NF-YA) or NF-Yam29 (pIRES-NF-YAm29) was introduced into NIH 3T3 cells, resulting in significant transfection efficiency as examined by RT-PCR (Fig. 7B). Vectors pIRES-NF-YA or pIRES-NF-Yam29 were then co-transfected with the promoter–reporter construct pGL-CP−1255/+48. Co-transfection resulted in an enhancement of luciferase activity in a dose-dependent manner following NF-YA overexpression. Especially, 0.8 μg of pIRES-NFYA induced a 2.2 fold increase. In contrast, NF-YAm29 reduced the CP27 promoter activity (Fig. 7C).

To confirm our finding that the functional cooperation between NF-Y and CCAAT boxes influences endogenous cp27 gene expression, NIH 3T3 cells were transfected with pIRES-NF-YA or pIRES-NF-Yam29, and CP27 mRNA expression was quantified by real time RT-PCR. Our data indicate that NF-YA overexpression caused a 2-fold increase in endogenous CP27 mRNA expression. There was a slight decrease in CP27 transcription activity following NF-YAm29 treatment when compared to NIH3T3 cells (Fig. 7D). Together, these data suggest that NF-Y interacts with multiple CCAAT boxes to regulate cp27 gene expression.

DNA Sequence of the CP27 Promoter Region

```
CCGCGATGGC CCGGCTCAAA TAAATCTTAA AAAAAAAAAA ACAAAAAACA ACAACAAAAA AAGTAAGAAG TAAAACAAGA -2080

ACCAAACCAA ACCAAACCAA AAAAACCAAA CTTGATGCCG ATGTTCGGCC GTACTGCAGG ATGCAGAGGG TCAGCTAGCC -2000

CACTGTGGCT AACCTGCTCA ACTTTGGCTT GCTTCCTGAA AACCAAGGAC ACATAGGTGG TGCTTATTCT GCTGGAGAGA -1920

AGAGCGAGAC ACGTCAGCAT CCAGCGGTTC TACCCCAGGT GTTCGGTTCT CGCGGCTTGA TGAGGAGATG ACGTGATGAC -1840
                                            OCT-1
GTAAGCATTT TCCCCTCCCT CCCAGTCCTG CCTGAAAATT TGCATCATTC TTTTCTGCTT TGTTTCCTGC CTCATTCCTT -1760
GATA
TATCTTTTCT TTTTTTTCTT TTTTAATTAT TTTTTAAAAA TTGAGTATCA CAGCGAGGCA CAAACCCAAG TCTTTAATCC -1680
                                                        OCT-1
CAACACTCAG GAGGCAGAGA CAGGCGGATC TTTCAGTTCA CCGCCAGCCT GGTTTACATA GTGAGTTCCA GGACAGCCAG -1600

AGCTGCACAG AGAGACCCTG TCTCAAAAAA TCCTACCCCT GCCCCTCTAA AAAAGAGTAT TACTATGTAG TGTTGACTGA -1520
            OCT-1                                                                   OCT-1
CCTGGAACAC TTTATGAAGA TCAAGCTGGC CTTGAACTCA CAGAGATCTC CCTGTCTCTG TCTCCTGATT GTTGGAATTA -1440

AAATCGTGTG CCATCACCAC ACAGGGCTTT CTGCCTCATT CTGTTAAGCA TCTCAGCATA AGGGCCAGAG GAGGTGACAT -1360
                     NXK25                          AP1
GCTTAAATTT GAGGGCACAA TTAAGCATTG GGTCACATTC TTCTACGTCA CCTTCCCCAG CCCCCTTTAG ATGTATTCCA -1280
       OCT-1                                          OCT-1 CAT BOX
CACTGATATT TTGACGGCTG TGAACTCTTA GGCTGATTCC CATTGCCATC CCATTGGTCA ACTCCCACCA GTTTACCCAC -1200
           CAT BOX                                        CAT BOX
TCATCCAGAG CATTGGTTGG TCCTCCCGAT GTCTCTGCTA AAATTTCCTA TTGGTTGTTC CTACGGATTT CTCTGCTAAG -1120

ATTTCCTCAT CTTCCTCCTT CATGTGCTCC GAGAGTTCGA TTATTCTCAG TACAGTATGC ATTATATTCT CATCACAGTT -1040

TTAAAAAAAT GTGTGTATAT ATATATATAT ATAAAGGCGT GCGCCACCAC GCCCGGCAGA AGGTGATTTC TGAGGGACTA -960

GGGGCATGGC TCAGTGGGTG AAGGTGCTTG CTGCACTGTA CTACATACAT GCCTGGTGCC TATTGAGGTC AGAACCAGGG -880

CGGTAGTGAA CCGCCATGTT GGGGATGCTA GGAACCAAAC CTAGTTTTGC TGCAGAAGCA ACAAGTACTG TTAACCTTTG -800
          CAT BOX
GGCCGTCTCG CCAATCCTCA CATACTCACA AATTTAACTG CTTTTCCATC CATCTTTCCC GTTGTTTCAA AAGTGTCAAT -720
                                  GATA
CTAGCACTTT GTGTAGTGGC TTCCCTCACA GATAAGCGGA TTTCCTTTTG TCTTTTAGTG ATTATCGGAT TGTTGATTCA -640

TTAATGCTGA ACTTACTGCC AACAGTACTT GTAACTCAGG CCTGAATGTA GCTTACTTAA CAGGCCGAGT TTCTCAGGAA -560

AGAGCGTCGC AGTCTTCTTG CGCTTAGAAT ATTAGACAGA GTTTCGGTAG TGTTCTTGGG AGCAATTTTA GGCAGAAAAA -480

AAAAAAAAAA CAAACAAAAA CAAAAATGCA GGGAAAAGGC ACAAAAACTG CATTAAAGAA TTCGATTCTA GCGAGAGAAT -400

TGAATCAAAA AGGCAGAGCC TCAGCCTTGC TCAAAAGTTG ATGGGAACTT TAGCATCTAT CTATTCAGCT TTCAGTTTTT -320
         OCT-1
ACTCGCTGAG CATATCCGGG AGCGACATTT TAATCTCTGA TTTTAGAGTT AGAAAAAATA TTAGCTTGTG AGCAAATTTC -240
                                            GATA            NKX25                C-MYB
AAAATAAAAA GACAAGTATA AAGAGAAAGT ACTATTTCCG CAGATAAGCC ATTCTCCATT AAGGACGCAC GGTACCGTTG -160

AAAACTACAA GCCCCAGCAT GCATCGCTTC TGAGAGGTGG GGGTCCGGAA TCCCACAAGG GCCCGGTGAG TGTAGACTGA -80
CAT BOX     UNKNOWN                    E-BOX
CCAATCGCAG CAGCCGGAAG TGTCGTCTCT GACCACGTGG CACTGCCTGC GCATGTGCGC TCGCCTCTAG GGCGGCCCTA +1

GCTGCTGGTC CTGTACCCCT ATGGTCTCGC CCTATATCTA GCTTCGC                                    +48
```

Fig. 1. Nucleotide sequence and putative regulatory elements of the 5′ flanking region of the mouse cp27 gene. The numbering of the nucleotides starts at the first nucleotide of the cDNA (+ 1). The first nucleotide 5′ of the preferred transcription start site is labeled −1. Selected potential transcription factor binding sequences have been labeled. Abbreviations: consensus binding site for the transcription factor oct-1 (OCT-1), consensus binding site for the gata transcription factor (GATA), consensus binding site for the transcription factor nxk-25 (NXK25), consensus binding site for the transcription factor c-myb (C-MYB), consensus binding site for transcription factor ap1 (AP1), CCAAT box (CAT BOX), E-box (E-BOX), unknown binding site (UNKOWN).

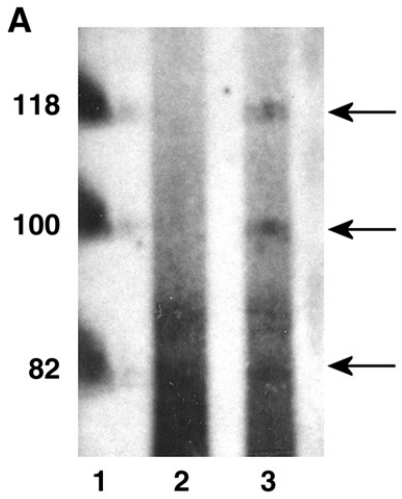

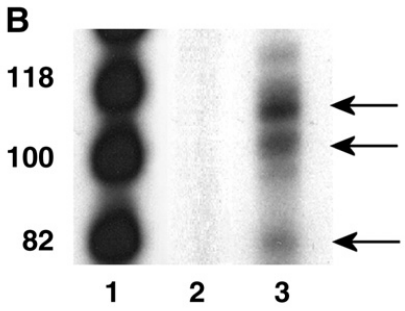

C

```
TGCATCGCTT CTGAGAGGTG GGGGTCCGGA ATCCCACAAG GGCCCGGTGA GTGTAGACTG  -81

ACCAATCGCA GCACCCGGAA GTGTCGTCTC TGACCACGTG GCACTGCCTG CGCATGTGCG  -21
                                                 *
                         +1
CTCGCCTCTA GGGCGGCCCT AGCTGCTGGT CCTGTACCCC TATGGTCTCG CCCTATATCT   40
                         *

AGCTTCGCTA TTTTGGGGCA GTGGCGCAGT CGTGTGGGTA GCAGGCCCCA AGTGACAGCA  100

GCATGGAGGA ATTCGACTCC GAAGACTTCT CCACATCGGA CGAGGATGAG GACTACTTGC  160
  M  E  E   F  D  S   E  D  F  S   T  S  D   E  D  E   D  Y  L  P   20
```

Fig. 2. Determination of the transcription start sites of the mouse cp27 gene. A, primer extension. The oligonucleotide CP 82/61 was end-labeled with (r-32P) ATP and hybridized with 10 μg of total RNA from NIH 3T3 cells or tRNA. The products of the primer extension reaction were size fractionated and autoradiographed. Lane 1, φX174 Hinf I DNA markers; lane 2, primer extension with tRNA; lane 3, primer extension reaction with RNA from NIH 3T3 cells. B, ribonuclease protection assay. The (r-32P) ATP-labeled RNA probe was generated using the TOPO-207/+82 plasmid containing a PCR fragment amplified by the sense oligonucleotide CP −207/−186 and the antisense oligonucleotide CP82/61. The labeled probe was hybridized with 10 μg of total RNA from NIH 3T3 cells or yeast RNA. The RNase-resistant products were sized-fractioned and autoradiographed. Lane 1, φX174 Hinf I DNA markers; lane 2, no RNase-resistant product from yeast RNA; lane 3, RNase-resistant products from NIH 3T3 cells. C, mapping transcription start sites by 5′ RACE assay. Rapid amplification of cDNA 5′ ends using total RNAs extracted from NIH 3T3 cells mapped two transcription start sites of the cp27 gene indicated with stars. The first start site corresponded to an A purine residue 140 nucleotides upstream of the ATG initiation codon, and the second one to an A purine residue located 102 nucleotides upstream of the ATG codon.

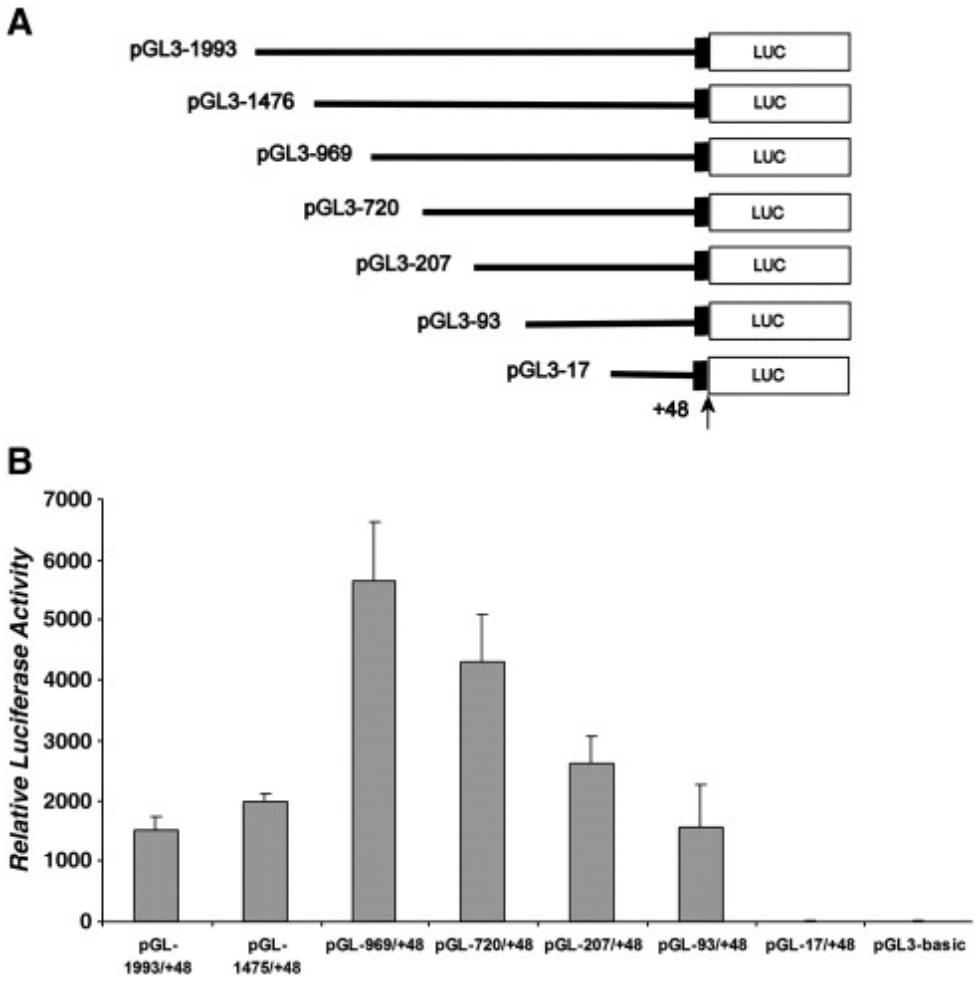
A
pGL3-1993
pGL3-1476
pGL3-969
pGL3-720
pGL3-207
pGL3-93
pGL3-17
LUC
+48
B
Relative Luciferase Activity
7000
6000
5000
4000
3000
2000
1000
0
pGL-1993/+48
pGL-1475/+48
pGL-969/+48
pGL-720/+48
pGL-207/+48
pGL-93/+48
pGL-17/+48
pGL3-basic

Fig. 3. Promoter activity in the 5′ flanking region of mouse cp27 gene. A, schematic representation of promoter–reporter plasmids. 1993 bp DNA and 5′-truncated fragments of the CP27 promoter upstream of the preferred transcription start site were inserted into the luciferase reporter vector pGL3-Basic in sense orientation. The arrow indicates the preferred transcription start site. The name of each reporter construct was assigned according to the 5′-end nucleotide number and the inserted promoter sequence. All constructs contain a partial exon 1. B, Luciferase activity resulting from the expression of the CP27 promoter–reporter gene constructs. The promoter–reporter gene constructs were transfected into NIH 3T3 cells, and specific luciferase activity was measured 48 h post transfection. The results were normalized by co-transfection with a pRL-TK reporter plasmid. Error bars represent the standard error for three samples in five independent experiments. The activity of the pGL3-Basic vector transfected in the same experiment is indicated.

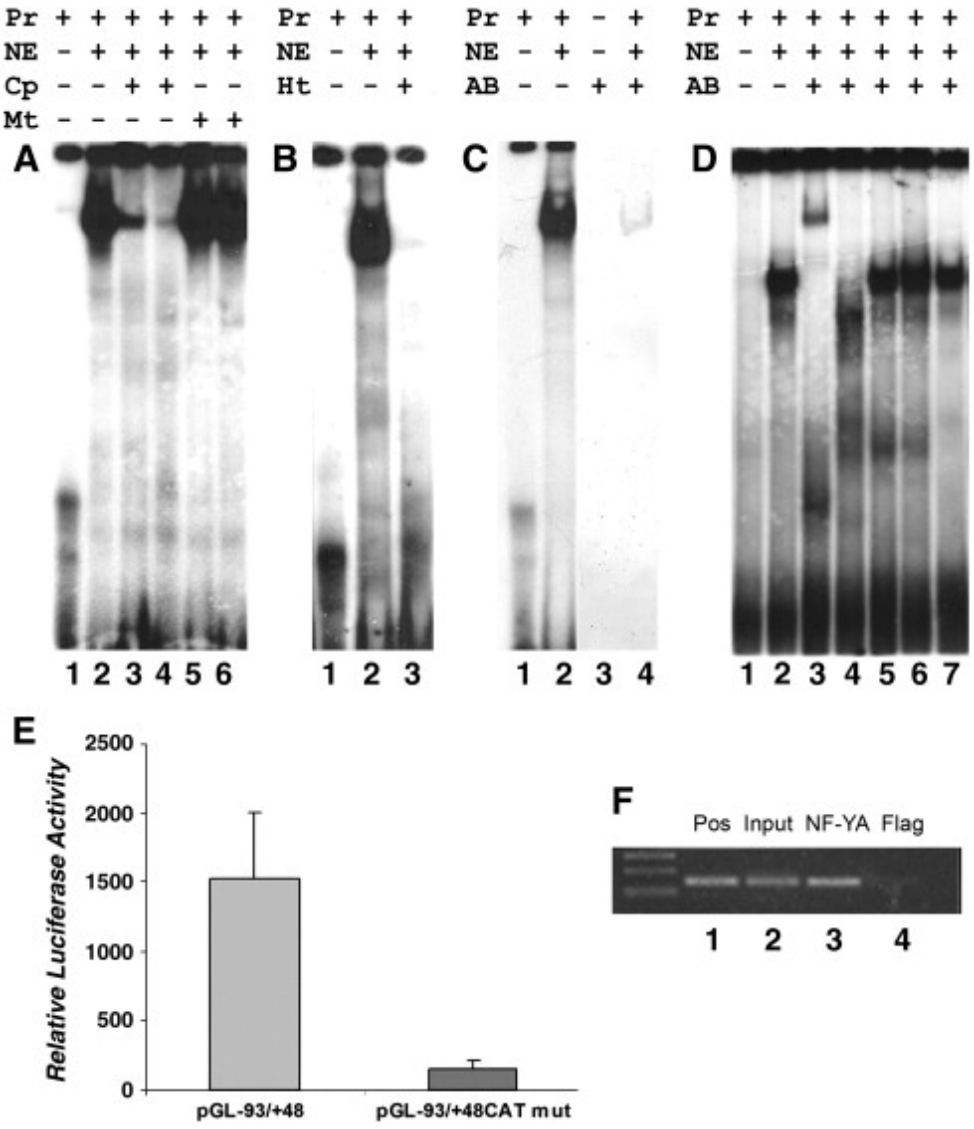
Pr + + + + + +
NE - + + + + +
Cp - - + + - -
Mt - - - - + +
A
1 2 3 4 5 6
Pr + + +
NE - + +
Ht - - +
B
1 2 3
Pr + + - +
NE - + - +
AB - - + +
C
1 2 3 4
Pr + + + + + + +
NE - + + + + + +
AB - - + + + + +
D
1 2 3 4 5 6 7
E
Relative Luciferase Activity
2500
2000
1500
1000
500
0
pGL-93/+48
pGL-93/+48CAT mut
F
Pos Input NF-YA Flag
1 2 3 4

Fig. 4. Identification of NF-Y as the CCAAT box binding protein of the mouse CP27 proximal promoter. Nuclear extracts were prepared from NIH 3T3 cells. The extracts were incubated with the 32P-labeled double-stranded oligonucleotides CP-93/-56 containing the CCAAT box of the mouse CP27 proximal promoter. A, Electrophoretic mobility shift analysis. Nuclear extracts from NIH 3T3 cells were incubated with 32P-labeled oligonucleotide CP-93/-56 probe in the presence of the various competitors. Lane 1,32P-labeled probe only; lane 2, probe plus nuclear extracts; lane 3, twenty-five-fold molar excess of unlabeled wild-type(WT) double-stranded oligonucleotides; lane 4, fifty-fold WT; lane 5, twenty-five-fold molar excess of unlabeled mutated (MUT) double-stranded oligonucleotides; lane 6, fifty-fold molar excess of unlabeled mutated (MUT) double-stranded oligonucleotides. The labels above individual lanes read Pr = probe, NE = nuclear extract, Cp = competition, Mt = mutation. B, effect of heat-treated nuclear extract on the DNA–protein complex. Lane 1, probe only; lane 2, nuclear extracts were incubated with the 32P-labeled probe; lane 3, the extracts were heated to 85 °C for 5 min, centrifuged and then added to the reaction mixture. C, Immunoblot analysis. Nuclear extracts were analyzed by EMSA in the presence of the double-stranded oligonucleotides CP-93/-56. Lanes 1 and 3, probe only; lanes 2 and 4, probe plus nuclear extracts. The EMSA gels were dried and subjected to autoradiography (lane 1 and 2) or blotted onto a nitrocellulose membrane, which was then immunoblotted with anti-NF-YA antibody (lane 3 and 4). D, supershift analysis. Lane 1, probe only; lane 2, nuclear extracts were incubated with a 32P-labeled probe; lane 3-7, the extracts were pre-incubated with anti-NF-YA, NF-YC, NF1, Est1/2 or SOX5 antibodies (respectively) for 15 min and then added to the reaction mixture. The labels above individual lanes read Pr = probe, NE = nuclear extract, Ht = heat treatment, AB = antibody. E, transient transfection experiments. The plasmid pGL-93/-56 CCAATmut is a construct in which the CCAAT box has been mutated. Equal amounts of the mutated or wild-type constructs were transiently transfected into NIH 3T3 cells. pRL-TK was used as internal control for transfection efficiency. The values for relative luciferase activity including standard deviation were derived from at least five independent experiments with triplicate wells. There was a significant difference in luciferase activity between the wild-type and the mutated construct. F, ChIP assay. Chromatin fragments immunoprecipitated with anti-NF-YA antibody were amplified by PCR using primers spanning the CP27 proximal promoter region. Immunoprecipitation with anti-Flag antibody was used as a negative control. Lane 1, positive control; lane2, Input DNA fragment amplified by mouse CP27 primers; lane3, CP27 target immunoprecipitated by anti-NF-YA antibody; lane 4, anti-Flag antibody control.

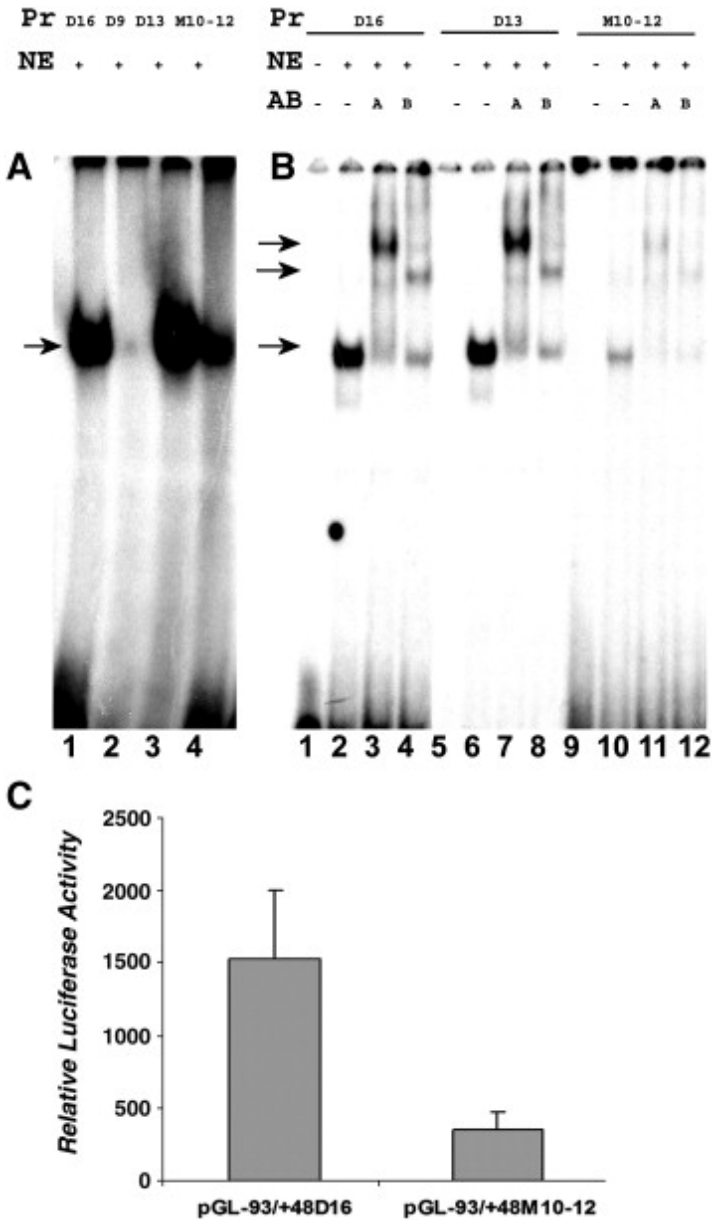
Pr D16 D9 D13 M10-12
NE + + + +
A
1 2 3 4
Pr D16 D13 M10-12
NE - + + + - + + + - + + +
AB - - A B - - A B - - A B
B
1 2 3 4 5 6 7 8 9 10 11 12
C
Relative Luciferase Activity
2500
2000
1500
1000
500
0
pGL-93/+48D16
pGL-93/+48M10-12

Fig. 5. Effect of site-specific mutation on the NF-Y binding in the 3′ flanking region of the CCAAT box of the mouse CP27 proximal promoter. A, Binding efficiency analysis of the NF-Y on the binding site. Wild-type oligonucleotides or mutated oligonucleotides were labeled with 32P. These probes were incubated with nuclear extracts and the formation of NF-Y–DNA complexes was analyzed using EMSA. Lane 1, wild-type oligonucleotide probe CP-93/-56; lane 2, deletion-mutated probe CP-93/-56D9; lane 3, deletion-mutated probe CP-93/-56D13; lane 4, site-specific mutated probe CP27-93/-56M10-12. B, Antibody supershift assay. Lanes 1–4, wild-type probe CP-93/-56; lanes 5-8, deletion-mutated probe CP-93/-56D13; lanes 9–12, site-specific mutated probe CP-93/-56M10-12; lanes 1, 5, and 9, probe only; lanes 2, 6, and 10, probe plus nuclear extract; lanes 3, 7, and 11, probe plus nuclear extract and anti-NF-YA antibody; lanes 4, 8, and 12, probe plus nuclear extract and anti-NF-YB antibody. The labels above individual lanes in Figs. 6A-C read Pr = probe, NE = nuclear extract, Cp = competition, AB = antibody. C, Transient transfection assays. The oligonucleotide containing the mutated CGGA motif in the 3′ flanking region was substituted for the plasmid pGL-93/-56 M10-12. Equal amounts of the wild-type or mutated constructs were transiently transfected into NIH 3T3 cells and luciferase activity was measured. The data represent the means and standard deviation from five separate experiments. There was a significant difference in luciferase activity between the wild-type and the mutated construct.

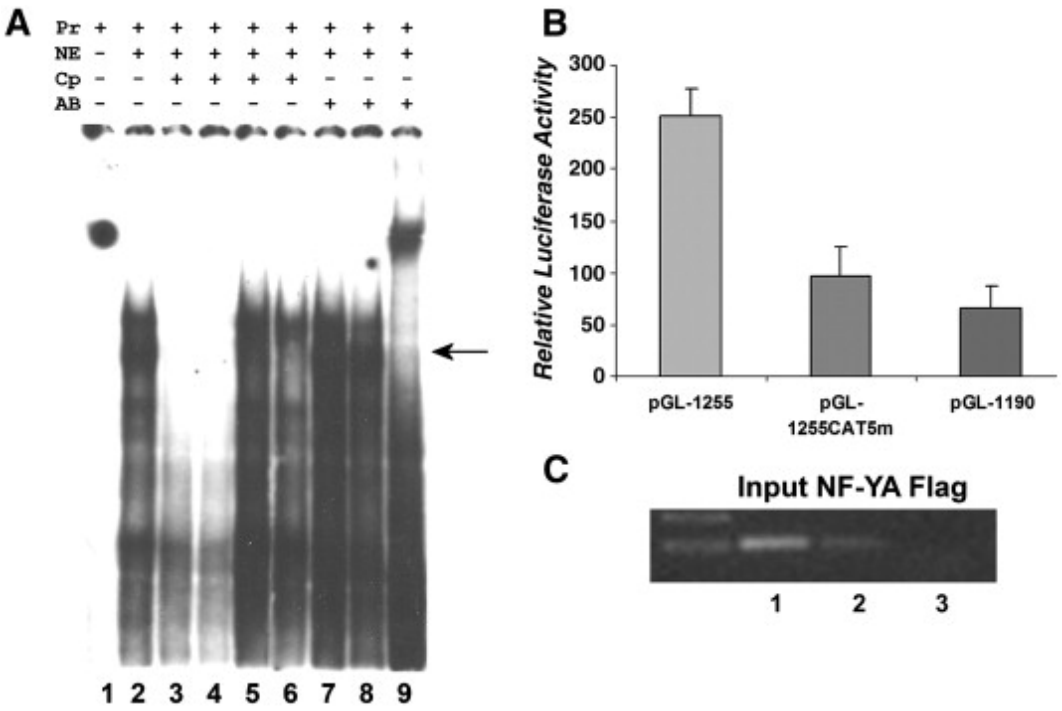
A
Pr + + + + + + + + +
NE - + + + + + + + +
Cp - - + + + + - - -
AB - - - - - - + + +
1 2 3 4 5 6 7 8 9
B
Relative Luciferase Activity
300
250
200
150
100
50
0
pGL-1255
pGL-1255CAT5m
pGL-1190
C
Input NF-YA Flag
1 2 3

Fig. 6. Multiple NF-Y binding elements in the mouse CP27 promoter. A, EMSA. Nuclear proteins were extracted from NIH 3T3 cells. The extracts were incubated with the 32P-labeled CCAAT box-containing oligonucleotide CP-1255/-1207. lane1, probe only; lane2, probe plus nuclear extracts; lane3, twenty five-fold and lane4, fifty-fold molar excess of unlabeled WT double-stranded oligonucleotides CP-1255/-1213; lane5, fifty-fold molar excess of unlabeled WT double-stranded oligonucleotides CP-1255/-1234; lane6, fifty-fold molar excess of unlabeled WT double-stranded oligonucleotides CP-1233/-1213 (Table 2); lanes 7–9, supershift with anti-NF1, SOX5 or NF-YA antibodies. The labels above individual lanes read Pr = probe, NE = nuclear extract, Cp = competition, AB = antibody. B, Mutation analysis of CAT5 box. The wild type promoter–reporter construct pGL-1255/+48 or its 5′ deletion mutation pGL-1180/+48 or its mutated homologues pGL-1255/+48CAT5-mut was introduced into NIH3T3 cells, and luciferase activity was measured. The values for relative luciferase activity including standard deviation were presented in triplicates in five independent experiments as described before. C, ChIP assay. Chromatin fragments immunoprecipitated with anti-NF-YA antibody were amplified by PCR using primers spanning the CP27 promoter regions from −1254 to −1133 bp. Immunoprecipitation with anti-Flag antibody was used as a negative control. Lane 1, input DNA fragment amplified by mouse CP27 primers; Lanes 2, CP27 target immunoprecipitated by Anti-NF-YB antibody; lane3, anti-Flag antibody control.

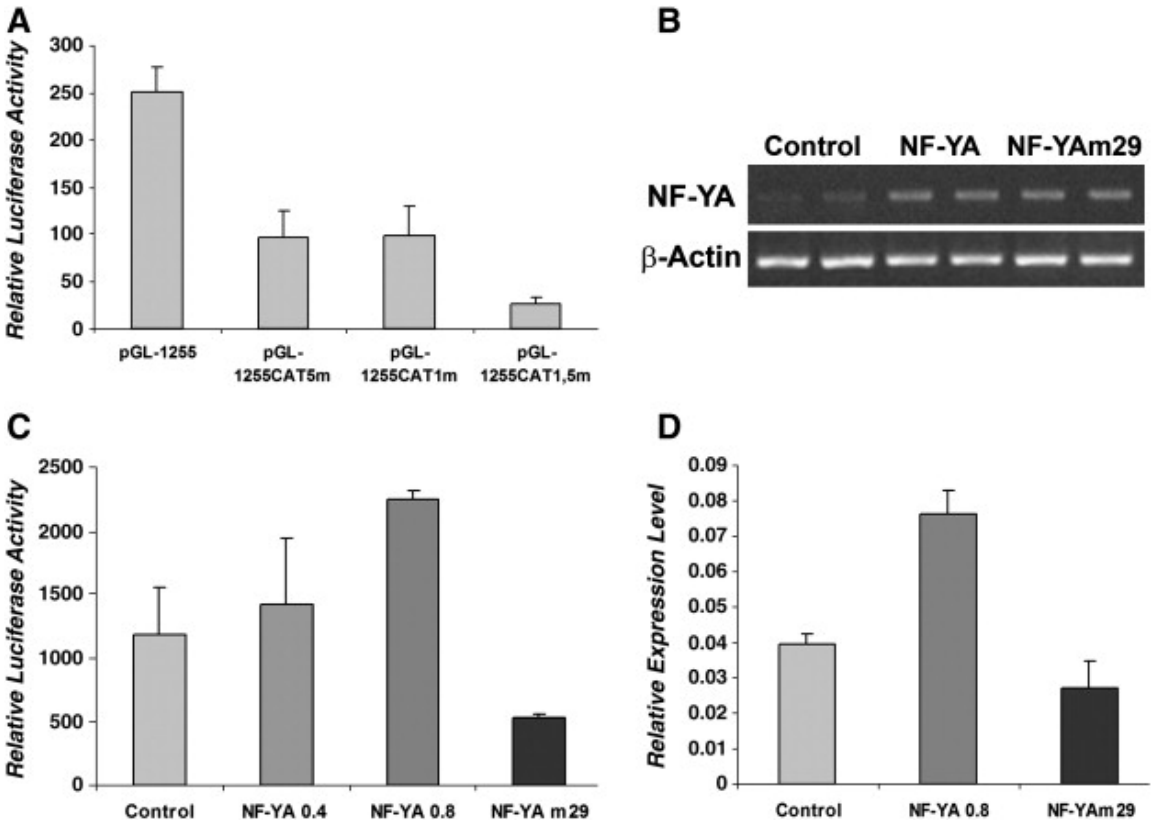
A
Relative Luciferase Activity
300
250
200
150
100
50
0
pGL-1255
pGL-1255CAT5m
pGL-1255CAT1m
pGL-1255CAT1,5m
B
Control
NF-YA
NF-YAm29
NF-YA
β-Actin
C
Relative Luciferase Activity
2500
2000
1500
1000
500
0
Control
NF-YA 0.4
NF-YA 0.8
NF-YA m29
D
Relative Expression Level
0.09
0.08
0.07
0.06
0.05
0.04
0.03
0.02
0.01
0
Control
NF-YA 0.8
NF-YAm29

Fig. 7. Effect of NF-Y on the cp27 gene expression. A, function study on the cooperation of multiple CCAAT-boxes to regulate the CP27 promoter. The wild type promoter–reporter construct pGL-1255/+48 or its mutated homologues pGL-1255/+48CAT1-mut, pGL-1255/+48CAT5-mut or pGL-1255/+48CAT1, 5-mut was transfected into NIH3T3 cells, and luciferase activity was measured in triplicates in five independent experiments as described before. B, RT-PCR analysis of NF-YA or NF-YAm29 overexpression efficiency. NIH3T3 cells were transfected with expression vectors pIRES-NF-YA or pIRES-NF-YAm29. After 24 h, total RNA was isolated from transfected cells and reverse transcribed. NF-YA expression level was detected by PCR analysis. RT-PCR products of four separate experiments were loaded onto 1% agarose gels and stained with ethidium bromide. β-actin served as an internal control. C, Luciferase activity of CP27 promoter–reporter gene constructs regulated by overexpression of NF- YA or NF-YAm29. The construct pGL-1255/+48 was co-transfected with either the expression vectors pIRES-NF-YA or pIRES-NF-YAm29 into NIH3T3 cells. Transfection with pIRES-GFP was used as control. Forty-eight hours after transfection, cells were harvested and luciferase activity was measured as described above. Results are presented as relative luciferase activity. D, qRT-PCR analysis of CP27 mRNA expression modulated by gene manipulation of NF-YA. NIH3T3 cells were transfected with the expression vectors pIRES-NF-YA or pIRES-NF-YAm29. After 48 h, total RNA was isolated from the transfected cells and reverse transcribed. CP27 expression levels were measured using real time RT-PCR analysis. Changes in expression levels were measured as n-fold increases of stimulation over the control group using the $2^{-\Delta\Delta Ct}$ method. CP27 expression was 1.93-fold higher when cells were transfected with NF-YA.

B. 1. Two regulatory elements, a CCAAT-box and an E-box, are located in the mouse CP27 proximal promoter region

To understand how CP27 expression is regulated in ES cells, putative cis-acting elements within the CP27 proximal promoter region were localized by progressive 5′ deletion mutations using reporter gene constructs in mouse ES cells with or without LIF (Fig. 8A). Luciferase activity assays demonstrated that the region between −93 and −56 contained a strong enhancer activity because the 5′ deletion mutation from nucleotides −93 to −56 resulted in a 9.6 times decrease in luciferase activity. The construct pGL −55/+48 had a 60 times higher luciferase activity than the pGL3-basic control. The activity of the pGL −17/+48 construct was on the same level with the pGL3-basic vector (Fig. 8B).

The transient transfection experiments described above indicate the presence of two positive regulatory elements within 93 bp of the mouse CP27 proximal promoter region. In order to elucidate the nuclear factor binding sites, DNase I footprint assays were performed. Using end-labeled probe CP − 207/+48 and nuclear extracts from ES cells, two major protected DNA regions were identified between nucleotides −83 and −61, and from −52 to −37 (Fig. 8C, lane 3). These protected sequences were identified as a CCAAT-box and an inverted E-box by comparison with a DNA ladder.

B. 2. Transcription factors binding to corresponding cis-regulatory elements on the CP27 proximal promoter *in vitro* and *in vivo*: NF-Y binds to the CCAAT-box and USF1 binds to an E-box

To confirm that the CCAAT-box and the E-box are regulatory elements in the mouse CP27 proximal promoter, oligonucleotides containing the CCAAT-box (CP-93/-56) or the E-box (CP-55/-27) were subjected to EMSA. The EMSA revealed formation of

protein–DNA complexes using nuclear extracts from ES cells and the radioactively labeled oligonucleotide CP-93/-56 or oligonucleotide CP-55/-27. Competition experiments were performed to determine the sequence specificity of the protein–DNA complex. Twenty-five- or 50-fold molar excess of unlabeled CP-93/-56 or CP-55/-27 eliminated the formation of the complexes (Fig. 9A and B, lanes 3 and 4). However, when a mutation in the CCAAT-box was introduced by mutating CCAAT to CACAT or a mutation in E-box was generated by mutating CGTG to AATG, the mutated oligonucleotides did not affect protein/DNA bindings (Fig. 9A and B, lanes 5 and 6).

To determine which transcription factors contributed to the complexes formed with the CCAAT-box or the E-box, the proximal CP27 promoter region was analyzed using MatInspector (www.genomatrix.de) and Signal Scan (www.bimas.dcrt.nih.gov). This analysis identified a NF-Y binding site and a USF1 binding site. To further confirm that NF-Y and USF1 bind to the CCAAT-box and the E-box in the CP27 proximal promoter, respectively, super-gel shift assays were performed. Incubation of anti-NF-YA antibody together with the CP27 −93/−56 DNA–protein complex led to the formation of slower migrating supershifted bands (Fig. 9A, lane 7). The anti-NF1 antibody did not form a supershifted band with CP27 proximal promoter sequences (Fig. 9A, lane 8). The antibody to USF1 completely obliterated the CP27 −55/−27 DNA/protein complex (Fig. 9B, lane 7), whereas the antibody to USF2 did not recognize this band (Fig. 9B, lane 8), indicating that USF1 binds to the E-box within the CP27 proximal promoter. Note that the USF1 antibody did not supershift but caused the disappearance of the cognate ESMA band. These results further confirmed that the CP27 −93/−56 DNA–protein complex contained the NF-Y transcription factor (Fig. 9A, lane 7) while the CP27

−55/−27 DNA–protein complex contained the USF1 transcription factor (Fig. 9B, lane 7).

Chromatin immunoprecipitation was performed in order to verify the binding of NF-Y and USF1 to the CP27 promoter in ES cells *in vivo*. The cross-linked chromatin of ES cells was immunoprecipitated with anti-NF-YA or anti-USF1 antibodies and subjected to PCR amplification using primers spanning the CP27 promoter region (Table 3), resulting in the amplification of a 141 bp fragment corresponding in size to the CP27 proximal promoter fragment (Fig. 9C, lanes 2 and 3). In contrast, a control anti-flag antibody failed to precipitate a chromatin fragment containing the endogenous CP27 promoter (Fig. 10C, lane 1). These results confirmed the presence of an active CCAAT-box and an active E-box in the CP27 proximal promoter.

To determine whether the CCAAT-box and the E-box are involved in the regulation of the CP27 promoter, the CCAAT-box and the E-box of the intact CP27 promoter were mutated (Table 3). Specifically, the activity of the mutated plasmid pGL-93/+48 CCAAT-m was compared with that of the wild-type pGL-93/+48 and the mutated plasmid pGL-55/+48 E-m was compared with that of the wild-type pGL-55/+48. The mutations had significant effects on the activity of the CP27 promoter. Mutation in the CCAAT-box reduced CP27 promoter activity by 80.74% (Fig. 9D), while mutation of the E-box decreased CP27 promoter activity by 53.12% (Fig. 9D). These results demonstrate that the CCAAT-box and the E-box are functionally significant regulatory elements located in the mouse CP27 proximal promoter.

B. 3. NF-Y interacts with USF1 on the CP27 proximal promoter

DNase I footprinting and functional studies described earlier have identified two active cis-regulatory elements in the proximal CP27 promoter, an E-box and an adjacent CCAAT-box. Previous studies have suggested that a combined CCAAT-box–E-box motif regulates gene expression directly and co-operatively (Zhu et al., 2003 and Grskovic et al., 2007). To explore the possibility of an interaction between the CCAAT-box and the E-box in the CP27 proximal promoter, we subjected oligonucleotide (CP-93/-27) containing both the CCAAT-box and the E-box to EMSA. The CP-93/-27 probe generated three EMSA bands from ES cell nuclear extracts (Fig. 10A, lane 1). The fastest migration band was generated by USF1 because the USF1 antibody completely abolished the band (Fig. 10A, lane 3). The second fast migrating band was generated by NF-Y because the NF-YA antibody obliterated the band and formed a supershifted band (Fig. 10A, lane 2). The slowest band was generated by both NF-Y and USF1 since inclusion of antibody against either USF1 or NF-YA into the promoter/NE reaction disrupted the formation of this band (Fig. 10A, lanes 1–3). The USF2 antibody did not interact with any protein/DNA complexes (Fig. 10A, lane 4).

To determine whether NF-Y and USF1 were co-localized in ES cells, NF-YA and USF1 expression were examined by immunohistochemistry. Immunofluorescent assays illustrated that NF-YA and USF1 proteins were expressed and overlapped in the nucleus with and without addition of the growth factor LIF (Fig. 10B).

To confirm that NF-Y interacts with USF1 *in vivo*, we performed coimmunoprecipitation experiments. ES cell lysates were used for immunoprecipitation with antibodies against NF-YC or USF1. Flag antibody was served as a negative control.

As shown in Fig. 10C, USF1 was detected in anti-NF-YC immunoprecipitates but not in immunoprecipitates with Flag antibody. Conversely, NF-YC was detected in the USF1 immunoprecipitates. These results provide additional evidence that NF-Y and USF1 physically interact *in vivo*.

B. 4. Synergistic activation of CP27 expression by NF-Y and USF1

To investigate the involvement of NF-Y–USF interactions in the regulation of the CP27 promoter, mutated CCAAT-box and E-box constructs of the intact CP27 promoter were generated (Table 3). Specifically, the activity of the mutated plasmid pGL-93/+48 CAT-m or pGL-93/+48 E-m was compared with that of the wild-type pGL-93/+48. The mutation in the CCAAT-box reduced luciferase activity by 90.49% (Fig. 11A). Surprisingly, the mutation in the E-box completely abolished the activity of the CP27 proximal promoter even though the CCAAT-box remained intact (Fig. 11A). These results suggest that the function of the CCAAT-box is dependent on the E-box as an essential regulatory element located in the mouse CP27 proximal promoter.

To determine whether NF-Y and USF1 can function synergistically in activation of the CP27 promoter, expression vectors for NF-YA (pIRES-NF-YA) or USF1 (pCMV-SPORT6.1-USF1) were introduced into ES cells and expression levels in transfected cells were significantly higher than in control cells as demonstrated by RT-PCR (lanes 5–8 compared to lanes 1–4, determined by densitometry) (Fig. 11B). Vectors pIRES-NF-YA, pCMV-SPORT6.1-USF1 or a combination were then co-transfected with the promoter–reporter construct pGL-CP-93/+48 containing both the CCAAT-box and the E-box and a high degree of synergy (2.19 folds) between NF-YA and USF1 was observed (Fig. 11C).

To confirm that the functional collaboration between NF-Y and USF1 influences endogenous CP27 gene expression, ES cells were transfected with pIRES-NF-YA or pCMV-SPORT6.1-USF1 or a combination of both, and CP27 mRNA was quantified by real time RT-PCR. The endogenous CP27 mRNA expression was increased by 1.93-fold following NF-YA overexpression, 2.06-fold following USF1 overexpression, and 2.69-fold following NF-YA-USF1 overexpression, respectively (Fig. 11D).

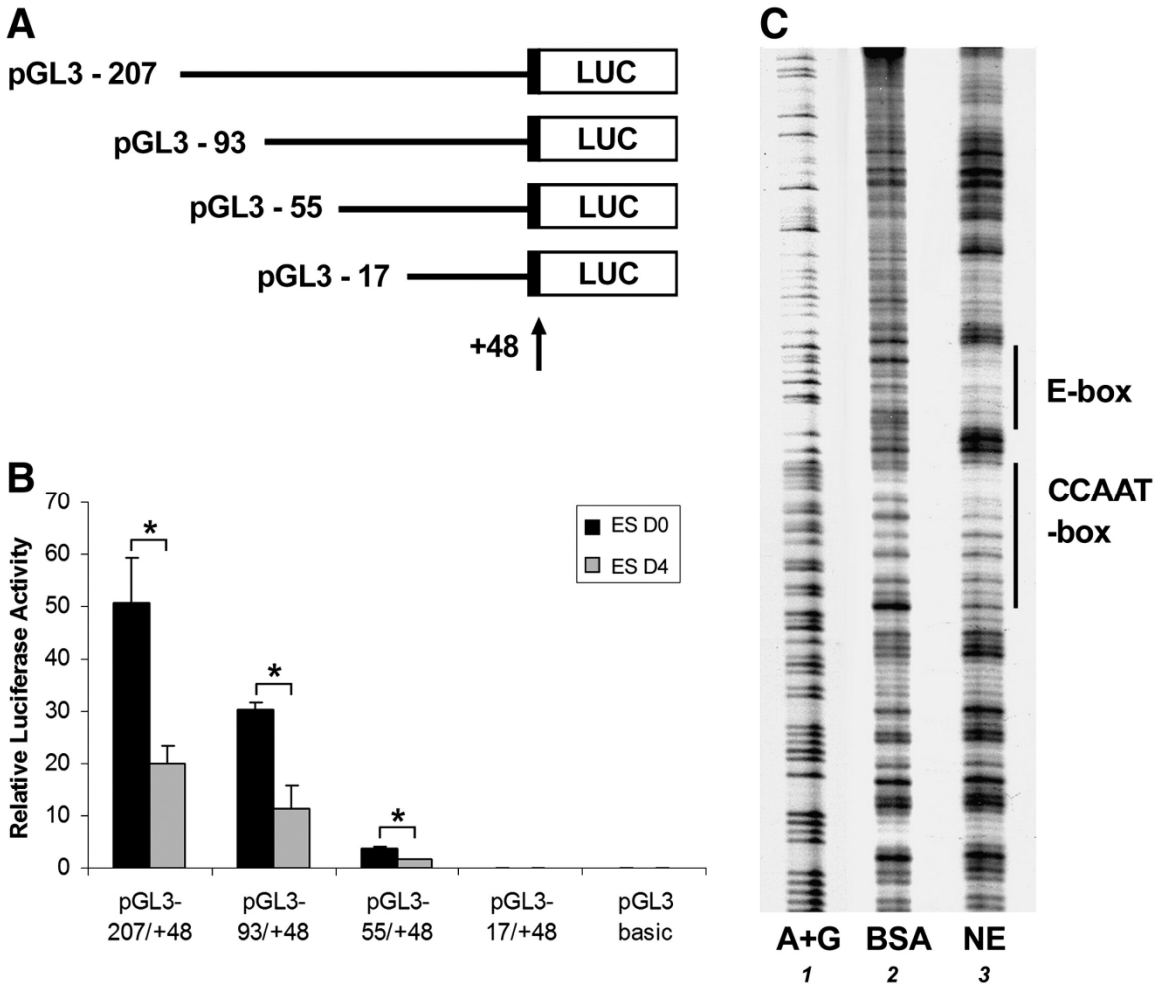
A
pGL3 - 207
LUC
pGL3 - 93
LUC
pGL3 - 55
LUC
pGL3 - 17
LUC
+48
B
Relative Luciferase Activity
70
60
50
40
30
20
10
0
ES D0
ES D4
*
*
*
pGL3-
207/+48
pGL3-
93/+48
pGL3-
55/+48
pGL3-
17/+48
pGL3
basic
C
E-box
CCAAT
-box
A+G
1
BSA
2
NE
3

Fig. 8. Characterization of the mouse CP27 proximal promoter activity in ES cells. *A*, schematic representation of reporter plasmids. The arrow indicates the position of the transcription start site. Reporter constructs descriptors indicate the 5′-end nucleotide number of the inserted promoter sequence. *B*, luciferase activity resulting from the expression of the CP27 promoter–reporter gene constructs. D0 represents cell culture in the presence of LIF and D4 represents LIF-withdrawal for 4 days. The results were normalized by co-transfection with a pRL-TK reporter plasmid. Error bars represent the standard error for three samples in five independent experiments. *C*, DNase I footprinting analysis. The DNA fragment CP-207/+48 was 3′-end labeled and incubated with BSA (lane 2) or nuclear extract from ES cells (lane 3). Lane 1 represents a G + A Maxam–Gilbert sequencing ladder. Two DNase I protected regions are recognized, and their sequences match the E-box and the CCAAT-box consensus sequences of the proximal CP27 promoter. The asterisks in B indicate significant differences ($P < 0.05$).

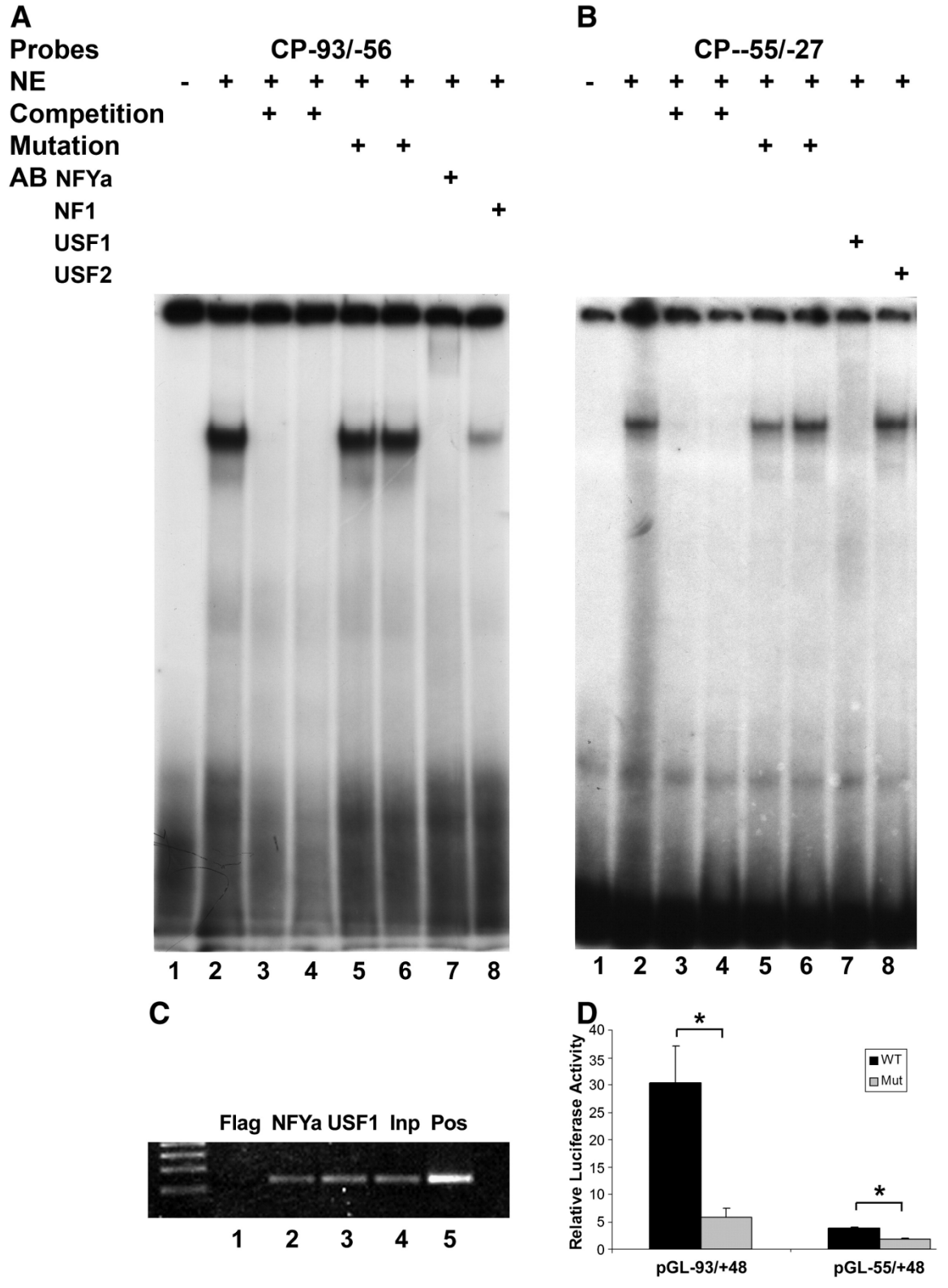
A
Probes
CP-93/-56
NE
Competition
Mutation
AB NFYa
NF1
USF1
USF2
1 2 3 4 5 6 7 8
B
CP--55/-27
1 2 3 4 5 6 7 8
C
Flag NFYa USF1 Inp Pos
1 2 3 4 5
D
Relative Luciferase Activity
WT
Mut
pGL-93/+48
pGL-55/+48

Fig. 9.

Identification of two active cis-regulatory elements and corresponding transcription factors on the CP27 proximal promoter: NF-Y binds to the CCAAT-box and USF1 binds to an E-box. *A* and *B*, electrophoretic mobility shift analysis. Nuclear extracts from ES cells were incubated with ^{32}P-labeled oligonucleotide probes CP-93/-56 (A) or CP-55/-27 (B) in the presence of various competitors, mutants and antibodies. The labels above individual lanes read NE = nuclear extract, AB = antibody. *C,* chromatin immunoprecipitation. NF-YA (lane 2) or USF1 associated DNA fragments (lane 3) were immunoprecipitated using anti-NF-YA or USF1 antibodies. Flag antibody served as negative control. *D,* transient transfection experiments. The plasmid pGL-93/+48 CCAAT-m is a modified construct of pGL-93/+48 in which the CCAAT-box had been mutated; the plasmid pGL-55/+48 Em is a mutated construct of pGL-55/+48 in which the E-box was modified. The asterisks in D indicate significant differences ($P < 0.05$).

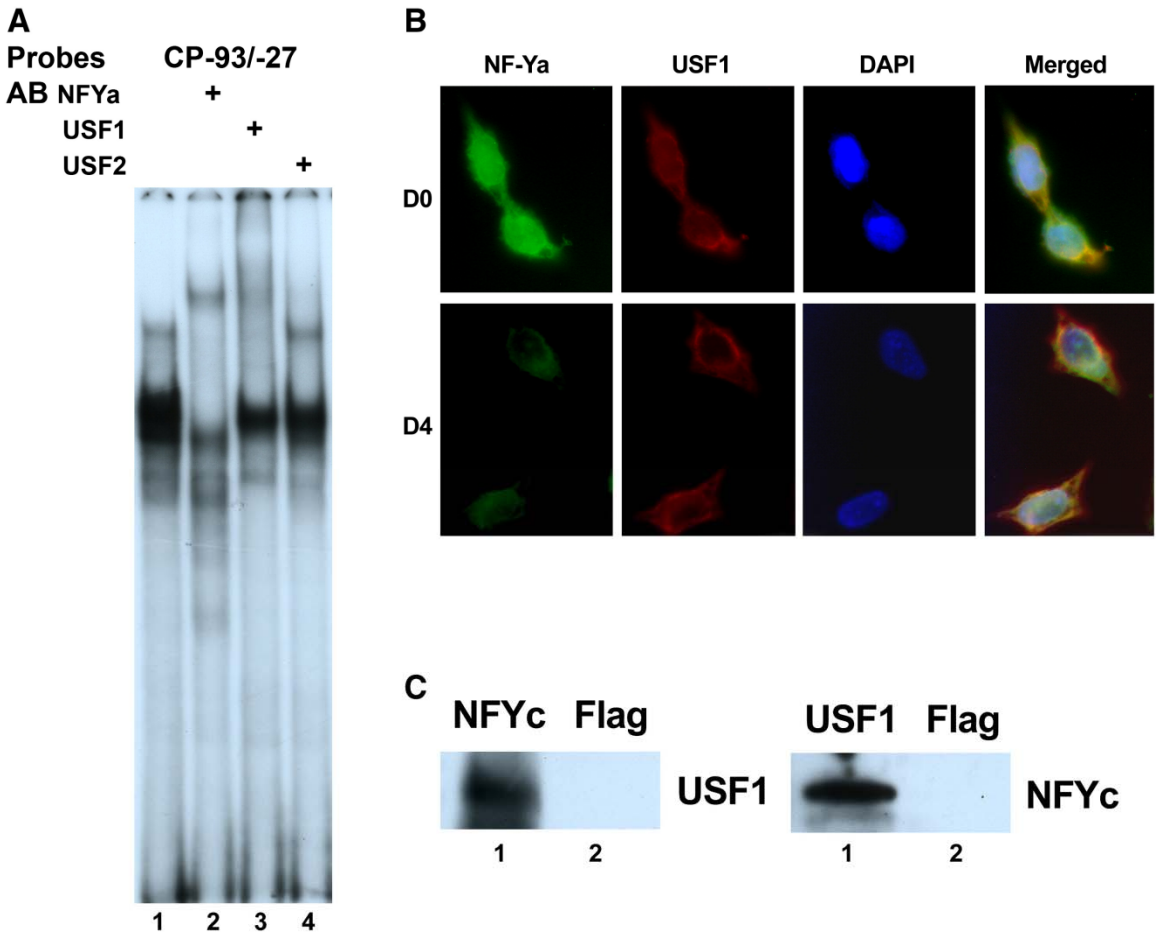
A
Probes
CP-93/-27
AB NFYa
+
USF1
+
USF2
+
1 2 3 4
B
NF-Ya
USF1
DAPI
Merged
D0
D4
C
NFYc Flag
USF1
1 2
USF1 Flag
NFYc
1 2

Fig. 10.

Interaction between NF-Y and USF1 on the CP27 proximal promoter. *A,* supershift assay. Oligonucleotide CP-93/-27 containing both the CCAAT-box and the E-box was ^{32}P-labeled and incubated first with NE from ES cells and then with various antibodies. AB = antibody. *B*, immunofluorescent assay for NF-YA and USF1 expression. ES cells were cultured in the presence of LIF or without LIF for 4 days, fixed and subjected to double immunofluorescence staining using NF-YA (green) and USF1 (red) antibodies. The nucleus was stained with DAPI (blue). D0 represents cell culture in the presence of LIF and D4 represents LIF-withdrawal for 4 days. *C*, coimmunoprecipitation. ES cell lysates were precipitation with either NF-YC antibody or USF1 antibody. Flag antibody was used as negative control.

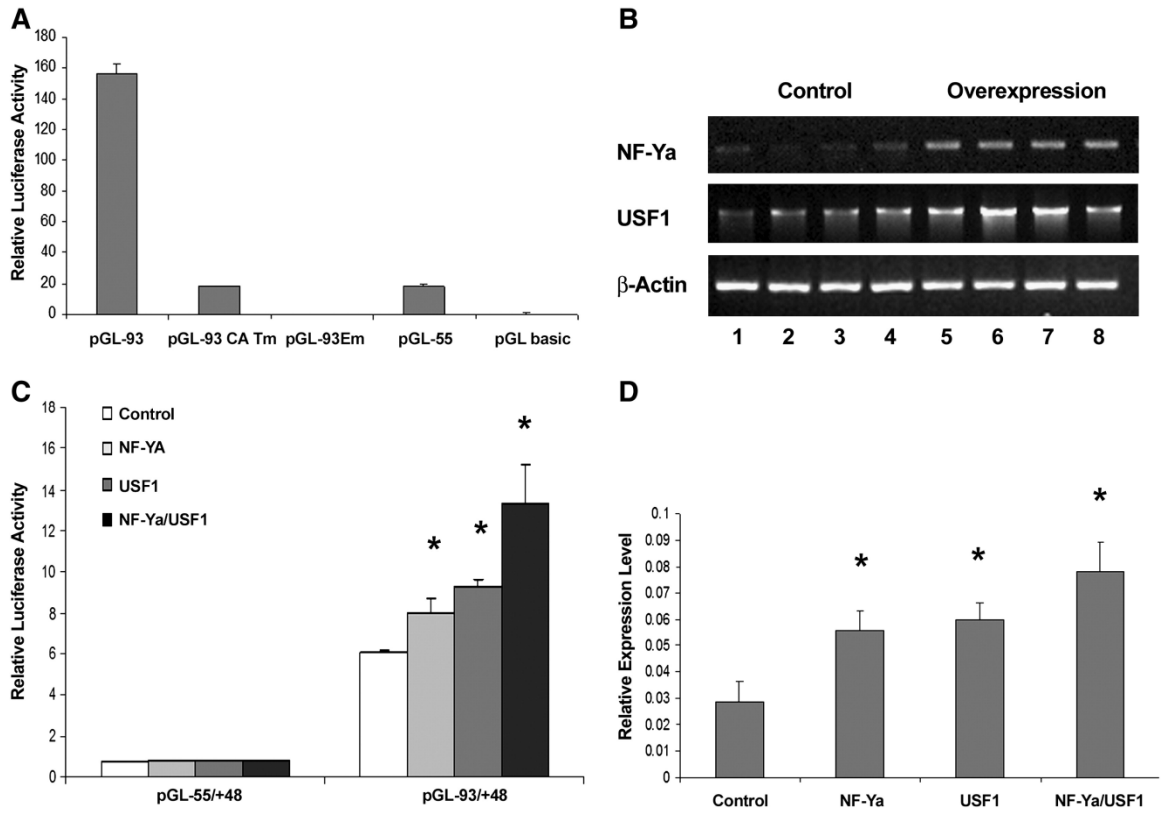
A
Relative Luciferase Activity
180
160
140
120
100
80
60
40
20
0
pGL-93
pGL-93 CA Tm
pGL-93Em
pGL-55
pGL basic
B
Control
Overexpression
NF-Ya
USF1
β-Actin
1 2 3 4 5 6 7 8
C
Control
NF-YA
USF1
NF-Ya/USF1
Relative Luciferase Activity
18
16
14
12
10
8
6
4
2
0
*
*
*
pGL-55/+48
pGL-93/+48
D
Relative Expression Level
0.1
0.09
0.08
0.07
0.06
0.05
0.04
0.03
0.02
0.01
0
*
*
*
Control
NF-Ya
USF1
NF-Ya/USF1

Fig. 11.

Effect of the interaction between NF-Y and USF1 on CP27 gene expression. *A*, function study to determine whether the CCAAT-box and the E-box are essential regulatory elements of the CP27 promoter. The wild type promoter–reporter construct pGL-93/+48 and its mutated homologues pGL-93/+48CCAATm or pGL-93/+48Em were transfected into ES cells. *B,* RT-PCR analysis of NF-YA or USF1 overexpression efficiency. ES cells were transfected with expression vectors pIRES-NF-YA or pCMV-SPORT6.1-USF1. Each lane (1–8) represents RNA extracts from individually cultured wells. Lanes 1–4 are from controls and 5–8 are from overexpressing mouse ES cells. *C,* regulation of CP27 promoter activity by overexpression of NF-YA or USF1 or a combination of both. The construct pGL-93/+48 was co-transfected with the expression vectors pIRES-NF-YA or pCMV-SPORT6.1-USF1 or a combination of both into ES cells. Transfection with pIRES-GFP or pCMV-SPORT6.1 was used as controls. *D,* qRT-PCR analysis of CP27 mRNA expression regulated by gene manipulation of NF-YA or USF1 or a combination of both. The asterisk indicates a statistically significant increase in luciferase activity and gene expression levels. CP27 expression levels were calculated in relationship to the β-actin internal control using the $2^{-\Delta\Delta Ct}$ method (Livak and Schmittgen, 2001).

C. 1. Structure and evolution of the SWR-C/SRCAP complex member CP27

Previous studies have noted the unique developmental expression pattern (Diekwisch et al. 1999) and functional potency (Diekwisch and Luan 2002) of the *cp27* gene and highlighted its role in fibroblast proliferation (Luan and Diekwisch 2002, Luan et al. 2010, Ito et al. 2011). To further define its role, we have placed CP27 in the broader context of the mammalian ATP-ase dependent chromatin remodeling complex SRCAP (Fig. 1A). Based on sequence homology analysis, CP27 is the mouse counterpart of the yeast protein Swc5, a member of the yeast SWR complex, which is the equivalent of the mammalian SRCAP complex (Chrivia, Diekwisch 1999). The yeast SWR complex is a multi-protein complex known for its ability to exchange the canonical histone H2A with the variant histone Htz1 (Figs. 12A,B; Wu et al. 2005). In yeast, SWR complex members Swc2, Arp6, Swc5, Swc6 have been associated with Htz1 exchange (Wu et al. 2005). CP27 is characterized by a number of unique sequence attributes suggestive of its biological function, including alternating α-helices and β-sheets indicative of an interactive secondary structure, a high level of sequence conservation representative of an evolutionarily conserved function, and unusual isoelectric point polarity of the CP27 molecule, ranging from a highly acidic N-terminus (pH 2.8) to a basic C-terminus (pH 9.9)(Fig. 12C-E). Remarkably, during the course of CP27 evolution from mycoplasm to human, the pI of the conserved region of the N-terminus (Supplement 1) gradually decreased from pH6 to pH 3, while the C-terminus became increasingly alkaline (from pH9 to 11)(Fig. 12F).

C. 2. CP27 is part of SRCAP complex to regulate stem cell differentiation and progression.

As a next step, we have asked the question whether CP27 is a member of the SRCAP complex. Previous studies have shown that the CP27 yeast homologue swc5 is a part of the SWR1 chromatin remodeling complex (Wu et al. 2005), an ATPase containing chromatin complex which plays a key role in H2A/H2A.Z histone variant exchange. H2A/H2A.Z variant exchange is one of the pivotal events in the life of a cell that prevents the spreading of heterochromatin and thus keeps DNA accessible to transcription. As long as CP27 has remained an swr/SRCAP complex member throughout its evolution from yeast to man, the mammalian CP27 with its 45% homology to swc5 has likely retained its role in histone exchange based on the highly conserved function of this complex in deuterostomes. However, many chromatin complex members change or lose their association with complexes. We therefore decided to probe whether CP27 was a member of the mammalian SRCAP complex. In order to ask this question, we used co-immunoprecipitation assays to test whether CP27 co-immunoprecipitates with conserved swr/SRCAP complex members such as DMAP1, TIP49A, TP49B, and BAF53 (Morrison and Shen, 2009). In these studies, our anti-CP27 antibody recognized a single band representing CP27 indicative of CP27/TIP49A and TIP49B protein interaction in western blots (Fig. 13A-C). In addition, the anti CP27 antibody employed for this western blot recognized the presence of DMAP1 and BAF53A (Fig. 13A-C). Together our co- immunoprecipitation experiment indicates that CP27 interacts with SRCAP complex subunits and thus is a member of the SRCAP complex.

Furthermore, we used chromatin immunoprecipitation (ChIP) assays to test whether CP27 binds to matching regions on the FAD synthetase promoter, a promoter that demonstrates high levels of SRCAP binding (Wong, et al. 2007). FAD synthetase promoter studies allowed us to ask whether matching CP27 and SRCAP complex subunit binding regions were also occupied by H2A.Z, suggesting a role in H2A.Z deposition. ChIP assays were performed using antibodies against H2A.Z, CP27, TIP49A, and DMAP1 to pull down chromatin immunoprecipitates. Our study yielded overlapping regions of CP27, TIP49A, and DMAP1 binding within the FAD promoter (Fig. 13D), suggesting that CP27 binding sites are related to SRCAP complex binding sites.

C. 3. CP27 affects H2A.Z expression pattern and levels.

CP27 is a homologue to yeast swc5, a subunit of SWR1 complex (SRCAP complex in mammalian cells) which catalyzes ATP-dependent exchange of the nucleosomal histone H2A for H2A.Z. Furthermore, a histone variant H2A.Z mutant mouse was reported to fail shortly after implantation and prior to gastrulation (E6) (Faast et al, 2001). In comparison between *cp27* and *H2A.Z* null mice, both null phenotypes were similar (Faast et al. 2001, Ridgway et al. 2004). Based on its homology with swc5 as described above, we have hypothesized that CP27 plays an essential role in the exchange of the histone variant H2A.Z. Here we tested CP27 and H2A.Z protein localization in ES cells and blastocysts, and involvement in histone variant H2A.Z exchange. Immunofluorescence experiments demonstrated CP27 and H2A.Z co-localization in blastocysts (Figs. 14A-D) and ES cells (Figs.3E-H). CP27 was localized in the inner cell mass and in the trophoblast (Fig. 14A). In comparison, H2A.Z expression was mostly restricted to the inner cell mass. However, CP27 reactivity in the

trophoblast was stronger than H2A.Z reactivity (Fig. 14B compared to 14A). CP27 and H2A.Z were co-localized in the inner cell mass (Fig. 14C). On a cellular level, CP27 and H2A.Z co-localized in mouse embryonic stem cells. CP27 expression was not only in the nucleus but also expressed at low levels in cytoplasm; in contrast, H2A.Z expression was exclusively restricted to the nucleus (Figs. 14E-H). Together, null phenotype and protein localization were supportive of the concept that CP27 and H2A.Z were involved in early embryogenesis. Next, we asked the question whether loss of CP27 function affects H2A.Z expression pattern and levels using whole mount immunoreactions with antibodies against H2A.Z in CP27 knockout and control blastocysts. Our data revealed that only wild-type blastocysts detected H2A.Z expression (Fig. 14I), while blastocysts without CP27 did not (Fig 14J). Together, these data suggested that CP27 expression and association in the ICM is critical for H2A.Z expression and may play important roles in H2A/H2A.Z exchange. Analysis of mRNA levels in CP27 knockout blastocysts by real time qPCR suggested that H2A.Z mRNA levels were decreased by 70% (Fig. 14K).

Based on the similarities between H2A.Z and CP27 in terms of expression, localization, and null phenotype, and CP27 mutant affect H2A.Z expression in blastocysts, we decided to explore whether CP27 involved in H2A.Z exchange on a chromatin level. Using chromatin immunoprecipitation (ChIP) assay, we demonstrated that CP27 and H2A.Z precipitate together as part of the same chromatin complex. The anti-H2A.Z antibody employed for this Western blot recognized a single band at 14kDa representing H2A.Z as part of a Flag/CP27/H2A.Z chromatin complex pulled down by an anti-Flag antibody (Fig. 14L). Also the anti-Flag antibody reacted with the □CP27/Flag fusion protein, however failed to pull down the ΔCP27/H2A.Z chromatin complex

(compare with Fig.14L Lane 2), suggesting that the mutated swc5-like CP27 domain (BCNT) is necessary for the interaction of CP27 with the H2A.Z containing chromatin complex.

In addition, cell culture studies to confirm the effect of CP27 on H2A.Z localization and expression by CP27 knockdown experiments resulted in a 42% reduction of H2A.Z and 44% reduction of CP27 protein expression in the cells on Western blots (Fig. 14S, measured by densitometry) and on immunohistochemistry micrographs analysis (Figs. 14M-R) to verify CP27 affects H2A.Z localization pattern and heterochromatin confirmation. Besides ES cell plasticity is regulated through chromatin dynamics and epigenetic mechanisms involving DNA methylation, histone modifications, and histone exchenge, which in turn affect the promoter regions. In light of the pivotal role of the histone variant H2A.Z in the protection of euchromatin from ectopic heterochromatin spreading (Meneghini et al., 2003) we hypothesized that changes in CP27 expression might affect H2A.Z localization and heterochromatin confirmation. A CP27 knockdown approach was used to test the effect of CP27 on heterochromatin/euchromatin boundaries. Following CP27 siRNA transfection, nuclei became enriched in DAPI fluorescence, indicative of enhanced heterochromatin levels (Fig. 14N versus 14Q). H2A.Z immunopositive regions co-localized with DAPI-unstained heterochromatin nuclear areas in overlay micrographs (Figs. 14O and 14R). Note that the generalized low-level H2A.Z expression found in control nuclei was lost in CP27 knockdown nuclei and replaced by more restricted H2A.Z expression within the boundaries of circumscribed euchromatin regions (Figs. 14P/R versus Figs. 14M/O). In addition, we tested how relationship between CP27 and heterochromatin by treating the

cells with Trichostatin A (TSA) to remove the heterochromatin, our results indicates CP27 expression pattern in treatment cells are widely extended (Supplement 2A), that suggesting CP27 involved in eu- / hetero-chromatin formation associate with H2A.Z. Together, these findings document that CP27 co-localizes with H2A.Z and affects its expression and chromatin conformation.

C. 4. CP27 is essential for early development / Lack of CP27 mis-regulates formation of three germ layers

In order to determine the effect of *cp27* loss of function, targeted ES cells were used to produce germ-line chimeras via blastocyst injection (Fig. 15A-C). Homozygous progeny was observed from E3.5 blastocysts to E7.5 embryos. From E8.5 until newborn, homozygous offspring was missing, while the number of resorbed/degrading embryonic masses peaked at days E10 and E12, that suggesting early embryonic lethality between implantation and embryonic day E8 (Fig. 15D). In E3.5 blastocysts, whole mount wild-type and *cp27* knockout embryos were indistinguishable from each other (Figs. 15E,F). In contrast, E7.5 *cp27* mutant mice displayed rudimentary embryonic tissues lacking germ layer organization while same-stage mid-gastrulation wild-type mouse embryos featured differentiated germ layers (Fig. 15K,L). Immunoreactions using an anti-CP27 antibody revealed strong reactivity in wild-type blastocysts and embryos compared to complete absence of CP27 in knockout samples (Figs. 15G,H). In order to determine the viability of *cp27* mutant progeny, E3.5 blastocysts were cultured in ES cell medium without LIF, resulting in trophoblast ectoderm cellular outgrowth in both *cp27* mutant and wild-type blastocysts (Fig. 15I,J). The wild-type group featured distinct inner cell mass condensations while the inner cell mass was lost in the $cp27^{-/-}$ group and only a few

single cells remained (Fig. 15I,J). Both wild-type and mutant embryos as late as E6.5 were incorporating BrdU (Fig. 15M,N) and indicating that prior to the onset of gastrulation the embryos were relatively intact.

At E6.5, *cp27* null intraembryonic tissues were greatly compressed (Fig. 15P) and the conceptus was populated by a condensation of extraembryonic endoderm (een) identified by the endoderm marker GATA4 (Fig. 15O). There was no distinct epiblast in the *cp27* null phenotype (Fig. 15P,R,T versus 15O,Q,S) although the anterior pole of the embryo retained a rudimentary extraembryonic ectoderm layer (ee) labeled by the ectoderm marker EED (Fig. 15Q,R). At E7.5, embryos were further degraded and there was no evidence of mesoderm formation (Fig. 15T), while the SNAIL marker clearly identified the mesoderm of control embryos (Fig. 15S).

In search for potential explanations for *cp27* null lethality, obvious similarities between nanog-deficient (Mitsui et al. 2003) and *cp27*-deficient mice were noted, since both phenotypes highlighted survival of extraembryonic endoderm-like cells in conjunction with epiblast failure. CP27 was abolished in the inner cell mass (ICM) of *cp27* null blastocysts already at E3.5 (Fig. 15H vs. 15G), while wild-type counterparts featured strong CP27 expression in the ICM. Loss of CP27 in blastocyst ICM dramatically reduced Nanog (Fig. 16A), and this reduction was likely to cause a failure in ICM derivation as seen in the failure to form an epiblast. In contrast, Nanog reduction did not affect the extraembryonic endoderm, which continued to proliferate (Fig. 15M,N BrdU) and occupied the majority of the *cp27* null rudiment during the final days prior to degradation. The lack of mesoderm and archenteron development in *cp27* null mice was also consistent with mutant phenotypes observed in another CP27 interaction partner, the

variant histone H2A.Z, which failed shortly after implantation and prior to gastrulation (E6)(Faast et al. 2001, Ridgway et al. 2004). In comparison to *Nanog* and *H2A.Z* null mice, the *cp27* null phenotype was less severe, consistent with low levels of Nanog and H2A.Z expression in CP27 mutant mice (Fig. 14K, 16A).

C. 5. CP27 regulates Nanog promoter via H2A.Z exchange

In search for potential explanations for *cp27* null lethality, analysis of core pluripotent transcription factors such as Nanog, Oct4, and Sox2 after CP27 siRNA treatment of ES cells was conducted. Since Nanog homozygous mutant mouse die between E3.5 and E5.5 with abnormal embryonic and extraembryonic tissue development, Oct4 homozygous knockout results in peri-implantation lethality with failure to develop a pluripotent inner cell mass, Sox2 null mutations implant but fail to develop an epiblast, and die shortly thereafter. CP27 knockout experiments for Nanog expression demonstrate an over 70% loss of Nanog mRNA.

Our CP27siRNA experiments demonstrate a 40% downregulation of Nanog expression in ES cells as revealed by western blot (Fig. 16B). However, Oct4 and Sox2 did not result in a significant change in siRNA treatmented cells. Moreover, Nanog mRNA expression was reduced by 77% and 67% respectively compare to wild type control in E3.5 and E6.5 day knockout embryos (Fig. 16A). Also we observed obvious similarities between Nanog mutant (Mitsui et al. 2003) and cp27 deficient mice, both displaying phenotype differentiation into endoderm-like cells in conjunction with epiblast failure; nevertheless, in cp27 null embryos, ectoderm like cells were still intact,

suggesting that loss of CP27 function affects not only pluripotent transcription factor Nanog, but also involves transcriptional activation during early development.

Here we focus on analyzing ES cell differentiation, whether the CP27/SRCAP complex regulates pluripotency transcription factors. CP27 knockout studies suggested that one of the important pluripotency transcription factors: Nanog, is downregulated in CP27 knockout mice. We tested whether the CP27/SRCAP complex binds the Nanog promoter region (Fig. 16C). ChIP assays were carried out using an antibody that recognized CP27, TIP49A, and DMAP1 (SRCAP complex subunit proteins), as well as an H2A.Z antibody for measuring levels of H2A.Z deposition. Our results demonstrate that CP27 and SRCAP complex subunits overlapped within Nanog promoter sites, and these binding sites were corresponding with those of H2A.Z deposition (Fig. 16C). Together, the CP27/SRCAP complex affects Nanog expression through the exchange of histone H2A with the variant H2A.Z within the Nanog promoter. Our assay suggested that CP27 is essential for ES cell differentiation during early development.

Next we tested how loss of CP27 affects H2A.Z deposition. Knockdown of CP27 experiment in mouse ES cells decreases H2A.Z deposition at the FAD synthetase and Nanog promoter sites as revealed by ChIP assay as shown with the antibody against H2A.Z (Fig. 16D). Here we demonstrate reduction of H2A.Z deposition at the -300 to -1000 and 200 to 500 regions of both the FAD and Nanog promoter. However, the -200 to 200 regions of the promoter were slightly decreased (Supplemental data), CP27 siRNA treatment reduced CP27 expression 40 to 60%, which may suggest that the -200 to 200 regions of H2A.Z deposition were not affected, explaining survival of CP27 siRNA treated cells. This region may be critical for transcriptional activity at the TSS site. Our

experiments also indicate that loss of CP27 affects the transcriptional activity of Nanog expression. However, H2A.Z siRNA treatment in ES cells demonstrates that H2A.Z depleted cells do not affect Oct4 and Nanog expression (Creyghton et al. 2008). In addition to explaining our data, the SRCAP complex (SWR1 in yeast) does not have a physiological role in transcriptional activation independent of H2A.Z, suggesting that SRCAP complex subunits including CP27 may have unique functions related to gene regulation.

Homologous SWR-C and SRCAP complex members

	S.cerevisiae		Homo sapiens	
Sub unit type				
ATPase	Swr1		SRCAP	
RubB-like	Rvb1	Rvb2	TIP49a	TIP49b
Actin	Act1		β-actin	
Actin-related protein	Arp4	Arp6	BAF53	ARP6
YEATS domain protein	Yaf9		GAS41	
Non-conserved subunit	Bdf1	Swc2	DMAP1	YL1
	Swc3	Swc4	XPG	tubulin
	Swc5	Swc6	**CP27**	ZnF-HIT1
	Swc7			

A

SRCAP complex

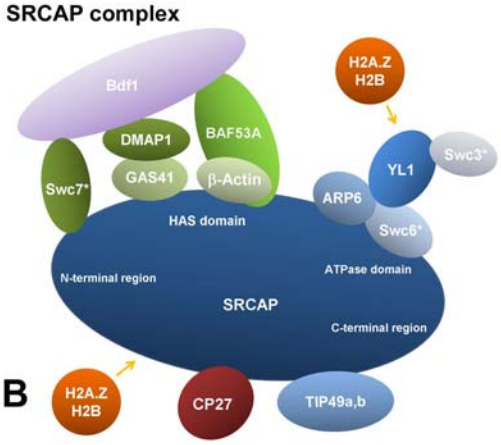

B

CP27 structure

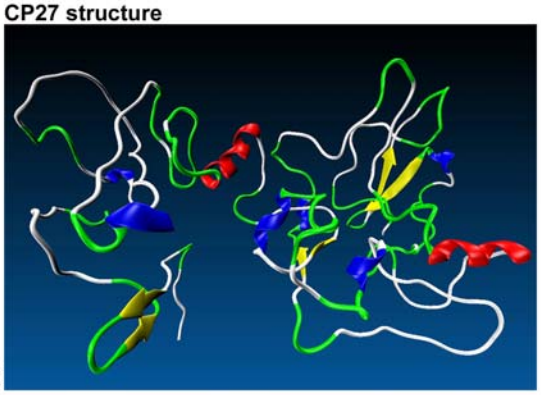

C

CP27 phylogenetic tree

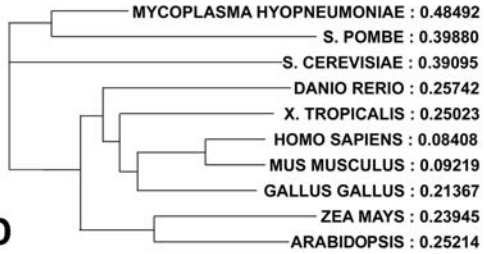

D

CP27 pI polarity

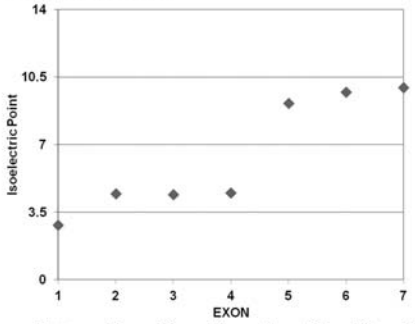

Exon	E1	E2	E3	E4	E5	E6	E7
AA position	1 to 22	to 61	to 130	to137	to 213	to 266	to 295
pI	2.833	4.466	4.417	4.493	9.136	9.733	9.968

E

Evolutionary shift in pI

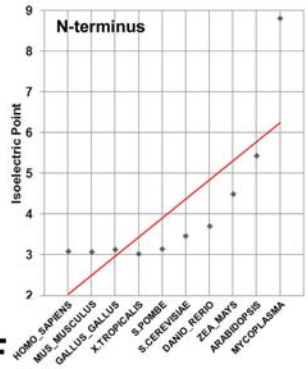

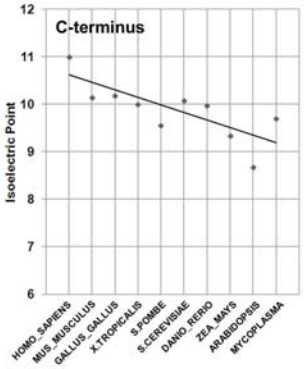

F

Fig. 12.

Structure and evolution of the SWR-C/SRCAP complex member CP27. (A) Comparison between conserved and non-conserved members of the yeast SWR-C and mammalian Snf-2-related CREB-binding protein activator protein (SRCAP) chromatin complex. CP27 is the mammalian homologue of yeast Swc5 based on sequence homology and domain organization. (B) Model of the mammalian SRCAP is a multiprotein chromatin remodeling complex. The SRCAP complex is organized around a principal component, the Snf-2-related CREB-binding protein activator protein (SRCAP), and contains multiple other members such as YL1, ZnF-HIT1, TIP49a, TIP49b, BAF53a, ARP6, GAS41, and DMAP1. In this sketch, CP27 was added because of its homology to Swc5 of the yeast SWR-C complex. (C) Predicted structure of CP27 containing multiple loops, turns and helices indicative of a highly interactive protein. (D) Phylogenetic relationship between CP27 homologues in living organisms indicative of conservation from plants to humans. (E) Isoelectric point distribution along the CP27 protein sequence reveals a highly acidic N-terminal half (exons 1-4, pI 3-4) set against a basic C-terminus (exons 5-7, pI 9-10). (F) Evolutionary trends in N-terminal and C-terminal isoelectric point. The C-terminal pI only marginally increased from plants to mammals from pI9 to pI11, while there was a steep decrease in N-terminal pI from pI5 to pI3.

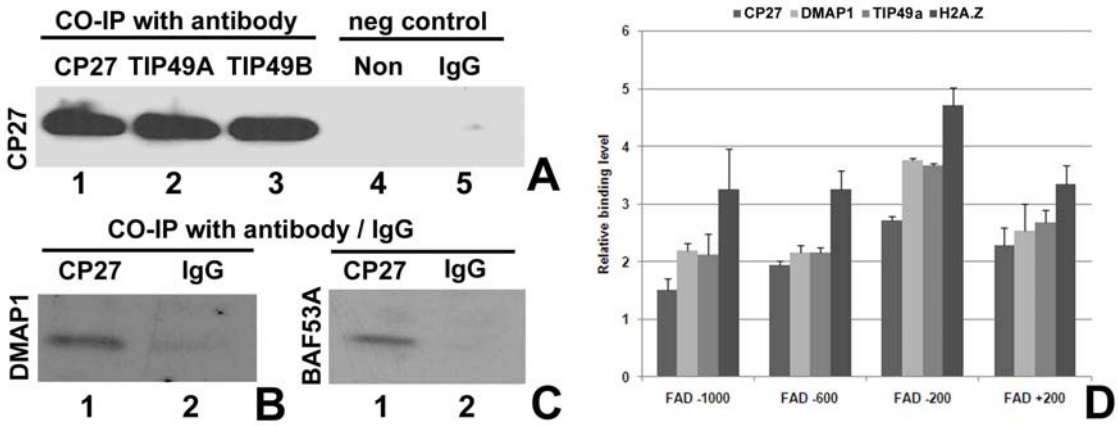
CO-IP with antibody
neg control
CP27 TIP49A TIP49B
Non IgG
CP27
1 2 3 4 5
A
CO-IP with antibody / IgG
CP27 IgG
DMAP1
1 2
B
CP27 IgG
BAF53A
1 2
C
CP27 DMAP1 TIP49a H2A.Z
Relative binding level
0 1 2 3 4 5 6
FAD -1000
FAD -600
FAD -200
FAD +200
D

Fig. 13.

CP27 is a member of the SRCAP complex. (A-C) Co-Immunoprecipitation of SRCAP complex subunits and CP27. (A) Lanes 1-3 were loaded with cell lysate precipitates generated by pull-down with antibodies against CP27 (lane 1), TIP49A (lane 2), and TIP49B (lane3). Lanes 4 and 5 are negative controls that were either incubated without antibody (lane 4) or with IgG (lane 5). The presence of CP27 in these precipitates was assessed by Western blot using an anti-CP27 antibody. (B,C) In both blots, lane 1 was loaded with the anti-CP27 antibody precipitate from cell lysate while lane 2 was loaded with IgG. Western blot was used to either identify DMAP1 (B) or BAF53A in these precipitates. (D) Promoter occupancy map of the proximal FAD promoter for CP27, and H2A.Z, and SRCAP complex subunits TIP49A and DMAP1. Overlapping occupancy at multiple sites would be suggestive of concerted activity of subunits within a complex. The Flavin adenine dinucleotide synthetase (FAD synthetase) promoter region has been previously identified as a high level SRCAP binding site. ChIP assays against four promoter fragments were performed using antibodies that recognized H2A.Z, CP27, TIP49A, and DMAP1. CP27, H2A.Z, TIP49a, and H2A.Z chromatin immunoprecipitates bound to the same location on the FAD promoter.

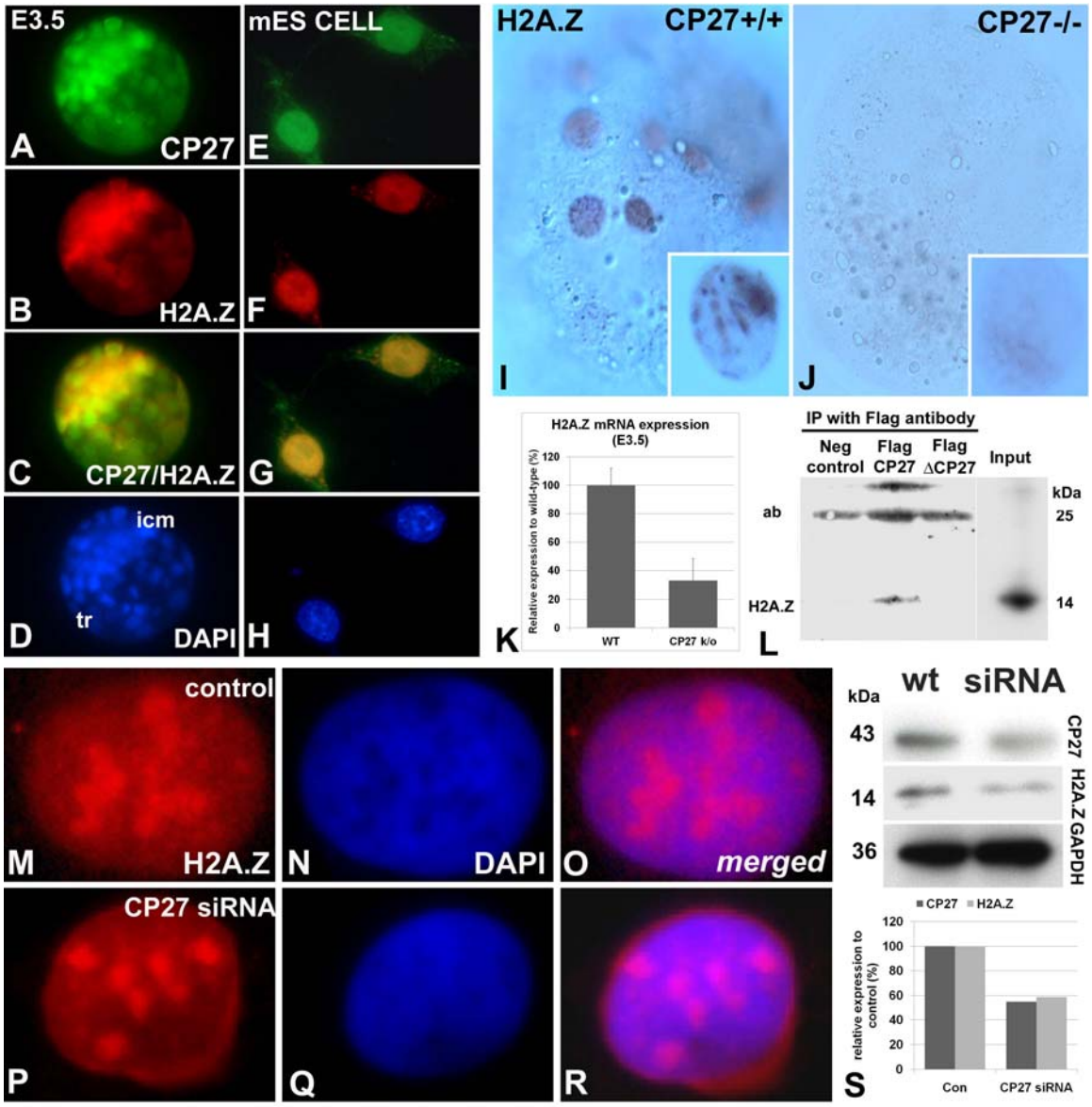
E3.5
mES CELL
A
CP27
E
B
H2A.Z
F
C
CP27/H2A.Z
G
icm
tr
D
DAPI
H
H2A.Z
CP27+/+
CP27-/-
I
J
H2A.Z mRNA expression (E3.5)
Relative expression to wild-type (%)
120
100
80
60
40
20
0
WT
CP27 k/o
K
IP with Flag antibody
Neg control
Flag CP27
Flag ΔCP27
Input
kDa
25
14
ab
H2A.Z
L
control
M
H2A.Z
N
DAPI
O
merged
CP27 siRNA
P
Q
R
wt
siRNA
kDa
43
14
36
CP27
H2A.Z
GAPDH
CP27
H2A.Z
relative expression to control (%)
120
100
80
60
40
20
0
Con
CP27 siRNA
S

Fig. 14.

Relationship between CP27 and H2A.Z. (A-H) Comparison of CP27 and H2A.Z localization in mouse E3.5 embryonic blastocysts (A-D) and mouse embryonic stem cells (E-H). This panel shows immunofluorescence micrographs for CP27 (green; A,E), H2A.Z (red; B,F), CP27/H2A.Z overlay (green/red; C,G) and DAPI (blue; D,H). H2A.Z and CP27 immunofluorescence overlapped and were strongly identified in the inner cells mass, with only a few areas of the trophoblast also displaying positive immunoreactivity (B and C). The position of inner cell mass (icm) and trophoblast (tr) are indicated as a reference (D). The broader expression pattern for CP27 as compared to H2A.Z was also observed on a cellular level in mouse embryonic stem cells (E-H). The overlay image i(G) shows yellow staining indicative of both CP27 and H2A.Z in the nucleus, while the cytoplasm fluoresced in green, representative of CP27 immunofluorescence. (I,J) Whole-mount immunoreactions against H2A.Z for E3.5 blastocysts from CP27-/- mice (J) and CP27+/+ mice (I) using an antibody against H2A.Z. Only wild-type blastocysts reacted with the antibody (Fig. 3I). Note the distinct H2A.Z immunoreactivity in the inner cell mass (I, insert). (K) H2A.Z mRNA expression levels in cp27 null and wild-type blastocysts as assessed by real-time qPCR, indicating reduced H2A.Z levels in CP27 null mice. (L) Chromatin immunoprecipitation with FLAG antibody identifies H2A.Z within a FLAG-tagged CP27 containing complex. Here, ES cells were co-transfected with a FLAG tagged empty vector (lane 1) as negative control, FLAG-tagged CP27 (lane 2) or a FLAG-tagged CP27 mutant (lane 3), respectively. Cells were then subjected to Chromatin immunoprecipitation with an anti-FLAG antibody using protein A beads. Western blots employing anti-H2A.Z antibody were used to identify H2A.Z in the lysate (lane 4; input) and in the immunoprecipitates (lane 1-3). The light chain of the Flag antibody was identified at 25kDa. The anti-H2A.Z antibody used for this Western blot recognized a single band at 14kDa representing H2A.Z as part of a Flag/CP27/H2A.Z chromatin complex pulled down by an anti-Flag antibody, but not when mutated CP27 was part of the Flag/ΔCP27/ chromatin complex. (M-R) Immunolocalization of H2A.Z in wild-type (M-O) and CP27 siRNA treated cells (P-R). (M,P) H2A.Z immunofluorescence, (N,Q) DAPI-positive euchromatin, (O,R) merged H2A.Z/DAPI overlays. Following CP27 siRNA transfection, nuclei became DAPI-positive throughout, and dark areas indicative of euchromatin were greatly reduced (Q). H2A.Z immunopositive regions co-localized with DAPI-unstained euchromatin nuclear areas in overlay micrographs (O,R). As a result, DAPI/H2A.Z-merged micrographs highlighted alternating regions for H2A.Z (red color) and euchromatin (blue color) with only little overlap. (S) Western blot analysis of CP27 siRNA treated cells. The CP27 knockdown experiment in ES cells resulted in a 42% reduction of H2A.Z and 44% reduction of CP27 protein expression as detected by densitometry.

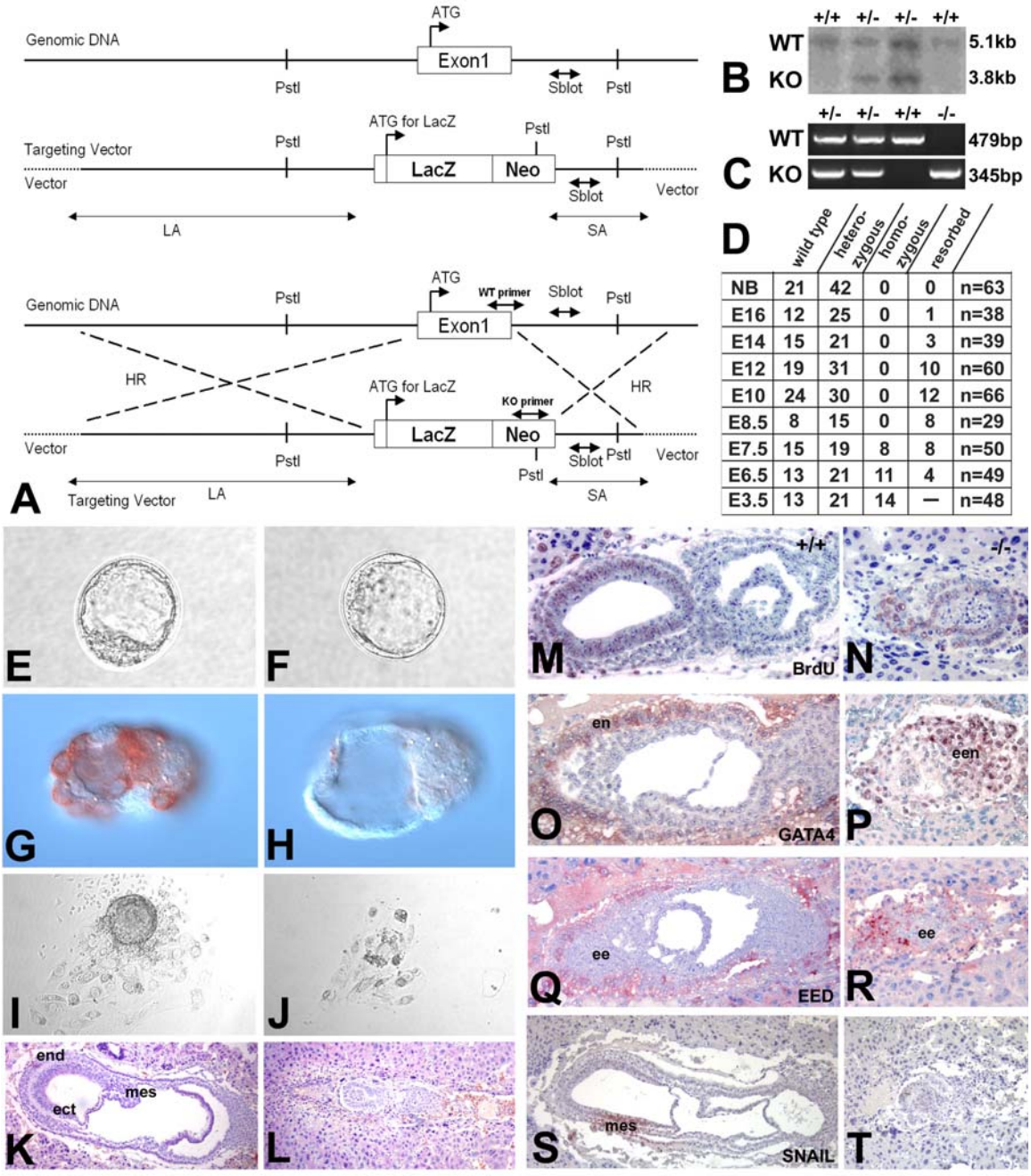
A
Genomic DNA
ATG
Exon1
PstI
SblotI
PstI
Targeting Vector
Vector
ATG for LacZ
PstI
PstI
LacZ
Neo
SblotI
Vector
LA
SA
Genomic DNA
ATG
WT primer
SblotI
PstI
Exon1
HR
HR
ATG for LacZ
KO primer
Vector
LacZ
Neo
SblotI
PstI
Vector
PstI
PstI
Targeting Vector
LA
SA
B
+/+ +/- +/- +/+
WT
KO
5.1kb
3.8kb
C
+/- +/- +/+ -/-
WT
KO
479bp
345bp
D
wild type
hetero-zygous
homo-zygous
resorbed
NB 21 42 0 0 n=63
E16 12 25 0 1 n=38
E14 15 21 0 3 n=39
E12 19 31 0 10 n=60
E10 24 30 0 12 n=66
E8.5 8 15 0 8 n=29
E7.5 15 19 8 8 n=50
E6.5 13 21 11 4 n=49
E3.5 13 21 14 — n=48
E
F
G
H
I
J
K
end
mes
ect
L
M
+/+
BrdU
N
-/-
O
en
GATA4
P
een
Q
ee
EED
R
ee
S
mes
SNAIL
T

Fig. 15.

***cp27* conventional knockout mouse targeting results in collapse of the embryo during early gastrulation.** (A-D) Mouse targeting. **(**A) Targeting construct. PstI; restriction enzyme site for Southern blot; HR, region of homologous recombination. (B) Southern Blot of mouse genomic DNA from *cp27* k/o and wild type mice digested with PstI. This probe detected a band of ~5.1kb size for the wild type allel and a band of ~3.8kb for the mutant allel. (C) PCR analysis of genotypes. Wild-type embryos were identified using a 479bp fragment based on the WT primer from our map in (A) while mutant embryos were identified by a 345bp fragment amplified using the K/O primer (A). (D) Survival rates after crossing *cp27* heterozygous mice. Homozygous progeny was observed from E3.5 blastocysts to E7.5 embryos. From E8.5 until newborn, there was no homozygous offspring, while the number of resorbed/degrading embryonic masses peaked at days E10 and E12. (E-L) CP27 blastocyst and embryonic phenotype analysis. There were no obvious morphological differences between wild-type (E,G) and CP27 mutant blastocysts (F,H). (G,H) Whole mount immunohistochemistry against CP27 for wild-type blastocysts (G) and mutant blastocysts (H). Only wild-type blastocysts reacted with the antibody. (I,J) Comparison of inner cell mass (ICM) growth between *cp27* null and WT E3.5 blastocysts cultured in ES cell medium without LIF. The WT group featured distinct inner cell mass (ICM) condensations (I) while the inner cell mass was lost in the *cp27* null group and only a few single cells remained (J). At embryonic stage E7.5, the *cp27* null mice (L) displayed rudimentary embryonic tissue compared to the same-stage, mid-gastrulation wild-type mouse embryos featuring differentiated germ layers ectoderm (ect), mesoderm (mes), and endoderm (end) (K). (M-T) Analysis of WT and CP27 mutant embryos using markers for proliferation (M,N) and germ layers (O-T). Both the wild-type (M) and the knockout tissue sections (N) reacted positively for BrdU, with BrdU in the null section restricted to the distal extraembryonic endoderm (N). (O-T) Immunohistochemical analysis of germ layer organization in developing mouse embryos (O,Q,S) and their same-stage *cp27* null counterparts (P,R,T). The endoderm marker GATA4 recognized the extraembryonic endoderm layer (een) in E6.5 control sections (O), while it only recognized a set of cuboidal individual cells in the cp27 null embryo (een). The ectoderm marker EED (ee) was greatly diminished in *cp27* null progeny (R) and only formed a narrow layer when compared to wild-type counterparts (Q). The SNAIL mesoderm marker gene was entirely absent in *cp27* null embryos (T) while there was highly specific SNAIL expression in late E7 wild-type embryos (S). Note the missing amniotic cavity in *cp27* knockout embryos (N,P,R,T) compared to wild-type controls (adjacent panel on the left).

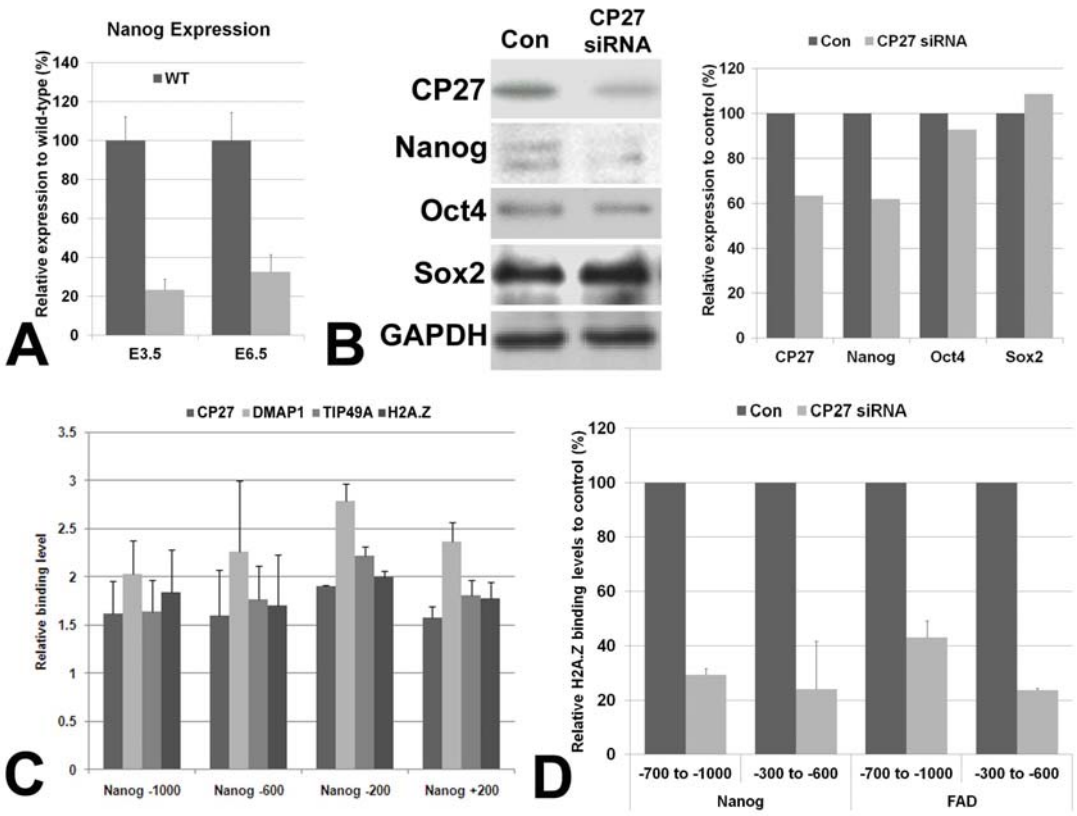
A
Nanog Expression
WT
Relative expression to wild-type (%)
140
120
100
80
60
40
20
0
E3.5
E6.5
B
Con
CP27 siRNA
CP27
Nanog
Oct4
Sox2
GAPDH
Con
CP27 siRNA
Relative expression to control (%)
120
100
80
60
40
20
0
CP27
Nanog
Oct4
Sox2
C
CP27
DMAP1
TIP49A
H2A.Z
Relative binding level
3.5
3
2.5
2
1.5
1
0.5
0
Nanog -1000
Nanog -600
Nanog -200
Nanog +200
D
Con
CP27 siRNA
Relative H2A.Z binding levels to control (%)
120
100
80
60
40
20
0
-700 to -1000
-300 to -600
-700 to -1000
-300 to -600
Nanog
FAD

Fig. 16.

CP27 affects histone H2A.Z deposition and expression. (A) Comparison of H2A.Z expression between cp27 null and wild type blastocysts (E3.5) and E6.5 embryos. (B) Lack of CP27 affects only the pluripotent transcription factor Nanog, but not Sox2 and Oct4. Western blot analysis indicates that the CP27 knockdown experiment in ES cells resulted in a 39% reduction of Nanog and 37% reduction of CP27 protein expression as detected by densitometry. (C) Promoter occupancy map of the Nanog promoter for CP27, and H2A.Z, and SRCAP complex subunits TIP49A and DMAP1. Overlapping occupancy at multiple sites would indicate the presence of an active SRCAP complex on the Nanog promoter. ChIP assays indicated that CP27, H2A.Z, TIP49a, and H2A.Z chromatin immunoprecipitates bound to the same location on the Nanog promoter. (D) CP27 siRNA treated ES cells reduced H2A.Z deposition. ES were transfected with CP27 siRNA and control (Con), and ChIP assays were performed using an antibody that recognized H2A.Z. ChIP assays revealed high levels of H2A.Z and reduction in H2A.Z after CP27 siRNA treatment at Nanog (-700 to -1000, -300 to -600) and FAD synthetase (-700 to -1000, -300 to -600) promoter sites that had shown high binding levels in our previous ChIP assay.

Supplement 1

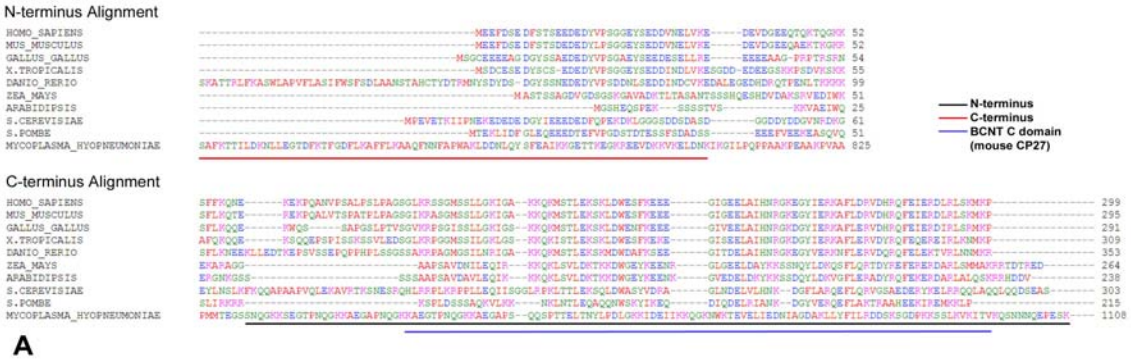

A

Isoelectric Point

	HOMO_SAPIENS	MUS_MUSCULUS	GALLUS_GALLUS	X.TROPICALIS	S.POMBE	S.CEREVISIAE	DANIO_RERIO	ZEA_MAYS	ARABIDOPSIS	MYCOPLASMA
N-terminus	3.091	3.07	3.136	3.032	3.152	3.469	3.704	4.502	5.433	8.803
C-terminus	10.99	10.132	10.173	10	9.505	10.076	9.97	9.331	8.677	9.703

Alignment Position

	HOMO_SAPIENS	MUS_MUSCULUS	GALLUS_GALLUS	X.TROPICALIS	S.POMBE	S.CEREVISIAE	DANIO_RERIO	ZEA_MAYS	ARABIDOPSIS	MYCOPLASMA
N-terminus	1-36	1-36	1-31	1-39	1-37	1-47	1-83	1-36	1-10	726-805
C-terminus	197-299	193-295	194-291	207-309	145-215	186-303	245-353	157-246	184-238	978-1108

B

ORGANISM	ACCESSION NUMBER	Symbol
Mycoplasma hyopneumoniae 232	YP_115696	p97
Schizosaccharomyces pombe 972h	NP_588440.1	swc5
Saccharomyces cerevisiae S288c	NP_009790.1	SWC5
Danio rerio	ENSDARP00000073626	cfdp1
X. tropicalis	NP_001017329.1	cfdp1
Homo sapiens	NP_006315.1	CFDP1
Mus musculus	NP_035931.1	CP27
Gallus gallus	NP_001001189.1	CFP1
Zea mays	GRMZM2G113391	cfdp1
Arabidopsis lyrata	XP_002872335	ARALYDRAFT

C

Supplement 2

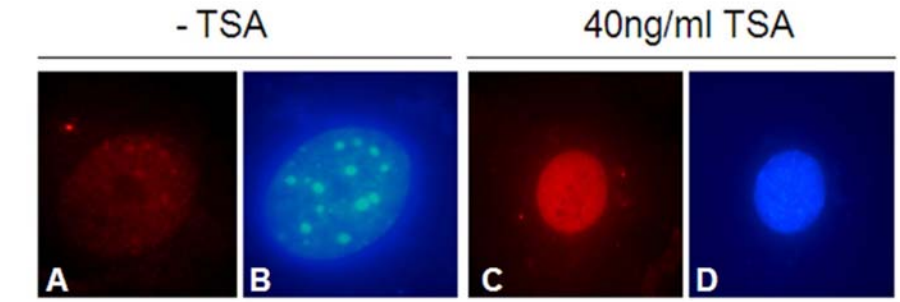

A

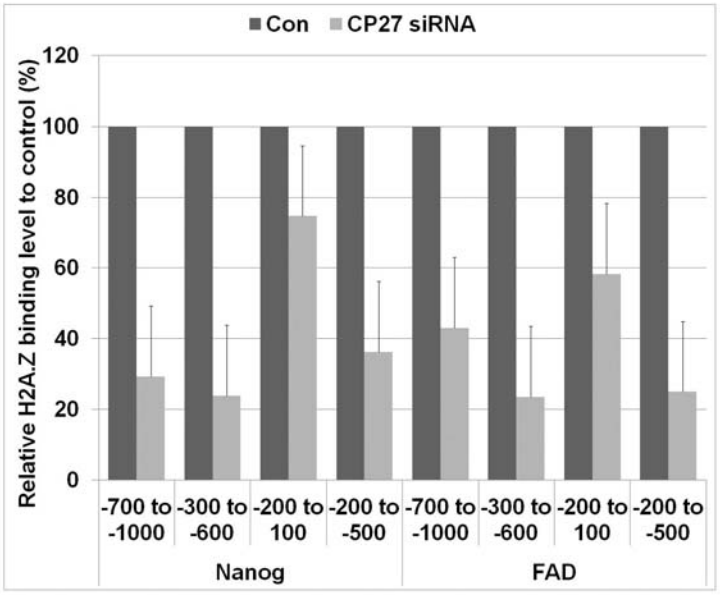

B

IV. DISCUSSION

A. Characterization of the mouse CP27 promoter and NF-Y mediated gene regulation

The present study is the first analysis of the CP27 promoter structure and function. For our analysis we have cloned the promoter of the mouse CP27 gene, examined its transcriptional activity, and identified a transcription factor in the proximal promoter region. Our studies demonstrated that the similar patterns of CP27 transcriptional activity were displayed in NIH 3T3 cells. Two major transcription start sites were mapped adjacent to exon 1. Functional analysis of the 5′ flanking region by progressive 5′deletion mutations revealed transcription repression elements between −1993 bp and −969 bp as well as several positive elements between −968 bp and the preferred transcription start site. Furthermore, deletion analyses identified an enhancer element within 93 bp of the CP27 proximal promoter. EMSA experiments and function study demonstrated that NF-Y was involved in the activation of the CP27 proximal promoter through two CCAAT boxes. A binding site in the 3′ flanking region of CCAAT box 1 affected the efficiency of NF-Y binding. Together, these studies provide a basis for our understanding of the regulation of the CP27 gene.

NF-Y binding CCAAT boxes have been identified as crucial determinants of proper gene regulation related to cell growth (Bhattacharya et al., 2003, Elkon et al., 2003 and Testa et al., 2005). The histone-like NF-Y substitutes H2A-H2B and finely tunes histone methylation and acetylation on CCAAT-containing promoters (Gatta and

Mantonani, 2008 and Gurtner et al., 2008). As a bifunctional transcription factor, NF-Y binding is associated with both positive and negative histone marks (Ceribelli et al., 2008 and Donati et al., 2008). Most cell-cycle regulated promoters contain CCAAT boxes and promoters of genes with key roles in the G2/M transition have multiple CCAAT motifs, such as cyclin B1 (two), cyclin B2 (three), cdc25c (three), and HSP 70 (two) (Li et al., 1998, Salsi et al., 2003 and Muller et al., 2007). These promoters rely on multiple CCAAT boxes activated by NF-Y, whose binding to DNA is temporally regulated during the cell cycle (Alder et al., 1992, Wasner et al., 2008 and Zwicker et al., 1995). Inhibition of NF-Y mediated transcription activation arrested cells at G2/M phase and suppressed expression of genes activated at G2/M phase of the cycle (Hu et al., 2006). P53/NF-Y complexes binding to NF-Y target promoters are associated with direct p53 transcriptional repression during the G2/M phase (Di Agostino et al., 2006 and Imbriano et al., 2006). The functional implementations of these studies have been confirmed in cell lines as well as in knock-out animal model in vivo. For example, expression of the domain-negative mutant of CBF/NF-Y in mouse fibroblasts resulted in a retardation of cell growth. Furthermore, deletion of both NF-YA alleles caused a specific block of cell proliferation and cell death in embryonic fibroblasts (Bhattacharya et al., 2003, Chae et al., 2004 and Hu et al., 2000). Lastly, a conditional knockout animal model in which the inactivation of NF-YA caused early embryonic lethality (Bhattacharya et al., 2003) provided support for a pivotal role of NF-Y-mediated transcription in embryonic development.

The mouse CP27 promoter features multiple CCAAT boxes. NF-Y interacts with these CCAAT boxes and enhances cp27 gene expression. Studies from our laboratory

have demonstrated that similar to other NF-Y target genes, CP27 plays significant roles in cell proliferation and mouse organogenesis (Diekwisch and Luan, 2002 and Luan and Diekwisch, 2002). Loss of CP27 function inhibited cell growth and induced apoptosis in embryonic fibroblast cells (Luan and Diekwisch, 2002). Deletion of both CP27 alleles in knock-out mice resulted in early embryo lethality and knock-down of the cp27 gene caused cell death (unpublished data). Here we are proposing that NF-Y regulation of CP27 expression provides a meaningful explanation for the powerful effects of CP27 that we have documented in previous studies (Diekwisch and Luan, 2002) and that we are currently confirming in knockout and transgenic models in our laboratory (data not published). Besides CP27, NF-Y affects a number of other genes essential to early embryonic and craniofacial development, including the chondrogenesis gene SOX9 (Pan et al., 2009), the early fibroblast growth factor FGF4 (Bermadt et al., 2005), the fibroblast growth factor receptor 2 promoter in osteoblasts (Sun et al., 2009), the tooth enamel gene amelogenin (Xu et al., 2006), and the tooth dentin gene dentin sialophosphoprotein (Chen et al., 2008). Underscoring NF-Y's essential role in early mouse development and cell proliferation, gene targeting studies have resulted in early embryonic lethality (Bhattacharya et al., 2003).

NF-Y has been demonstrated to interact with the CCAAT box in both forward and reverse orientation in eukaryotic promoters and has been shown to absolutely require all 5 nucleotides of the CCAAT box (Pan et al., 1999, Hu et al., 2000, Xiong et al., 2000, and Zhou and Snead, 2000). Our mutation analysis established that a mutation from CCAAT to CACAT almost abolished NF-Y binding activity and CP27 promoter function, which further confirmed the importance of the intact CCAAT pentanucleotides

in cp27 gene regulation. In addition to the functional importance of the CCAAT core sequence, database analysis and functional studies revealed that the adjacent flanking nucleotides (C, Pu, Pu, on the 5′-side and C/G, A/G, G A/C, G on the 3′-site) of the CCAAT box are required for efficient binding of NF-Y (Mantovani, 1998). In comparison to the CCAAT consensus sequence including its flanking regions, the mouse CP27 CCAAT motif (TGACCAATCGCAG) has 85% homology with the common consensus sequence (Mantovani, 1998), indicating that the mouse CP27 CCAAT motif may demonstrate similar binding behavior as CCAAT promoter regions of other genes and species.

Interactions between NF-Y and more distal flanking regions of the CCAAT box have been established by previous footprinting experiments (Bi et al., 1997). The sequences protected from hydroxyl radical cleavage are located on both 5′ and 3′ flanking regions. The function of these protected regions is suggested to provide minimal DNA fragments required for proper binding by NF-Y. Partial removal of one of these regions leads to a decrease in binding (Romier et al., 2003). Complete removal of the protected region from the 3′ flanking side not only alters the affinity of NF-Y for its binding site but also the electrophoretic mobility of the NF-Y–DNA complex (Romier et al., 2003, and Sugira and Takishima, 2003). It is not known whether the DNA sequence of the distal region is specific for the NF-Y binding or only necessary for proper distortion of the DNA. In the present study, we have provided evidence that the specific sequence of the protected binding site is critical for NF-Y to interact with the CCAAT box. Sequence analysis of the 3′ protected region in the pro-α1(I) collagen, pro-α2(I) collagen (Bi et al., 1997) and CP27 promoter revealed that the binding sites are located between

10 and 16 bp downstream of the CCAAT box, in an equivalent position to the CP27 CGGA motif. Our supershift assays indicate that a crucial CGGA binding site in the 3′ flanking region of the CCAAT box affected NF-Y binding, resulting in lower binding activity for the mutated CGGA motif (mutated to TACA) interacting with NF-Y. Thus, our studies introduce CGGA as a CP27-related motif for CCAAT-box mediated NF-Y binding.

Using primer extension assay, ribonuclease protection assays and 5′ RACE, we identified two candidate sites as potential CP27 transcription start sites 140 and 98 bp upstream of the ATG initiation codon. The presence of several different transcription start sites is a common feature of mammalian genes. Splicing of exons is one way to shift the location of transcription start sites (Rustighi et al., 1999 and Yu et al., 1999). In the present study, we have detected two different transcripts of the cp27 gene in the odontoblast cell line OB1 by Northern blot analysis (data not shown). In other cases, one gene may contain several hitherto unidentified 5′ untranslated regions (Menon et al., 1995, and Mu and Burt, 1999). To date, only two full-length mouse CP27 cDNA sequences have been reported (GenBank NM_011801 and BC_005589). These are only a few nucleotides apart from each other. Multiple transcription start sites are often cell line specific (Schrodeder and Myers, 2008), and the multiplicity of transcription start sites may play a role in the tissue-specific expression of the cp27 gene at various stages of development. Transcription start sites differ between various sub-species or strains since 5′-RACE assays using different cell lines established from various mouse strains yielded different transcription start sites of the cp27 gene (data not shown). Based on our 5′ RACE study and published information on CP27 cDNA clone regions, we have defined

the start site 102 nucleotides upstream of the initiation codon as preferred transcription start site. In addition, this site is the shortest 5′ transcription start site. Together, our CP27 function studies in tandem with studies on the NF-Y transcriptional network indicate that CP27 may act in synchronicity with other NF-Y regulated genes to modulate cell proliferation and cell survival in craniofacial development. In this context, the present study uncovers the contribution of NF-Y in cp27 gene regulation and provides a further explanation of cp27 gene function in the NF-Y-mediated transcriptional network of genes.

B NF-Y and USF1 transcription factor binding to CCAAT-box and E-box elements activates the CP27 promoter

In the present study we have identified a CCAAT-box and an E-box as cis-acting promoter elements of the TATA box-less CP27 promoter and characterized their regulation in ES cells through the transcription factors NF-Y and USF1. The CP27 gene encodes a novel chromatin factor required for mouse development and germ layer differentiation, and CP27 is highly expressed in inner cell mass (ICM) of developing blastocysts. Loss of CP27 caused severely disturbed epiblast development (not published). The distinct expression of CP27 in the ICM and the effect of CP27 on epiblast development were the reason for selecting ES cells as a model system to study the regulation of CP27 in ES cells.

Two cis-regulatory elements, a CCAAT-box and an E-box, were identified in the CP27 proximal promoter by deletion mutation and footprint analysis. Among several transcription factor binding candidates, NF-Y was identified as the CCAAT-box binding protein and USF1 as the E-box binding protein. Previous studies have reported combined CCAAT-box/E-box structures in the HOXB4 proximal promoter (Zhu et al., 2003) and in HOXC4 and HOXD4 promoters of both human and mouse (Zhu et al., 2005). The close relationship between the CCAAT-box and the E-box and the interaction between NF-Y and USF1 suggests that NF-Y and USF1 might cooperate in the regulation of CP27 gene expression. In our studies, overexpression of exogenous NF-YA and USF1 upregulated CP27 promoter activity and endogenous CP27 gene expression, suggesting a synergistic interaction between NF-Y and USF1. Explaining the function of a combined CCAAT-box/E-box structure, previous studies have indicated that NF-Y is not a powerful

transcription activator but rather a promoter organizer which co-operates with neighboring transcription factors to modulate the transcriptional activity of target genes (Testa et al., 2005, Ceribelli et al., 2008 and Nicolas et al., 2003). In the case of the CP27 proximal promoter, this would imply that NF-Y might cooperate with USF1 to regulate CP27 transcription. In support of a functional interaction between NF-Y and USF1 we have shown that CCAAT-box mutation reduced the activity of the CP27 proximal promoter by 80.74%, while maintaining the CP27 basal promoter function. In contrast, mutation of CP27 E-box completely abolished the function of the CP27 proximal promoter even though the CCAAT-box structure remained intact. These results indicate that the regulatory role of NF-Y may depend on the transcriptional regulatory partners to which it binds in a given genomic and cellular context (Zhu et al., 2003 and Matuoka, 1999).

On a biological level, these data indicate that the effect of the ES cell proliferation transcription factor NF-Y on the CP27 promoter is synergistically modulated by a second transcription factor, USF-1. Here we have shown that in tandem with NF-Ya downregulation, USF-1 shuttles from the center of the nucleus to the nuclear envelope, a potential transcription factor resting place (Heessen and Fornerod, 2007). Thus, regulation of CP27 gene expression to facilitate ES cell proliferation may require the physical interaction between USF-1 and NF-Ya in ES cell nuclei.

We conclude that through CCAAT-box and E-box promoter elements, the CP27 proximal promoter is jointly and interactively regulated by two important transcriptional factors, NF-Y and USF1. NF-Y is a ubiquitous transcription factor that promotes proliferation while USF1 has been linked to the inhibition of cell differentiation (Zhu et

al., 2003, Grskovic et al., 2007 and Jiang and Mendelson, 2003 B. Jiang and C.R. Mendelson), USF1 and USF2 mediate inhibition of human trophoblast differentiation and CYP19 gene expression by Mash-2 and hypoxia. (Jiang and Mendelson, 2003). Our studies provide a functional link between the transcriptional regulators NF-Y and USF1 and ES cell growth through the regulation of CP27 gene expression.

C. The H2A.Z Exchange Histone Chaperone CP27 regulates ES cell Pluripotency through Nanog

Here we report that a highly conserved chromatin factor, CP27, is essential for proliferation and germ layer differentiation during early postimplantation-stage embryonic development. In order to explain the mechanisms behind CP27's essential role in development, we demonstrate that CP27 regulates Nanog expression on a chromatin level. CP27 also dramatically affects the histone variant H2A.Z, a key chromatin component in embryonic development, positioning CP27-containing chromatin complexes in a unique role related to pluripotency maintenance and germ layer differentiation. The effect of loss of CP27 on H2A.Z was accompanied by dramatic changes in the chromatin transcriptional configuration as revealed by a shift in euchromatin/heterochromatin boundaries. We propose here that CP27 affects embryonic development by regulating both Nanog and H2A.Z and by modulating chromatin-mediated pluripotency of germ layer cells.

cp27 Null mice were lethal prior to E8 suggesting that CP27 plays an essential role during early development. Already in earlier studies, CP27 gene products have demonstrated dramatic effects during organogenesis (Diekwisch and Luan, 2002a). In addition, knockdown of *Drosophila* Bcnt (Yeti) by RNA interference caused larval stage lethality (personal communication, cited in Iwashita et al., 2006), and *Drosophila* DOM mutants lost germline stem cell self-renewal (Xi and Xie, 2005). In contrast, deletions of Swc5 in yeast remained viable, but demonstrated a number of sensitivities.

In order to exploit the *cp27*$^{-/-}$ phenotype for clues toward potential pathways or mechanisms that might be affected by its function as a chromatin complex member, we compared gastrulation stage events in *cp27*$^{-/-}$ mice with similar defects in other, possibly related mouse models. Early embryonic lethality is a common feature in many epigenetic machineries affecting stem cell pluripotency, including polycomb repressive complexes, the RNAse III Dicer1, and chromatin remodeling/histone exchange proteins (reviewed in Niwa, 2007). Embryonic lethalities also occur when other pluripotency factors are lost, albeit in germ layer manifestations different from the *cp27* phenotype: *Sox2* null mice die at implantation and fail to generate an epiblast (Avilion et al., 2003) while *Oct4* mutant offspring lacks a pluripotent inner cell mass and differentiates along extraembryonic trophoblast lineages (Nichols et al., 1998). The embryonic lethalities caused by deficiencies in two CP27 interacting partners studied here, H2A.Z and Nanog, are characterized by implantation stage death (*H2A.Z*, Faast et al. 2001) and epiblast formation failure together with extraembryonic endoderm proliferation (*Nanog*, Mitsui et al. 2003). In comparison to *H2A.Z* and *Nanog* null embryos, *cp27*$^{-/-}$ postimplantation development was slightly more successful, featuring epiblast failure and endoderm lineage differentiation. The slightly further advanced development of *cp27*$^{-/-}$ embryos over their *H2A.Z* and *Nanog* counterparts is consistent with the finding that both H2A.Z and Nanog were clearly reduced but not abolished by CP27. Another factor that is likely to contribute to the early lethality in *cp27* null mice was the thinning and disruption of Reichert's membrane, since disruption of the barrier function of Reichert's membrane could lead to lethality due to a toxic effect of direct exposure of the embryo to the maternal circulation or uterine environment (Williamson et al. 1997).

Our findings indicate that CP27 function significantly affects the prominent ES cell pluripotency factor Nanog. Based on analyses of *Nanog* loss of function (Mitsui et al. 2003), the effect of CP27 on Nanog expression might play a significant role in the early lethality and the failure of germ layer organization in *cp27*$^{-/-}$ mice, a result that was further supported by our cell culture and the prominent GATA4 labeled endoderm-like cells in the center of *cp27*$^{-/-}$ embryos described here. Low levels of *Nanog* expression that were still present in *cp27* null blastocysts might consequently account for slightly further development of *cp27*$^{-/-}$ compared to *Nanog* null mice. Explaining the effect of Nanog during the development of the *cp27*$^{-/-}$ phenotype we found that a CP27 containing chromatin complex directly bound two regions on the *Nanog* promoter, one together with H2A.Z and a second that was exclusive to CP27. This finding suggests some degree of interaction between CP27 and H2A.Z in the regulation of Nanog expression, while CP27 alone might have additional unique mechanisms to interact with Nanog.

Our studies on the effect of CP27 on H2A.Z documented (i) a dramatic reduction of H2A.Z in *cp27*$^{-/-}$ mice (immunoreactions and Real-Time PCR), (ii) changes in H2A.Z nuclear expression pattern in CP27 knockdown cells, (iii) overlapping expression patterns between CP27 and H2A.Z in blastocysts and ES cells, and (iv) interaction between CP27 and H2A.Z through a CP27 containing chromatin complex (ChIP assay). Together, these data provide ample evidence that CP27 interacts with H2A.Z on a chromatin level and affects H2A.Z expression and function. Our findings are supported by a number of earlier findings suggesting a possible relationship between CP27 and H2A.Z, including (i) yeast genetics studies related to Swc5, the yeast orthologue of CP27 that shares 45% homology with CP27 and is part of the yeast SWR complex (Diekwisch et al., 1999) implicated the

SWR chromatin remodeling complex in the exchange of the chromatin-bound histone H2A with the histone variant H2A.Z (Krogan et al., 2003; Kobor et al., 2004, Mizugushi et al., 2004; Wu et al., 2005; Ruhl et al., 2006; Wong et al., 2007), (ii) striking similarities between the previously described *H2A.Z* null phenotype (Faast et al., 2001; Ridgway et al., 2004) to our *cp27*$^{-/-}$ mouse, including a failure of mesoderm formation in tandem with collapse of the archenteron, and (iii) remarkable similarity between CP27 and H2A.Z expression in the chordal mesoderm during early mouse development (Diekwisch et al., 1999; Ridgway et al., 2004).

There are a number of possibilities as to how CP27 might modulate H2A.Z that remain yet to be uncovered, but one likely scenario involves helix-loop-helix protein interactions between CP27 and H2A.Z since both proteins contain helix-loop-helix configurations (Diekwisch et al., 1999, Suto et al., 2000). In such a scenario, a close relationship between CP27 and H2A.Z would allow for other SWR complex members to alter H2A.Z function through ATP-dependent chromatin remodeling via the Swi2/Snf2 ATPase and histone acetylation through the NuA4 histone acetyltransferase. Evidence for such a model has been provided by recent studies indicating that H2A.Z acetylation plays an essential role in restricting silent chromatin (Babiarz et al., 2006) and that the acetylation of H2A.Z by NuA4 is a prerequisite for its exchange by the SWR-C (Kobor et al., 2004). In this setting, CP27 might act as a co-activator or co-regulator of H2A.Z function. Alternatively, both CP27 and H2A.Z might also act directly on chromatin, and their combined effects might fine-tune transcriptional activity in ES cells. Sequence comparison between mouse *cp27* and the yeast *cp27* orthologue *Swc5* reveals that only the *cp27* C-terminus is homologous between yeast and mouse (130AA, 60AA strong

homology). Our C-terminal *cp27* sequence modification and subsequent H2A.Z/CP27 ChIP IP study indicates that this region is important for the interaction with H2A.Z, suggesting that in its evolution from yeast to mammals, *cp27* might have developed an entirely new N-terminal domain that is functionally independent from the original H2A.Z interaction motif.

Here we have hypothesized that CP27 controls the nuclear transcriptional landscape through its interaction with the histone variant H2A.Z, and that these changes in chromatin configuration affect ES cell lineage specification by regulating Nanog expression. In support of our hypothesis, loss of CP27 eliminates low-level H2A.Z expression across the nucleus and enriches H2A.Z in transcriptionally active euchromatin regions. Low levels of H2A.Z expression in ES cells prevents heterochromatin spreading (Meneghini et al. 2003) which in turn allows the ES cell chromatin to remain transcriptionally open (Meshorer and Misteli 2006). Once CP27 is lost, H2A.Z reduction facilitates heterochromatin spreading and further rigidifies euchromatin/heterochromatin boundaries by eliminating residual levels of H2A.Z from transcriptionally inactive sites. The effect of CP27 on the ES cell nuclear landscape, perhaps in conjunction with H2A.Z, explains the role of CP27 in keeping the ES cell transcriptional machinery active and to facilitate the expression of Nanog and other pluripotency factors involved in germ layer differentiation and gastrulation.

V. CONCLUSION

CP27 function studies in tandem with studies on the NF-Y transcriptional network indicate that CP27 may act in synchronicity with other NF-Y regulated genes to modulate cell proliferation and cell survival in craniofacial development. In this context, the present study uncovers the contribution of NF-Y in *cp27* gene regulation and provides a further explanation of *cp27* gene function in the NF-Y-mediated transcriptional network of genes.

We conclude that through CCAAT-box and E-box promoter elements, the CP27 proximal promoter is jointly and interactively regulated by two important transcriptional factors, NF-Y and USF1. NF-Y is a ubiquitous transcription factor that promotes proliferation while USF1 has been linked to the inhibition of cell differentiation. Our studies provide a functional link between the transcriptional regulators NF-Y and USF1 and ES cell growth through the regulation of CP27 gene expression.

The effect of CP27 on the ES cell nuclear landscape, perhaps in conjunction with H2A.Z, explains the role of CP27 in keeping the ES cell transcriptional machinery active and to facilitate the expression of Nanog and other pluripotency factors involved in germ layer differentiation and gastrulation.

TABLE I

PRIMERS USED IN THE AMPLIFICATION OF PCR FRAGMENTS FOR PROMOTER–REPORTER GENE CONSTRUCTS

Primer	Oligonucleotide sequence	Orientation
−1993/−1973	5′TACCGAGCTCGGCTAACCTGCTCAACTTTGG3′	sense
−1255/−1234	5′TACCGAGCTCTCTTAGGCTGATTCCCATTGC3′	sense
−1190/−1169	5′TACCGAGCTCGCATTGGTTGGTCCTCCCGAT3′	sense
−969/−947	5′TACCGAGCTCAGGTGATTTCTGAGGGACTAGGG3′	sense
−720/−699	5′TACCGAGCTCTCTAGCACTTTGTGTAGTGGC3′	sense
−207/−186	5′TACCGAGCTCTATTAGCTTGTGAGCAAATT3′	sense
−93/−73	5′TACCGAGCTCTGAGTGTAGACTGACCAATCGC3′	sense
−17/+4	5′TACCGAGCTCCCTCTAGGGCGGCCCTAGCT3′	sense
+ 48/+25	5′TCGCAAGCTTGCGAAGCTAGATATAGGGCGAGAC3′	antisense

TABLE I

Each primer was labeled by the location of the 5′ and the 3′ first nucleotide in the CP27 5′ flanking region. Each sense oligonucleotide was paired with the only antisense oligonucleotide for PCR amplification. A SacI restriction enzyme site was added to the 5′ end of each sense oligonucleotide, while a HindIII site was added to the 5′ end of the antisense oligonucleotide. PCR products were then inserted into the vector pGL3-Basic to generate promoter–reporter gene constructs.

TABLE II

SENSE OLIGONUCLEOTIDES USED FOR EMSA, THE COMPETITION AND MUTATION ANALYSIS IN EMSA AND FOR THE CONSTRUCTION OF MUTANT PLASMIDS

Oligonucleotide code	Oligonucleotide sequence
CAT-box 1 mutation study	
cp-93/-56	5'TGAGTGTAGACTGA**CCAAT**CGCAGCAGCCGGAAGTGTC
	||
cp-93/-56CATm	5'TGAGTGTAGACTGA**CacAT**CGCAGCAGCCGGAAGTGTC^{mut}
CAT-box 1 flanking region study	
cp-93/-56 D16 wt	5'TGAGTGTAGACTGA**CCAAT**CGCAGCAGC**CGGA**AGTGTC
	|||
cp-93/-56 M10-12	5'TGAGTGTAGACTGA**CCAAT**CGCAGCAG**Ctac**AAGTGTC^{mut}
cp-93/-56 D9	5'TGAGTGTAGACTGA**CCAAT**CGCAGCAGC^{del}
cp-93/-56 D13	5'TGAGTGTAGACTGA**CCAAT**CGCAGCAGC**CGGA**^{del}
CAT-box 5 mutation study	
cp-1255/-1213	5'TCTTAGGCTGATTCCCATTGCCATCCC**ATTGG**TCAACTCCCA
	||
cp-1255/-1213CAT5m	5'TCTTAGGCTGATTCCCATTGCCATCCC**ATgtG**TCAACTCCCA^{mut}
cp-1255/-1234	5'TCTTAGGCTGATTCCCATTGCC^{comp}
cp-1233/-1213	5'ATCCCATTGGTCAACTCCCA^{comp}

TABLE II

Mutated oligonucleotides (mut) are listed below wild-type oligonucleotides and mutation sites are highlighted through vertical lines. Mutations were created directly between the nucleotides −93 and −56 at positions −78 and −77 (CP-93/-56CATm) or between the nucleotides −1255 and −1213 at positions −1225 and −1224 (CP-1255/1213CAT5m). The mutation oligonucleotide CP-93/-56 M10-12 was created by replacing the CGGA motif of the wildtype oligonucleotide with a TACA motif in the mutated sequence.The deletion oligonucleotides (del) CP-93/-56 D9 and CP-93/-56 D13 were generated by removal of the 3′ region from the wild-type oligonucleotide CP-93/-56 D16. Oligonucleotides cp-1255/-1234 and cp-1233/-1213 were used for competition studies (comp).Lower cases indicate mutated nucleotides. The corresponding wild-type sequences are marked in bold characters. These mutations were used for EMSA competition assays and for the generation of mutant plasmids. The CCAAT box was underlined.

TABLE III

OLIGONUCLEOTIDE SEQUENCES USED FOR CP27 PROMOTER ANALYSIS

Oligo name	Sequence	Experiment
−207/−186	TATTAGCTTGTGAGCAAATT	Construct
−93/−73	TGAGTGTAGACTGACCAATCGC	Construct/ChIP
-55/-36	GTCTCTGACCACGTGGCACT	Construct
−17/+4	CCTCTAGGGCGGCCCTAGCT	Construct
+ 48/+25	GCGAAGCTAGATATAGGGCGAGAC	Construct/ChIP
CP-93/-56	TGAGTGTAGACTGACCAATCGCAGCAGCCGGAAGTGTC	EMSA
CP-93/-56 CAATmut	TGAGTGTAGACTGAC**ac**ATCGCAGCAGCCGGAAGTGTC	EMSA
CP-55/-27	TCTCTGACCACGTGGCACTGCCTGCGCA	EMSA
CP-55/-27 Emut	TCTCTGACCA**tt**TGGCACTGCCTGCGCA	EMSA
CP sense	CGTCCAGACTTCTCCACATCGGA(FAM)G	PCR
CP antisense	CTCCACCGGACGGCATAGTAGT	PCR
NF-Ya sense	ATGGAGCAGTATACGACAAACAGCA	PCR
NF-Ya antisense	TTAGGACACTCGGATGATCTG	PCR
USF1 sense	ACCCCAACGTCAAGTACGTC	PCR
USF1 antisense	TATGTTGAGCCCTCCGTTTC	PCR
beta actin sense	TTCCTGACAGGATGCAGAAG	PCR
beta actin antisense	GTACTTGCGCTCAGGAGGAG	PCR

Oligonucleotide sequences are listed in 5′ to 3′ orientation.

TABLE IV

ANNOTATED SEQUENCE OF THE CP27 PROXIMAL PROMOTER

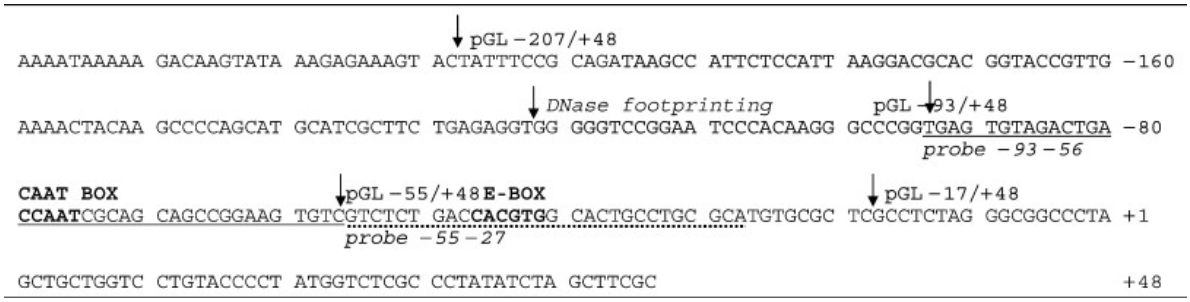

TABLE IV

LIST OF PRIMERS

Genotype PCR primer

Genotype		
WT (479bp)	ACTTCTCCACATCGGACGAG	ATGGGTAGCTCCTGCAAAGA
k/o (345bp)	GATCGGCCATTGAACAAGAT	ATACTTTCTCGGCAGGAGCA

Real time PCR analysis

Gene	5' Primer	3' primer
H2A.Z	CGTATCACCCCTCGTCACTT	TCAGCGATTTGTGGATGTGT
CP27	AGACTTCTCCACATCGGAG	CTCCACCGGACGGCAAGTAGT
Nanog	AGGTCTTCAGAGGAAGGGG	CAAGGGTCTGCTACTGAGATGCT
Ccnc	TGCTTCCTATGGGGAATCAG	ACGGCCTTAGGAGAGTCCAT

Primer for ChIP promoter assay

Gene	Promoter site	5' Primer	3' primer
RFad1	-700 to -1000	GTGATGTTCTGGAGGCAGGT	GGTGTGGAACCTTCGTTTGT
	-300 to -600	TGGGGCTCTGTCTGAACTGT	GTCGGGTGCTGCTTTGTAGT
	200 to -200	GAGCGACAGCCAAAATAACC	CTCTTTCCTTTCCGCATGTC
	100 to 500	AACTCAGGGTATGGCCTCCT	GGCTTTCCAGTAGCCACTCA
Nanog	-700 to -1000	GCCCTTCCCTCTCTGCTTAT	GTTTGCCGATCAGTCCTTGT
	-300 to -600	TTAAAAAGCCGCACTTTTGG	GACCTTGCTGCCAAAGTCTC
	200 to -200	GGAGAATAGGGGGTGGGTAG	CAGCCTATCTGAAGGCCAAC
	100 to 500	AAACGGGCTGAAGGGTTATT	CAAACTCAGAGGGGTTTCCA
Cyclin C	-1200 to -1600	AGATGGCTCAGCGGTTAAGA	GAGGGCATCAGGTTCCATTA
	-800 to -1200	TGGTCAGTGGGTCATGAAAA	CTGGGCAGAACATGACTCAA
	-400 to -800	ATTTTCAGGTGTGCCCAATC	CAGCCTAGGACAGGTGAGGA
	0 to -400	TTCAGCCCTAGGGAAAAAGC	ACGGTGTAGGCCTTCAGAAA
	0 to 400	CATTTGTATCAGGGCAAGCA	GCGAGAAAATGGAAGCTCAC

TABLE VI

LIST OF ANTIBODY AND CONDITION

	antibody information						
gene			IHC-P	IHC-F	WB	ChIP	CO-IP
CP27 (M)	Mouse monoclonal antibody IgG		1:100	1:100			
CP27	Rabbit polyclonal antibody IgG		1:100	1:100	1:1000	10ul/ml	10ul/ml
	souce	Cat #					
H2A.Z	abcam	ab4174	1:200	1:100	1:1000	5ug/ml	
DMAP1	abcam	ab2848			1:500	5ug/ml	
TIP49a	abcam	ab51500				5ug/ml	5ug/ml
Sox2	abcam	ab75179			1ug/ml	5ug/ml	
nanog	abcam	ab21624			1:1000		
Oct4	abcam	ab19857			1ug/ml		
TiP49b	abcam	ab36569					5ug/ml
BAF53A	abcam	ab3882			1ug/ml		
GAPDH	abcam	ab8245			1:2000		
Actin	Santa Cruz	sc-81178			1:1000		
Cyclin C	Santa Cruz	sc-1061			1:500		
GATA4	abcam	ab5245	1:100				
Snail	abcam	ab82846	1:100				
EED	abcm	ab4469	1:100				

V. CITED LITERATURE

Alder, H., Yoshinouchi, M., Prystowsky, M.B., Appasamy, P., Baserga, R., 1992. A conserved region in intro 1 negatively regulates the expression of the PCNA gene. Nucleic Acids Res. 11, 1769–1775.

Avilion, A. A., Nicolis, S. K., Pevny, L. H., Perez, L., Vivian, N., and Lovell-Badge, R. (2003). Multipotent cell lineages in early mouse development depend on SOX2 function. Genes Dev 17, 126-140.

Azara A, Piana A, Sotgiu G, Dettori M, Deriu MG, Masia MD, Are BM, Muresu E. 2006. Prevalence study of Legionella spp. contamination in ferries and cruise ships. BMC Public Health 6:100.

Babiarz, J. E., Halley, J. E., and Rine, J. (2006). Telomeric heterochromatin boundaries require NuA4-dependent acetylation of histone variant H2A.Z in Saccharomyces cerevisiae. Genes Dev 20, 700-710.

Bermadt, C.T., Nowling, T., Wiebe, M.S., Rizzino, A., 2005. NF-Y behaves as a bifunction transcription factor that can stimulate or repress the FGF-4 promoter in an enhancer-dependent manner. Gene Expr. 12, 193–212.

Bhattacharya, A., et al., 2003. The B subunit of the CCAAT box binding transcription factor complex (CBF/NF-Y) is essential for early mouse development and cell proliferation. Cancer Res. 63, 8167–8172.

Bi, W., Wu, L., Coustry, F., de Crombrugghe, B., Maity, S.N., 1997. DNA binding specificity of the CCAAT-binding factor CBF/NF-Y. J. Biol. Chem. 272, 26562–26572.

Boyer LA, Lee TI, Cole MF, Johnstone SE, Levine SS, Zucker JP, Guenther MG, Kumar RM, Murray HL, Jenner RG, Gifford DK, Melton DA, Jaenisch R, Young RA. 2005. Core transcriptional regulatory circuitry in human embryonic stem cells. Cell 122:947-956.

Boyer, L.A., et al., 2005. Core transcriptional regulatory circuitry in human embryonicstem cells. Cell 122, 947–956.

Bucher, P., Trifonov, E.N., 1988. CCAAT box revisited: bidirectionality, location and context. J. Biomol. Struct. Dyn. 5, 1231–1236.

Buszczak, M., and Spradling, A. C. (2006). Searching chromatin for stem cell identity. Cell 125, 233-236.

Caretti, G., Salsi, V., Vecchi, C., Imbriano, C., Mantovani, R., 2003. Dynamic recruitment of NF-Y and histone acetyltransferases on cell-cycle promoters. J. Biol. Chem. 278, 30435–30440.

Cavalli G. 2006. Chromatin and epigenetics in development: blending cellular memory with cell

Ceribelli, M., et al., 2008. The histone-like NF-Y is a bifunctional transcription factor. Mol. Cell. Biol. 28, 2047–2058.

Ceribelli, M., et al., 2008. The histone-like NF-Y is a bifunctional transcription factor. Mol. Cell. Biol. 28, 2047–2058.

Chae, H.D., Yun, J., Bang, Y.J., Shin, D.Y., 2004. Cdk2-dependent phosphorylation of the NF-y transcription factor is essential for the expression of the cell cycle-regulatory genes and cell cycle G1/S and G2/M transition. Ongogene 23, 4084–4088.

Chambers I. 2004. The molecular basis of pluripotency in mouse embryonic stem cells. Cloning Stem Cells 6:386-391.

Chen, S., et al., 2008. Bone morphogenetic protein 2 mediates dentin sialophosphoprotein expression and odontoblast differentiation via NF-Y signaling. J. Biol. Chem. 283, 19359–19370.

Cheung WL, Briggs SD, Allis CD. 2000. Acetylation and chromosomal functions. Curr Opin Cell Biol 12:326-333.

Coucouvanis, E., and Martin, G. R. (1995). Signals for death and survival: a two-step mechanism for cavitation in the vertebrate embryo. Cell 83, 279-287.

Coucouvanis, E., and Martin, G. R. (1999). BMP signaling plays a role in visceral endoderm differentiation and cavitation in the early mouse embryo. Development 126, 535-546.

Davidson, E.H., 1993. Later embryogenesis: regulatory circuitry in morphogenetic fields. Development 118, 665–690. Di Agostino, S., et al., 2006. Gain of function of mutant p53: The mutant p53/NF-Y protein complex reveals an aberrant transcriptional mechanism of cell cycle regulation. Cancer Cell 10, 191–202.

Didier, D.K., Schiffenbauer, J., Woulfe, S.L., Zacheis, M., Schwartz, B.D., 1988. Characterization of the cDNA encoding a protein binding to the major histocompatibility complex class II Y box. Proc. Natl. Acad. Sci. U. S. A. 85, 7322–7326.

Diekwisch TG, Luan X, McIntosh JE. 2002. CP27 localization in the dental lamina basement membrane and in the stellate reticulum of developing teeth. J Histochem Cytochem 50:583-586.

Diekwisch TG, Luan X. 2002. CP27 function is necessary for cell survival and differentiation during tooth morphogenesis in organ culture. Gene 287:141-147.

Diekwisch TG, Marches F, Williams A, Luan X. 1999. Cloning, gene expression, and characterization of CP27, a novel gene in mouse embryogenesis. Gene 235:19-30.

Diekwisch, T.G., Luan, X., 2002. CP27 function is necessary for cell survival and differentiation during tooth morphogenesis in organ culture. Gene 287, 141–147.

Diekwisch, T.G., Marches, F., 1997. cp27 novel gene expression during craniofacial development. J. Dent. Res. 76, 27.

Diekwisch, TGH 1999. EMBL Genbank Database Submission. Accession No. Y08219

Dillon, N. (2006). Gene regulation and large-scale chromatin organization in the nucleus. Chromosome Res 14, 117-126.

Donati, G., et al., 2008. An NF-Y-dependent switch of positive and negative histone methyl marks on CCAAT promoters. PLoS ONE 3, e2066.

Donati, G., Imbriano, C., Mantovani, R., 2006. Dynamic recruitment of transcription factors and epigenetic changes on the ER stress response gene promoters. Nucleic Acids Res. 34, 3116–3127.

Donovan PJ, Gearhart J. 2001. The end of the beginning for pluripotent stem cells. Nature 414:92-97.

Dorn, A., Bollekens, J., Staub, A., Benoist, C., Mathis, D., 1987. A multiplicity of CCAAT box-binding proteins. Cell 50, 863–872.

Downs JA, Allard S, Jobin-Robitaille O, Javaheri A, Auger A, Bouchard N, Kron SJ, Jackson SP, Cote J. 2004. Binding of chromatin-modifying activities to phosphorylated histone H2A at DNA damage sites. Mol Cell 16:979-990.

Eissenberg JC, Wong M, Chrivia JC. 2005. Human SRCAP and Drosophila melanogaster DOM are homologs that function in the notch signaling pathway. Mol Cell Biol 25:6559-6569.

Elkon, R., Linhart, C., Sharan, R., Shamir, R., Shiloh, Y., 2003. Genome-wide in silico identification of transcriptional regulators controlling the cell cycle in human cells. Genome Res. 13, 773–780.

Faast, R., Thonglairoam, V., Schulz, T. C., Beall, J., Wells, J. R., Taylor, H., Matthaei, K., Rathjen, P. D., Tremethick, D. J., and Lyons, I. (2001). Histone variant H2A.Z is required for early mammalian development. Curr Biol 11, 1183-1187.

Fan, J. Y., Gordon, F., Luger, K., Hansen, J. C., and Tremethick, D. J. (2002). The essential histone variant H2A.Z regulates the equilibrium between different chromatin conformational states. Nat Struct Biol 9, 172-176

Forsberg EC, Downs KM, Christensen HM, Im H, Nuzzi PA, Bresnick EH. 2000. Developmentally dynamic histone acetylation pattern of a tissue-specific chromatin domain. Proc Natl Acad Sci U S A 97:14494-14499.

Frontini, M., Imbriano, C., diSilvio, A., Bell, B., Bogni, A., Romier, C., Moras, D., Tora, L., Davidson, I., Mantovani, R., 2002. NF-Y recruitment of TFIID, multiple interactions with histone fold TAF(II)s. J. Biol. Chem. 277, 5841–5848.

Gatta, R., Mantonani, R., 2008. NF-Y substitutes H2A-H2B on active cell-cycle promoters: recruitment of CoREST-KDM1 and fine-tuning of H3 methylations. Nucleic Acids Res. 36, 6592–6607.

Griffiths, J.F.A., Miller, H.J., Suzuki, T.D., Lewontin, C.R., Gelbart, M.W., 2000. An introduction to genetic analysis, 7th edition. . New York.

Grskovic, M., Chaivorapol, C., Gaspar-Maia, A., Li, H., Ramalho-Santos, M., 2007. Systematic identification of cis-regulatory sequences active in mouse and human embryonic stem cells. PLoS Genet. 3, e145.

Guerra, R.F., Imperadori, L., Mantovani, R., Dunlap, D.D., Finzi, L., 2007. DNA compaction by the nuclear factor-Y. Biophys. J. 93, 176–182.

Gurtner, A., et al., 2008. NF-Y dependent epigenetic modifications discriminate between proliferation and postmitotic tissue. Plos One 23, 22047.

Hannan, N. J., and Salamonsen, L. A. (2008). CX3CL1 and CCL14 Regulate Extracellular Matrix and Adhesion Molecules in the Trophoblast: Potential Roles in Human Embryo Implantation. Biol Reprod.

Hattori N, Nishino K, Ko YG, Ohgane J, Tanaka S, Shiota K. 2004. Epigenetic control of mouse Oct-4 gene expression in embryonic stem cells and trophoblast stem cells. J Biol Chem 279:17063-17069.

Heessen, S., Fornerod, M., 2007. The inner nuclear envelope as a transcription factor resting place. EMBO Rep. 8, 914–919.

Holliday S, Schneider B, Galang MT, Fukui T, Yamane A, Luan X, Diekwisch TG. 2005. Bones, teeth, and genes: a genomic homage to Harry Sicher's "Axial Movement of Teeth". World J Orthod 6:61-70.

Hu, Q., Lu, J.F., Luo, R., Sen, S., Maity, S.N., 2006. Inhibition of CBF/NF-Y mediated transcription activation arrests cells at G2/M phase and suppressed expression of genes activated at G2/M phase of the cell cycle. Nucleic Acids Res. 34, 6272–6285.

Hu, Z., Jin, S., Scotto, K.W., 2000. Transcriptional activation of the MDR1 gene by UV irradiation. Role of NF-Y and Sp1. J. Biol. Chem. 275, 2979–2985.

Imbriano, C., et al., 2006. Direct p53 transcriptional repression: in vivo analysis of CCAAAT-containing G2/M promoters. Mol. Cell. Biol. 25, 3737–3751.

Ito, Y., Luan, X., Fan, J., Diekwisch, T., 2005. CP27 function related to early inner cell mass differentiation and pluripotent network maintenance. ASCB L349.

Iwashita, S., Ueno, S., Nakashima, K., Song, S. Y., Ohshima, K., Tanaka, K., Endo, H., Kimura, J., Kurohmaru, M., Fukuta, K., et al. (2006). A tandem gene duplication followed by recruitment of a retrotransposon created the paralogous bucentaur gene (bcntp97) in the ancestral ruminant. Mol Biol Evol 23, 798-806.

Jiang, B., Mendelson, C.R., 2003. USF1 and USF2 mediate inhibition of human trophoblast differentiation and CYP19 gene expression by Mash-2 and hypoxia. Mol. Cell. Biol. 23, 6117–6128.

Johnson, B. V., Rathjen, J., and Rathjen, P. D. (2006). Transcriptional control of pluripotency: decisions in early development. Curr Opin Genet Dev 16, 447-454.

Johnston H, Kneer J, Chackalaparampil I, Yaciuk P, Chrivia J. 1999. Identification of a novel SNF2/SWI2 protein family member, SRCAP, which interacts with CREB-binding protein. J Biol Chem 274:16370-16376.

Jorgensen HF, Giadrossi S, Casanova M, Endoh M, Koseki H, Brockdorff N, Fisher AG. 2006. Stem cells primed for action: polycomb repressive complexes restrain the expression of lineage-specific regulators in embryonic stem cells. Cell Cycle 5:1411-1414.

Kabe, Y., Yamada, J., Uga, H., Yamaguchi, Y., Wada, T., Handa, H., 2005. NF-Y is essential for the recruitment of RNA polymerase II and inducible transcription of several CCAAT box-containing genes. Mol. Cell. Biol. 25, 512–522.

Kaji K, Caballero IM, MacLeod R, Nichols J, Wilson VA, Hendrich B. 2006. The NuRD component Mbd3 is required for pluripotency of embryonic stem cells. Nat Cell Biol 8:285-292.

Kobor MS, Venkatasubrahmanyam S, Meneghini MD, Gin JW, Jennings JL, Link AJ, Madhani HD, Rine J. 2004. A protein complex containing the conserved Swi2/Snf2-related ATPase Swr1p deposits histone variant H2A.Z into euchromatin. PLoS Biol 2:E131.

Kobor, M. S., Venkatasubrahmanyam, S., Meneghini, M. D., Gin, J. W., Jennings, J. L., Link, A. J., Madhani, H. D., and Rine, J. (2004). A protein complex containing the conserved Swi2/Snf2-related ATPase Swr1p deposits histone variant H2A.Z into euchromatin. PLoS Biol 2, E131.

Kraus, W. L., and Wong, J. (2002). Nuclear receptor-dependent transcription with chromatin. Is it all about enzymes? Eur J Biochem 269, 2275-2283.

Krogan NJ, Baetz K, Keogh MC, Datta N, Sawa C, Kwok TC, Thompson NJ, Davey MG, Pootoolal J, Hughes TR, Emili A, Buratowski S, Hieter P, Greenblatt JF. 2004. Regulation of chromosome stability by the histone H2A variant Htz1, the Swr1 chromatin remodeling complex, and the histone acetyltransferase NuA4. Proc Natl Acad Sci U S A 101:13513-13518.

Krogan, N. J., Keogh, M. C., Datta, N., Sawa, C., Ryan, O. W., Ding, H., Haw, R. A., Pootoolal, J., Tong, A., Canadien, V., et al. (2003). A Snf2 family ATPase complex required for recruitment of the histone H2A variant Htz1. Mol Cell 12, 1565-1576.

Lee JH, Hart SR, Skalnik DG. 2004. Histone deacetylase activity is required for embryonic stem cell differentiation. Genesis 38:32-38.

Li J, Santoro R, Koberna K, Grummt I. 2005. The chromatin remodeling complex NoRC controls replication timing of rRNA genes. Embo J 24:120-127.

Li, Q., et al., 1998. Xenopus NF-Y pre-sets chromatin to potentiate p300 and acetylationresponsive transcription from the Xenopus hsp70 promoter in vivo. EMBO J. 17, 6300–6315.

Livak KJ, Schmittgen TD. 2001. Analysis of relative gene expression data using real-time quantitative PCR and the 2(-Delta Delta C(T)) Method. Methods 25:402-408.

Luan X, Diekwisch TG. 2002. CP27 affects viability, proliferation, attachment and gene expression in embryonic fibroblasts. Cell Prolif 35:207-219.

Luan X, Ito Y, Dangaria S, Diekwisch TG. 2006. Dental follicle progenitor cell heterogeneity in the developing mouse periodontium. Stem Cells Dev 15:595-608.

Luan, X., Diekwisch, T.G., 2002. CP27 affects viability, proliferation, attachment and gene expression in embryonic fibroblasts. Cell Prolif. 35, 207–219.

Luan, X., Ito, Y., Zhang, Y., Diekwisch, T.G., 2010. Characterization of the mouse CP27 promoter and NF-Y mediated gene regulation. Gene 460, 8–19.

MacDougald, O.A., Jump, D.B., 1991. Identification of functional cis-acting elements within the rat liver S14 promoter. Biochem. J. 280 (Pt 3), 761–767.

Magan, N., Szremska, A.P., Isaacs, R.J., Stowell, K.M., 2003. Modulation of DNA topoisomerase II alpha promoter activity by members of the Sp (specificity protein) and NF-Y (nuclear factor Y) families of transcription factors. Biochem. J. 374, 723–729.

Mantovani, R., 1998. A survey of 178 NF-Y binding CCAAT boxes. Nucleic Acids Res. 26, 1135–1143.

Mantovani, R., 1999. The molecular biology of the CCAAT-binding factor NF-Y. Gene 239, 15–27.

Matuoka, K., Yu Chen, K., 1999. Nuclear factor Y (NF-Y) and cellular senescence. Exp. Cell Res. 253, 365–371.

Meneghini, M. D., Wu, M., and Madhani, H. D. (2003). Conserved histone variant H2A.Z protects euchromatin from the ectopic spread of silent heterochromatin. Cell 112, 725-736.

Menon, R.K., Stephan, D.A., Singh, M., Morris Jr., S.M., Zou, L., 1995. Cloning of the promoterregulatory region of the murine growth hormone receptor gene. Identification of a developmentally regulated enhancer element. J. Biol. Chem. 270, 8851–8859.

Meshorer, E., and Misteli, T. (2006). Chromatin in pluripotent embryonic stem cells and differentiation. Nat Rev Mol Cell Biol 7, 540-546.

Meshorer, E., Yellajoshula, D., George, E., Scambler, P. J., Brown, D. T., and Misteli, T. (2006). Hyperdynamic plasticity of chromatin proteins in pluripotent embryonic stem cells. Dev Cell 10, 105-116.

Mitsui, K., Tokuzawa, Y., Itoh, H., Segawa, K., Murakami, M., Takahashi, K., Maruyama, M., Maeda, M., and Yamanaka, S. (2003). The homeoprotein Nanog is required for maintenance of pluripotency in mouse epiblast and ES cells. Cell 113, 631-642.

Mizuguchi, G., Shen, X., Landry, J., Wu, W. H., Sen, S., and Wu, C. (2004). ATP-driven exchange of histone H2AZ variant catalyzed by SWR1 chromatin remodeling complex. Science 303, 343-348.

Mu, W., Burt, D.R., 1999. The mouse GABA(A) receptor alpha3 subunit gene and promoter. Brain Res. Mol. Brain Res. 73, 172–180.

Muller, G.A., Heissig, F., Engeland, K., 2007. Chimpanzee, orangutan, mouse, and human cell cycle promoters exempt CCAAT boxes and CHR elements from interspecies differences. Mol. Biol. Evol. 24, 814–826.

Narlikar, L., Ovcharenko, I., 2009. Identifying regulatory elements in eukaryotic genomes. Brief. Funct. Genomics Proteomics 8, 215–230.

Nichols J, Zevnik B, Anastassiadis K, Niwa H, Klewe-Nebenius D, Chambers I, Scholer H, Smith A. 1998. Formation of pluripotent stem cells in the mammalian embryo depends on the POU transcription factor Oct4. Cell 95:379-391.

Nichols, J., Zevnik, B., Anastassiadis, K., Niwa, H., Klewe-Nebenius, D., Chambers, I., Scholer, H., and Smith, A. (1998). Formation of pluripotent stem cells in the mammalian embryo depends on the POU transcription factor Oct4. Cell 95, 379-391.

Nicolas, M., Noe, V., Ciudad, C.J., 2003. Transcriptional regulation of the human Sp1 gene promoter by the specificity protein (Sp) family members nuclear factor Y (NF-Y) and E2F. Biochem. J. 371, 265–275.

Niwa H. 2001. Molecular mechanism to maintain stem cell renewal of ES cells. Cell Struct Funct 26:137-148.

Niwa, H. (2007). How is pluripotency determined and maintained? Development 134, 635-646.

Nobukuni T, Kobayashi M, Omori A, Ichinose S, Iwanaga T, Takahashi I, Hashimoto K, Hattori S, Kaibuchi K, Miyata Y, Masui T, Iwashita S. 1997. An Alu-linked

repetitive sequence corresponding to 280 amino acids is expressed in a novel bovine protein, but not in its human homologue. J Biol Chem 272:2801-2807.

Nobukuni, T., et al., 1997. An Alu-linked repetitive sequence corresponding to 280 amino acids is expressed in a novel bovine protein, but not in its human homologue. J. Biol. Chem. 272, 2801–28071.

Novak, U., Paradiso, L., 1995. Identification of proteins in DNA–protein complexes after blotting of EMSA gels. Biotechniques 19, 54–55.

Pan, Q., et al., 2009. Bone morphogenetic protein-2 induces chromatin remodeling and modification at the proximal promoter of Sox9 gene. BBRC 379, 356–361.

Pan, Z., Hetherington, C.J., Zhang, D.E., 1999. CCAAT/enhancer-binding protein activates the CD14 promoter and mediates transforming growth factor beta signaling in monocyte development. J. Biol. Chem. 274, 23242–23248.

Pander, C. (1817). Historiam metamorphoseos quam ovum. Incubatum prioribus quinque diebus subit. (69 pp), Wuerzburg, Germany.

Papamichos-Chronakis M, Krebs JE, Peterson CL. 2006. Interplay between Ino80 and Swr1 chromatin remodeling enzymes regulates cell cycle checkpoint adaptationin response to DNA damage. Genes Dev 20:2437-2449.

Park JH, Roeder RG. 2006. GAS41 is required for repression of the p53 tumor suppressor pathway during normal cellular proliferation. Mol Cell Biol 26:4006-4016.

Poupko, J. M., Kostellow, A. B., and Morrill, G. A. (1977a). Histone acetylation associated with gastrulation in Rana pipiens. Differentiation 8, 167-174.

Poupko, J. M., Kostellow, A. B., and Morrill, G. A. (1977b). Changes in histone patterns during amphibian embryonic development. Differentiation 8, 61-70.

Puente LG, Borris DJ, Carriere JF, Kelly JF, Megeney LA. 2006. Identification of candidate regulators of embryonic stem cell differentiation by comparative phosphoprotein affinity profiling.

Rasmussen TP. 2003. Embryonic stem cell differentiation: a chromatin perspective. Reprod Biol Endocrinol 1:100.

Ridgway, P., Rangasamy, D., Berven, L., Svensson, U., and Tremethick, D. J. (2004). Analysis of histone variant H2A.Z localization and expression during early development. Methods Enzymol 375, 239-252.

Romier, C., Cocchiarella, F., Mantovani, R., Moras, D., 2003. The NF-YB/NF-YC structure gives insight into DNA binding and transcription regulation by CCAAT factor NF-Y. J. Biol. Chem. 278, 1336–1345.

Ruhl, D. D., Jin, J., Cai, Y., Swanson, S., Florens, L., Washburn, M. P., Conaway, R. C., Conaway, J. W., and Chrivia, J. C. (2006). Purification of a human SRCAP complex that remodels chromatin by incorporating the histone variant H2A.Z into nucleosomes. Biochemistry 45, 5671-5677.

Rustighi, A., Mantovani, F., Fusco, A., Giancotti, V., Manfioletti, G., 1999. Sp1 and CTF/NF- 1 transcription factors are involved in the basal expression of the Hmgi-c proximal promoter. Biochem. Biophys. Res. Commun. 265, 439–447.

Salsi, V., et al., 2003. Interaction between p300 and multiple NY-Y trimers govern cyclin B2 promoter function. J. Biol. Chem. 278, 6642–6650.

Scholer HR. 2004. [The potential of stem cells. A status update]. Bundesgesundheitsblatt Gesundheitsforschung Gesundheitsschutz 47:565-577.

Schrodeder, D.I., Myers, R.M., 2008. Multiple transcription start sites for FOXP2 with varying cellular specificities. Gene 413, 42–48.

Schuettengruber, B., Simboeck, E., Khier, H., Seiser, C., 2003. Autoregulation of mouse histone deacetylase 1 expression. Mol. Cell. Biol. 23, 6993–7004.

Slavkin HC, Diekwisch T. 1996. Evolution in tooth developmental biology: of morphology and molecules. Anat Rec 245:131-150.

Spivakov, M., and Fisher, A. G. (2007). Epigenetic signatures of stem-cell identity. Nat Rev Genet 8, 263-271.

Stern, C. D. (2004). The chick embryo--past, present and future as a model system in developmental biology. Mech Dev 121, 1011-1013.

Sugira, N., Takishima, K., 2003. Interaction of NF-Y with the 3′-flanking DNA sequence of the CCAAT box. FEBS Lett. 537, 58–62.

Sun, F., et al., 2009. Nuclear factor Y is required for basal activation and chromatin accessibility of fibroblast growth factor receptor 2 promoter in osteoblast-like cells. J. Biol. Chem. 284, 3136–3147.

Suto, R. K., Clarkson, M. J., Tremethick, D. J., and Luger, K. (2000). Crystal structure of a nucleosome core particle containing the variant histone H2A.Z. Nat Struct Biol 7, 1121-1124.

Sylvester, S.L., ap Rhys, C.M., Luethy-Martindale, J.D., Holbrook, N.J., 1994. Induction of GADD153, a CCAAT/enhancer-binding protein (C/EBP)-related gene, during the acute phase response in rats. Evidence for the involvement of C/EBPs in regulating its expression. J. Biol. Chem. 269, 20119–20125.

Tada T, Tada M. 2001. Toti-/pluripotential stem cells and epigenetic modifications. Cell Struct Funct 26:149-160.

Tam, P. P., and Loebel, D. A. (2007). Gene function in mouse embryogenesis: get set for gastrulation. Nat Rev Genet 8, 368-381.

Terada N, Hamazaki T, Oka M, Hoki M, Mastalerz DM, Nakano Y, Meyer EM, Morel L, Petersen BE, Scott EW. 2002. Bone marrow cells adopt the phenotype of other cells by spontaneous cell fusion. Nature 416:542-545.

Testa, A., et al., 2005. Chromatin immunoprecipitation (ChIP) on chip experiments uncover a widespread distribution of NF-Y binding CCAAT sites outside of core promoters. J. Biol. Chem. 280, 13606–13615.

Testa, A., et al., 2005. Chromatin immunoprecipitation (ChIP) on chip experiments uncover a widespread distribution of NF-Y binding CCAAT sites outside of core promoters. J. Biol. Chem. 280, 13606–13615.

Thesleff, I., 1995. Tooth morphogenesis. Adv. Dent. Res. 9, 12.

Thesleff, I., Sharpe, P., 1997. Signalling networks regulating dental development. Mech. Dev. 67, 111–123.

Thomson JA, Itskovitz-Eldor J, Shapiro SS, Waknitz MA, Swiergiel JJ, Marshall VS, Jones JM. 1998. Embryonic stem cell lines derived from human blastocysts. Science 282:1145-1147.

von Baer, K.E. (1828, 1837). Entwickelungsgeschichte der Thiere. Beobachtung und Reflexion. Bd. 1 & 2. Borntraeger, Koenigsberg, Germany.

Wasner, M., et al., 2008. Three CCAAT-box and a single cell cycle genes homology region (CHR) are the major regulating sites for transcription from the human cyclin B2 promoter. Gene 312, 225–237.

Weissman IL. 2000. Translating stem and progenitor cell biology to the clinic: barriers and opportunities. Science 287:1442-1446.

Wiren M, Silverstein RA, Sinha I, Walfridsson J, Lee HM, Laurenson P, Pillus L, Robyr D, Grunstein M, Ekwall K. 2005. Genomewide analysis of nucleosome density histone acetylation and HDAC function in fission yeast. Embo J 24:2906-2918.

Wolpert, L. (2004). Much more from the chicken's egg than breakfast--a wonderful model system. Mech Dev 121, 1015-1017.

Wong MM, Cox LK, Chrivia JC. 2007. The chromatin remodeling protein, SRCAP, is critical for deposition of the histone variant H2A.Z at promoters. J Biol Chem. 282(36):26132-9.

Wong, M. M., Cox, L. K., and Chrivia, J. C. (2007). The chromatin remodeling protein, SRCAP, is critical for deposition of the histone variant H2A.Z at promoters. J Biol Chem 282, 26132-26139.

Wu, W. H., Alami, S., Luk, E., Wu, C. H., Sen, S., Mizuguchi, G., Wei, D., and Wu, C. (2005). Swc2 is a widely conserved H2AZ-binding module essential for ATP-dependent histone exchange. Nat Struct Mol Biol 12, 1064-1071.

Xi, R., and Xie, T. (2005). Stem cell self-renewal controlled by chromatin remodeling factors. Science 310, 1487-1489.

Xiong, S., Chirala, S.S., Wakil, S.J., 2000. Sterol regulation of human fatty acid synthase promoter I requires nuclear factor-Y- and Sp-1-binding sites. Proc. Natl. Acad. Sci. U. S. A. 97, 3948–3953.

Xu, Y., et al., 2006. NF-Y and CCAAT/Enhancer-binding protein a synergistically activate the mouse amelogenin gene. J. Biol. Chem. 281, 16090–16098.

Yang XJ, Gregoire S. 2005. Class II histone deacetylases: from sequence to function, regulation, and clinical implication. Mol Cell Biol 25:2873-2884.

Ying QL, Nichols J, Evans EP, Smith AG. 2002. Changing potency by spontaneous fusion. Nature 416:545-548.

Yu, J.H., Schwartzbauer, G., Kazlman, A., Menon, R.K., 1999. Role of the Sp family of transcription factors in the ontogeny of growth hormone receptor gene expression. J. Biol. Chem. 274, 34327–34336.

Zang RY, Li ZT, Tang J, Huang X, Cai SM. 2006. Weekly induction intraperitoneal chemotherapy after primary surgical cytoreduction in patients with advanced epithelial ovarian cancer. World J Surg Oncol 4:4.

Zhang, Y., and Reinberg, D. (2001). Transcription regulation by histone methylation: interplay between different covalent modifications of the core histone tails. Genes Dev 15, 2343-2360.

Zhou, Y.L., Snead, M.L., 2000. Identification of CCAAT/enhancer-binding protein alpha as a transactivator of the mouse amelogenin gene. J. Biol. Chem. 275, 12273–12280.

Zhu, J., Giannola, D.M., Zhang, Y., Rivera, A.J., Emerson, S.G., 2003. NF-Y cooperates with USF1/2 to induce the hematopoietic expression of HOXB4. Blood 102, 2420–2427.

Zhu, J., Zhang, Y., Joe, G.J., Pompetti, R., Emerson, S.G., 2005. NF-Ya activates multiple hematopoietic stem cell (HSC) regulatory genes and promotes HSC self-renewal. Proc. Natl Acad. Sci. USA 102, 11728–11733.Bulger M. 2005. Hyperacetylated chromatin domains: lessons from heterochromatin. J Biol Chem 280:21689-21692.

Zorbas, H., Rein, T., Krause, A., Hoffmann, K., Winnacker, E.L., 1992. Nuclear factor I (NF I) binds to an NF I-type site but not to the CCAAT site in the human alpha-globin gene promoter. J. Biol. Chem. 267, 8478–8484.

Zwicker, J., et al., 1995. Cell cycle regulation of the cyclin A, cdc25c and cdc2 genes is based on a common mechanism of transcription repression. EMBO J. 14, 4514–4522.

VI. VITA

NAME: Yoshihiro Ito

EDUCATION:

2008-2012	PhD	UIC college of dentistry, MOST Program in Oral Science
1997-1999	USC Certificate	Continuing Education Program of Periodontology, USC, School of Dentistry
1996-1997	UCLA Certificate	Fellowship Course in Clinical Dentistry and Basic Dental Science at International Dental Academy, Tokyo Japan
1989-1996	D.D.S.	Nihon University, School of Dentistry, Tokyo Japan

EMPLOYMENT HISTORY

2004-2008	Research Specialist at UIC, Department of Oral Biology Collage of Dentistry, Chicago, IL
2000-2003	Research Associate, Center for Craniofacial Molecular Biology, School of Dentistry, University of Southern California, Los Angeles, CA
1997-1999	Clinical Periodontics training at School of Dentistry, University of Southern California, Los Angeles, CA
1996-1997	Clinical Dentistry training, International Dental Academy, Tokyo Japan

PUBLICATION:

Lu X, **Ito Y**, Kulkarni A, Gibson C, Luan X, Diekwisch TG. Ameloblastin-rich enamel matrix favors short and randomly oriented apatite crystals. Eur J Oral Sci. 2011 Dec;119 Suppl 1:254-60.

Dangaria SJ, **Ito Y**, Luan X, Diekwisch TG. Successful periodontal ligament regeneration by periodontal progenitor preseeding on natural tooth root surfaces. Stem Cells Dev. 2011 Oct;20(10):1659-68. Epub 2011 Mar 9.

Ito Y, Zhang Y, Dangaria S, Luan X, Diekwisch TG. NF-Y and USF1 transcription factor binding to CCAAT-box and E-box elements activates the CP27 promoter. Gene. 2011 Mar 1;473(2):92-9. Epub 2010 Nov 13.

Nakajima A, Tanaka E, **Ito Y**, Maeno M, Iwata K, Shimizu N, Shuler CF. The expression of TGF-β3 for epithelial-mesenchyme transdifferentiated MEE in palatogenesis.. J Mol Histol. 2010 Dec;41(6):343-55. Epub 2010 Oct 22.

Walker, C.G.*, Dangaria, S.*, **Ito, Y**., Luan, X., and Diekwisch, T.G.H.(2010).Osteopontin is Required for Unloading-Induced Osteoclast Recruitment and Modulation of RANKL Expression during Tooth Drift-associated Bone Remodeling, but Not for Super-Eruption. BONE 47, 1020-1029

Dangaria, S., Ito, Y., Yin, L.L., Valdrè, G., Luan, X., and Diekwisch, T.G.H. (2010). Apatite microtopographies instruct signaling tapestries for progenitor-driven new attachment of teeth. Tissue Engineering A. Pub Med ID: 20795795

Dangaria, S., **Ito, Y**., Luan, X., and Diekwisch, T.G.H. (2010). Differentiation of neural crest-derived intermediate pluripotent progenitors into committed periodontal populations involves unique molecular signature changes, cohort shifts, and epigenetic modifications. Stem Cells and Development. Pub Med ID: 20665818

Luan, X., **Ito, Y**., Zhang, Y., and Diekwisch, T.G.H. (2010). Characterization of the mouse CP27 promoter and NF-Y mediated gene regulation. Gene 460, 8-19.

Jin, T.*, **Ito, Y.*,** Luan, X., Dangaria, S., Walker, C., Allen, M., Kulkarni A., Gibson, C., Braatz, R., Liao, X., and Diekwisch, T.G.H. (2009). Supramolecular compaction through polyproline motif elongation as a mechanism for vertebrate enamel evolution. PLoS Biology 7(12): e1000262. doi:10.1371/journal.pbio.1000262.

Dangaria, S.J., **Ito, Y**., Walker, C., Druzinsky, R., Luan, X., and Diekwisch, T.G.H. (2009). Extracellular matrix-mediated differentiation of periodontal progenitor cells. Differentiation 78, 79-90.

Diekwisch, T.G.H., Jin, T., Wang, X., **Ito, Y**., Schmidt, M.K., Druzinsky, R., Yamane, A., and Luan, X. (2009). Amelogenin evolution and tetrapod enamel structure. Frontiers of Oral Biology 13, 74-79.

Walker, C., **Ito, Y.,** Dangaria, S., Luan, X., and Diekwisch, T.G.H. (2008). RANKL, osteopontin and osteoclast homeostasis in a hyper-occlusion mouse model. Eur. J. Oral Sci. 116, 312-318.

Xu X, Han J, **Ito Y**, Bringas P Jr, Deng C, Chai Y Ectodermal Smad4 and p38 MAPK are functionally redundant in mediating TGF-beta/BMP signaling during tooth and palate development.. Dev Cell. 2008 Aug;15(2):322-9.

Luan X, **Ito Y**, Holliday S, Walker C, Daniel J, Galang TM, Fukui T, Yamane A, Begole E, Evans C, Diekwisch TG. (2007) Extracellular matrix-mediated tissue remodeling following axial movement of teeth. J Histochem Cytochem. Feb;55(2):127-40. Epub 2006 Oct 2.

Nakajima A, **Ito Y**, Asano M, Maeno M, Iwata K, Mitsui N, Shimizu N, Cui XM, Shuler CF. (2007) Functional role of transforming growth factor-beta type III receptor during palatal fusion.Dev DynMar;236(3):791-801.

Luan, X., **Ito, Y**., Dangaria S. and Diekwisch, T.G.H. (2006) Dental follicle progenitor cell heterogeneity in the developing mouse periodontium. Stem Cells Dev. 2006 Aug;15(4):595-608.

Luan, X., **Ito, Y**., and Diekwisch, T.G.H**.** (2006). Evolution and development of Hertwig's Epithelial Root Sheath. Developmental Dynamics May;235(5):1167-80..

Oka K, Oka S, Sasaki T, **Ito Y**, Bringas P Jr, Nonaka K, Chai Y. The role of TGF-beta signaling in regulating chondrogenesis and osteogenesis during mandibular development. Dev Biol. 2007 Mar 1;303(1):391-404. Epub 2006 Nov 21

Wang, X., Fan, J.-L., **Ito, Y**., Luan, X., and Diekwisch, T.G.H. (2006). Identification and characterization of a squamate reptilian amelogenin gene: *Iguana iguana*. J. Exp. Zool. Mol. Dev. Evol. Jul 15;306(4):393-406

Diekwisch, T.G.H**.,** Wang, X., Fan, J.-L., **Ito, Y**., and Luan, X. (2006). Expression and characterization of a *Rana pipiens* amelogenin protein. Eur. J. Oral Sci. May;114 Suppl 1:86-92; discussion 93-5, 379-80

Xu X, Han J, **Ito Y**, Bringas P Jr, Urata MM, Chai Y. (2006) Cell autonomous requirement for Tgfbr2 in the disappearance of medial edge epithelium during palatal fusion. Dev Biol. 2006 Sep 1;297(1):238-48. Epub May 19.

Sasaki T, **Ito Y**, Bringas Jr. P, Chou S, Urata, M, Slavkin HC, Chai Y. (2005). TGF-beta-mediated FGF signaling is critical for regulating cranial neural crest cell proliferation during frontal bone development. *Development* Jan;133(2):371-81.

Choudhary, B, **Ito, Y**, Chai, Y, and Sucov, H (2005) Cardiovascular malformations with normal smooth muscle differentiation in neural crest-specific type II TGF-receptor (Tgfbr2) mutant mice. Dev Biol. 2006 Jan 15;289(2):420-9. Epub 2005 Dec 5.

Hosokawa R, Urata MM, **Ito Y**, Bringas P Jr., Chai Y. (2005). Functional significance of Smad2 in regulating basal keratinocyte migration during wound healing. *Journal of Investigative Dermatology* Dec; 125(6):1302-9.

Wang X, **Ito Y**, Luan X, Yamane A, Diekwisch T.G.H. Amelogenin sequence and enamel biomineralization in Rana pipiens. J Exp Zoolog B Mol Dev Evol. 2005 Mar 15;304(2):177-86

Cui XM, Shiomi N, Chen J, Saito T, Yamamoto T, **Ito Y**, Bringas Jr. P, Chai Y, Shuler CF. (2005) Overexpression of Smad2 in TGF-beta3-null mutant mice rescues cleft palate. *Dev. Biol*. 278, 193-202.

Sasaki T, **Ito Y**, Xu X, Han J, Bringas P Jr, Maeda T, Slavkin HC, Grosschedl R, Chai Y. (2005). LEF1 is a critical epithelial survival factor during tooth morphogenesis. *Dev.* Biol. 278,130-143.

Ito Y, Yeo JY, Chytil A, Han J, Bringas P Jr, Nakajima A, Shuler CF, Moses HL, Chai Y. (2003). Conditional inactivation of TGF-beta IIR in cranial neural crest causes cleft palate and calvaria defects. *Development* 130, 5269-5280..

Han J., **Ito Y**., Yeo J., Sucov H.M., Maas R., and Chai Y. (2003) Cranial neural crest-derived mesenchymal proliferation is regulated by Msx1-mediated $p19^{INK4d}$ expression during odontogenesis. *Dev. Biol*. In Press.

Cui XM, Chai Y, Chen J, Yamamoto T, **Ito Y**, Bringas P, Shuler CF. (2003). TGF - beta3-dependent SMAD2 phosphorylation and inhibition of MEE proliferation during palatal fusion. *Dev Dyn*. 227:387-94.

Chai Y., **Ito Y**., and Han J. (2003). TGF-beta signaling and its functional significance in regulating the fate of cranial neural crest cells. *Crit. Rev. Oral Biol. Med*. 14, 78-88

Xu X, Jeong L, Han J, **Ito Y**, Bringas P Jr, Chai Y. (2003). Developmental expression of Smad1-7 suggests critical function of TGF-beta/BMP signaling in regulating epithelial-mesenchymal interaction during tooth morphogenesis. Int J Dev Biol 47(1):31-9

Ito Y, Bringas P Jr, Mogharei A, Zhao J, Deng C, Chai Y. (2002) Receptor-regulated and inhibitory Smads in regulating TGF-beta-mediated Meckel's cartilage development. Dev. Dyn 224(1):69-78.

Ito Y, Zhao J, Mogharei A, Shuler CF, Weinstein M, Deng C, Chai Y (2001). Antagonistic effects of Smad2 versus Smad7 are sensitive to their expression level during tooth development. J Biol Chem 276(47):44163-44172

Ito Y, Sarkar P, Mi Q, Wu N, Bringas P Jr, Liu Y, Reddy S, Maxson R, Deng C, Chai Y (2001). Overexpression of Smad2 reveals its concerted action with Smad4 in regulating TGF-beta-mediated epidermal homeostasis. Dev. Biol. 236, 181-194

Chai Y, Jiang X, **Ito Y**, Bringas P Jr, Han J, Rowitch DH, Soriano P, McMahon AP, Sucov HM (2000). Fate of the mammalian cranial neural crest during tooth and mandibular morphogenesis. Development, 127,1671-1679.

Sarkar PS, Appukuttan B, Han J, **Ito Y**, Ai C, Tsai W, Chai Y, Stout JT, Reddy S (2000). Heterozygous loss of Six5 in mice is sufficient to cause ocular cataracts. Nature Genetics. 25, 110-114.

Membership

AADR	American association of Dental research
JADR	Japanese association of Dental research
IADR	International association of Dental research
ASCB	American Society for Cell Biology